'Corrosion of Aluminium in Contact with Cutting Fluids / Electrochemistry of Corrosion'

Victoria Jane Braham

Thesis submitted to THE UNIVERSITY OF NEWCASTLE UPON TYNE for the degree of Doctor of Philosophy

June 1997

Declaration

The work in this thesis was carried out between October 1993 and October 1996 at the University of Newcastle upon Tyne. The corrosion of aluminium and aluminium alloys in aqueous solutions and cutting fluid emulsions has been investigated. No part of this thesis has been submitted for a degree to this, or any other university.

Extracts from this work were presented at the 'Electrochem '95' conference (1995), which was held at Strathclyde University in Glasgow.

Two papers have been published in *Corrosion Science* (Vol. 37, p. 1489, (1995) and Vol. 38, p. 1463, (1996)) during the completion of this work.

"Any physical theory is always provisional, in the sense that it is only a hypothesis; you can never prove it. No matter how many times the results of experiments agree with some theory, you can never be sure the next time the results will not contradict the theory. On the other hand, you can disprove a theory by finding even a single observation that disagrees with the predictions of the theory. As philosopher Karl Popper has emphasised, a good theory is characterised by the fact that it makes a number of predictions that could in principle be disproved or falsified by observation. Each time new experiments are observed to agree with the predictions the theory survives, and our confidence in it is increased; but if ever a new observation is found to disagree, we have to abandon or modify the theory. At least that is what is supposed to happen, but you can always question the competence of the person that carried out the observation [1]."

[1] Stephen Hawking, *A Brief History of Time*, Bantem Press, London, (1988) p.10

Abstract

The work in this thesis concerns the behaviour of cutting fluids used for drilling aluminium. A cutting fluid which is useful must neither corrode nor stain aluminium unduly. The compositional factors which lead to a successful cutting fluid have been investigated using electrochemical techniques.

Linear sweep and impedance measurements were used to assess the corrosion of pure aluminium and aluminium alloys in contact with aqueous solutions in the pH range 8-11, in the presence and absence of oxygen. It was found that a low corrosion rate required that the solution pH was kept lower than 9.5.

Clear and stable cutting fluids were formulated with and without the use of amines and the corrosion of aluminium in contact with these cutting fluid emulsions was studied. The corrosion rate of aluminium was found to be a factor of ten times lower when in contact with a typical emulsion compared to contact with an aqueous borax solution of the same pH. The most important factor in respect of corrosion control was the pH. The presence/absence of amines did not significantly affect the corrosion rates.

In order to simulate the drilling process, a glass cell was designed with a glass frit situated at the base onto which an aluminium rotating disc electrode was lowered, and electrochemical measurements were made, *in situ* in this way. Abrasion of the electrode caused the anodic process on the metal to be affected to a greater extent than the cathodic process.

The electrochemical techniques used in this work have readily allowed us to assess the suitability of different cutting fluid formulations.

Contents

Page

Acknowledgments

CHAPTER 1

INTRODUCTION

1.0 Introduction

The work reported in this thesis is primarily concerned with the corrosion of aluminium in cutting fluid emulsions. This introductory chapter therefore, has been divided into two sections; the first outlines the background and principles of aluminium corrosion and the second gives an insight into cutting fluid concentrates and emulsions and their composition.

1.1 Basic Concepts of Corrosion

1.1.1 Definition

The 'electrochemical mechanism of corrosion' may be expressed concisely as;

'*An electrochemical reaction in which the metal itself is a reactant and is oxidised to a higher valency state, whilst another reactant, an electron acceptor, in solution is reduced to a lower valency state*'.

Corrosion may be defined as the attack of a material by its environment, generally leading to degradation in the properties of the material. When the material is not specified it is generally assumed to be a metal. The Corrosion Education Manual of the European Federation of Corrosion [1] provides a more comprehensive and exact definition of corrosion:

'*Corrosion : attack on a metal by the reaction with the environment with a consequential deterioration in properties. When no reference is made to the material it is normally understood that a metal is involved, and that the valency of the metal is increased; an exception is the dissolution of a metal in a liquid metal or a fused salt. The term corrosion may refer either to the process or to the damage caused. Implicit in the concept of corrosion as a process is the rate per unit area of the corrosion reaction; implicit in the damage caused is the extent and the nature of the damage in relation to the function of the component concerned*'.

1.1.2 Classification

The classification of corrosion processes is by no means simple, owing to the enormous variety of corrosive environments and the diversity of corrosion reactions. Implicit in the term 'dry' is the absence of water or an aqueous solution. The broad classification of corrosion reactions into 'wet' includes all reactions in which an aqueous solution is involved in the reaction mechanism [2].

'Dry' corrosion

These are generally metal/gas or metal/vapour reactions; oxidation, scaling and tarnishing are common examples of this. A characteristic of these reactions is that the initial oxidation of the metal and reduction of the non-metal involves the formation of a compound at the metal/non-metal interface. It is also observed that the formation of a continuous film of reactant product at the metal/non-metal interface results in a growth rate which, when the film becomes sufficiently thick to be rate determining, decreases as the film thickens.

For example, a bare aluminium surface which is exposed to dry air reacts spontaneously to form aluminium oxide according to the following equation;

$$4Al(s) + 3O_2(g) = 2Al_2O_3(s)$$

In the presence of water vapour the oxide may be converted to the hydroxide of which there are various forms,

$$Al_2O_3(s) + H_2O(g/l) = 2Al(OH)_3(s)$$

'Wet' corrosion

In 'wet' corrosion, the oxidation of the metal and the reduction of species in solution may occur at different areas on the metal surface. This involves electron transfer through the metal from the anodic area to the cathodic area. Hydrated ions (cations or anions) may be transported away from the interface by a processes such as migration, diffusion, or convection. Subsequent reaction with the solution may result in the formation of a stable solid phase, but if this forms away from the interface it will not be protective. Thermodynamically stable oxides will affect the kinetics of the corrosion reaction only if they form a film on the metal surface.

For example, when a bare aluminium surface is exposed to aqueous solution rapid corrosion results producing aluminium hydroxide,

$$Al(s) + 3H_2O(l) = Al(OH)_3 + 3/2H_2$$

In the case of aluminium, the film is strongly adherent to the metal surface. For the purpose of the work presented here, corrosion has been considered as a chemical reaction at the metal/environment interface which involves the metal itself as one of the reactants.

1.1.3 Cost of Corrosion

The main driving force for corrosion protection and inhibition is *economic*. Improved corrosion resistance can generally only be attained at an increased cost yet, in the majority of cases, it must be cheaper to protect the metal than allow it to corrode and incur the high cost of replacement. The addition of inhibiting chemicals can be regarded as a direct economic loss. A survey conducted in 1986 [3], estimated that the US industry spent $798M on corrosion inhibiting chemicals that year. However, in formulatory work, it is extremely important that the cost of the final product is not minimised at the expense of the final product quality or performance.

Other incentives for corrosion studies include *conservation*, and improvement of *safety*. Failure of airplane components, bridges and automotive steering mechanisms due to corrosion can all lead to catastrophic consequences. Often in industry, the required physical properties of constructional materials can be easily satisfied, but the selection of these materials can be seriously affected by their corrosion properties for example; carbon-steel may have adequate mechanical properties yet conditions might dictate the use of a more expensive corrosion resistant alloy.

1.2 Inhibitors

An inhibitor may be defined as;

'A *chemical substance which decreases the corrosion rate when present in the corrosion system at a suitable concentration, without significantly changing the concentration of any other corrosive agent* ' [4].

Aqueous systems are by far the most common corrosive environments to which corrosion inhibitors are applied, and generally increased corrosion resistance may only be obtained at increased cost. The use of chemical inhibitors remains the most practical and cost effective means of preventing corrosion, despite modern advances in corrosion resistant materials. Improved products can only be developed efficiently from greater understanding of corrosion and inhibition mechanisms.

The use of chemicals to inhibit the corrosion of metals in many environments is well established. In most cases inhibition is achieved through the interaction or reaction between the inhibitor and the metal surface which results in the formation of a protective surface film. In other cases the chemistry of the

environment may be modified to render it less corrosive, e.g. by adjusting the pH [3].

Although effective products are in use for many applications, certain chemicals are now being phased out. Inhibitors must be safe to use and enviromentally acceptable [5,6]. It is also important that the inhibitors do not interfere with functions of other components within the fluid concentrate. Problems may arise with chemical inhibitors interacting with other components in the solute rendering them ineffective for their particular application, and/or sometimes producing unsightly deposits on the surface of the metal.

In conclusion, an inhibitor must meet certain requirements for each specific application such as stability against temperature, time, and exposure to the corrosive environment. It must function at low concentrations and be easy to apply. It must be compatible with other chemicals in use, and must meet performance specifications, i.e. it must inhibit corrosion! It should not be too toxic. The raw materials must be readily available and not too expensive.

1.3 Thermodynamics

In this section the interaction of a metal with an aqueous solution will be considered from the viewpoint of the thermodynamics.

1.3.1 Introduction

The thermodynamics provides a means of measuring the equilibrium state of a system but provides no information on the detailed course of the reaction nor on the rate at which the system proceeds towards equilibrium. Although a reaction may have a thermodynamic tendency to proceed in a given direction, it may be regarded as not occurring at all due to the slow kinetics (slow rate) at which it reaches its equilibrium state. For example, when oxygen and hydrogen come into contact at 25°C, the conversion to water is extremely slow, despite the large decrease in the standard free energy that accompanies it.

$$H_2(g) + \tfrac{1}{2}O_2(g) \rightarrow H_2O \qquad \Delta G^\circ = -237\text{kJ}$$

Metals such as aluminium are relatively stable in oxygen whereas other reactive metals such as the alkali and alkaline earth metals undergo complete oxidation at a fast rate. Here the kinetics are determined by the nature of the oxide film formed on the surface which is protective for aluminium, and non-protective for the alkali and alkaline earth metals.

1.3.2 The Electrochemical Series

If a metal with a tendency to dissolve is immersed in a solution, it will establish a potential between the released positively charged metal cations and the subsequently negatively charged metal. The potential cannot be measured in absolute terms, but the potential difference between it and another electrode can be determined. If the potential of the other electrode is known and all of the other conditions are standardised, we can obtain a set of standard electrode potentials where the cation concentration is 1mol dm^{-3}. The known electrode is the standard hydrogen electrode which is arbitrarily assigned a potential of 0V. Thus, thermodynamics can provide us with an indication of whether or not a metal will corrode in a given environment due to hydrogen evolution/oxygen reduction.

A clear illustration of this is found by examination of the reduction potentials of a range of metals in deaerated 1M solutions of the metal cation:

$$Cu^{2+} + 2e^- = Cu \qquad E^o = +0.34V$$

$$H^+ + e^- = \tfrac{1}{2}H_2 \qquad E^o = 0.00V$$

$$Fe^{2+} + 2e^- = Fe \qquad E^o = -0.44V$$

$$Zn^{2+} + 2e^- = Zn \qquad E^o = -0.76V$$

$$Al^{3+} + 3e^- = Al \qquad E^o = -1.67V$$

Metals with a positive standard reduction potential (E^o) will not corrode in deaerated 1M $HClO_4$ solution, conversely iron and aluminium in this environment are thermodynamically unstable with respect to dissolution. In studying the reduction potentials above, no information is available on the possibility of surface film formation on the corroding metal. In the case of aluminium a very stable surface layer of alumina (Al_2O_3) forms and subsequently restricts further corrosion to a very low level. This phenomenon is called 'passivity'.

1.3.3 Definitions

Overpotential

'*When an electrochemical reaction occurs at an electrode which has been at equilibrium, the electrode potential changes from its initial value to a new value, and the difference is the overpotential* η'.

Any electrode process under specified conditions will require an activation overpotential in order for charge transfer at a finite rate to occur. The overpotential provides the activation energy required in order for the reactant to overcome the energy barrier that exists between the reactant and product. Most electrode processes involve more than one step and the activation energy therefore is that energy required to maintain the rate of the rate determining step, since the other steps are regarded as being at equilibrium.

Immunity [7]

'*A state of resistance to corrosion or anodic dissolution of a metal caused by thermodynamic stability of the metal*'.

Passivity [7]

'*A condition in which a piece of metal, because of an impervious covering of oxide or other compound, has a potential much more positive than that of the metal in the active state*'.

1.3.4 Pourbaix Diagrams

Data in the form of equilibrium diagrams showing pH vs E (the equilibrium potential), are known as 'Pourbaix diagrams' [8].

Three zones can be identified on these diagrams; immunity, corrosion and passivation. The horizontal lines represent reactions involving electron transfer only. Vertical lines represent reactions involving only chemical reactions and the diagonal lines show a combination of both types of reaction.

Various equilibria of the Al-H_2O system are shown in the Pourbaix diagram shown in Fig.1.1. The diagram indicates the conditions under which aluminium should theoretically corrode, be passive, and show immunity. It can be seen that aluminium will corrode forming Al^{3+} at low pH, and AlO_2^- at high pH. At near

neutral pH values, the system is passive and forms a protective layer of hydrargillite ($Al_2O_3.3H_2O$) on the surface. The nature of the oxide changes as the temperature is raised, with boehmite ($Al_2O_3.H_2O$) forming at temperatures above 75°C.

Cathodic Protection of Aluminium

The cathodic protection of aluminium is difficult to achieve (immunity without a protective oxide), owing to the very low equilibrium potential of the metal as can be seen in Fig.1.2(a). For the same reason, it is impossible to electrically deposit aluminium from aqueous solutions.

Limitations of the Pourbaix Diagram

It is assumed that species either side of any line in the Pourbaix diagram are in equilibrium. Generally for a corroding system, dissolution of the metal occurs continuously, which indicates that the metal and the metal ion are not in equilibrium. It is also assumed that the acid or alkali counter ions play no part in the corrosion process. For example, in acid solutions it is known that Cl^- ions are particularly aggressive towards aluminium so that passivity of the aluminium surface is not easily established. Passivity refers to any sparingly soluble products irrespective of their protective nature. It is possible that the product is loosely adherent to the metal surface and hence offers no corrosion protection at all.

Finally, Pourbaix diagrams provide a thermodynamic basis for the study of corrosion and offer no information on the rate of corrosion that may occur.

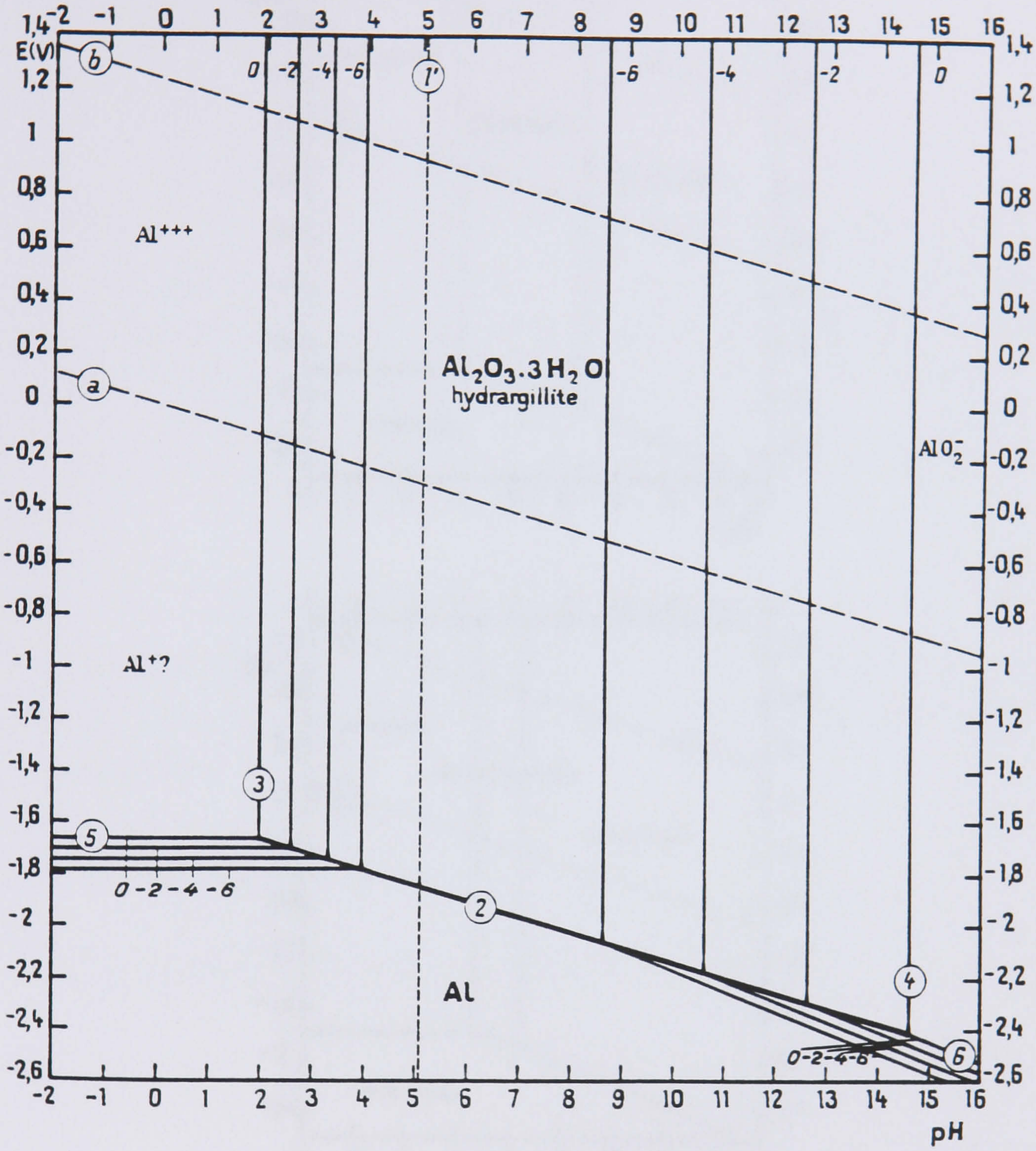

Fig. 1.1 Potential-pH diagram equilibrium diagram for the system aluminium-water, at 25°C

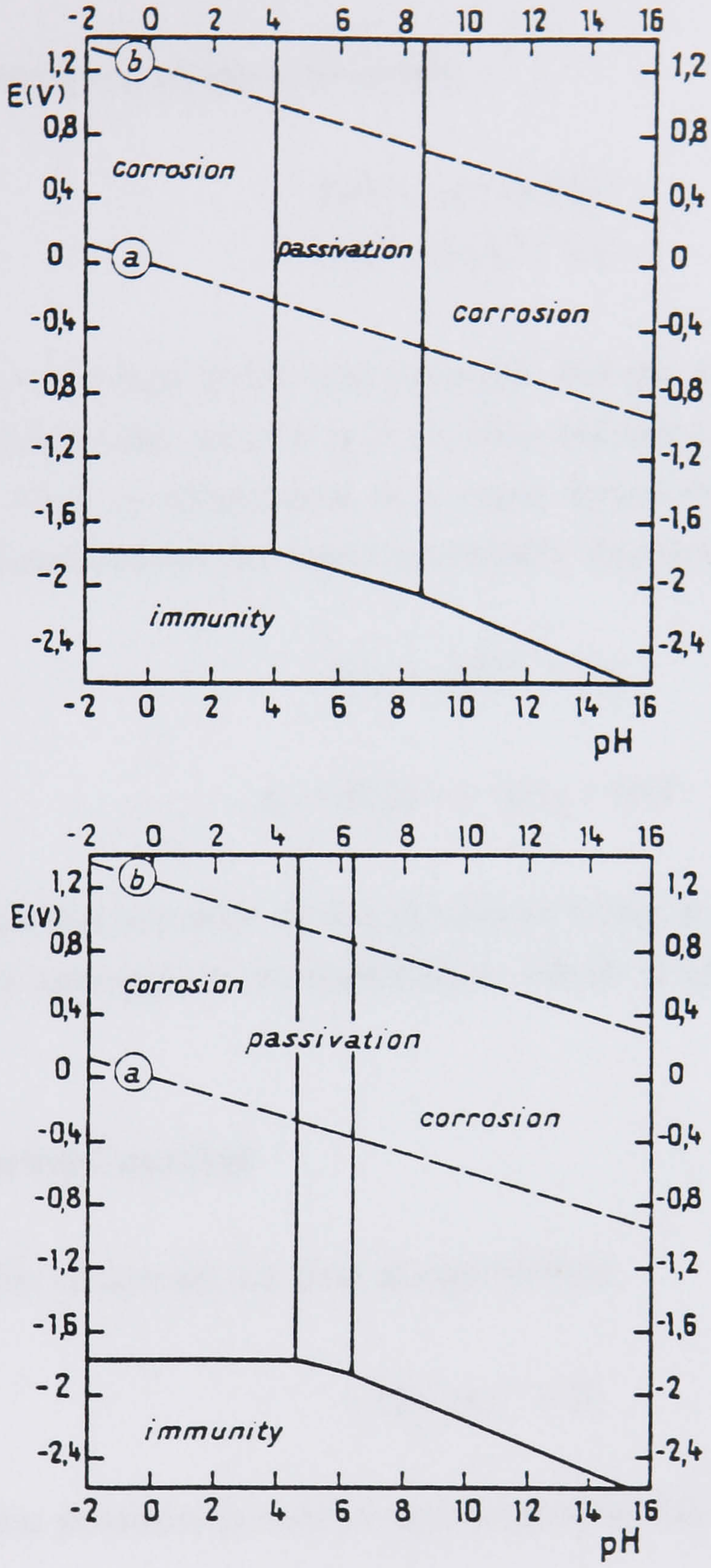

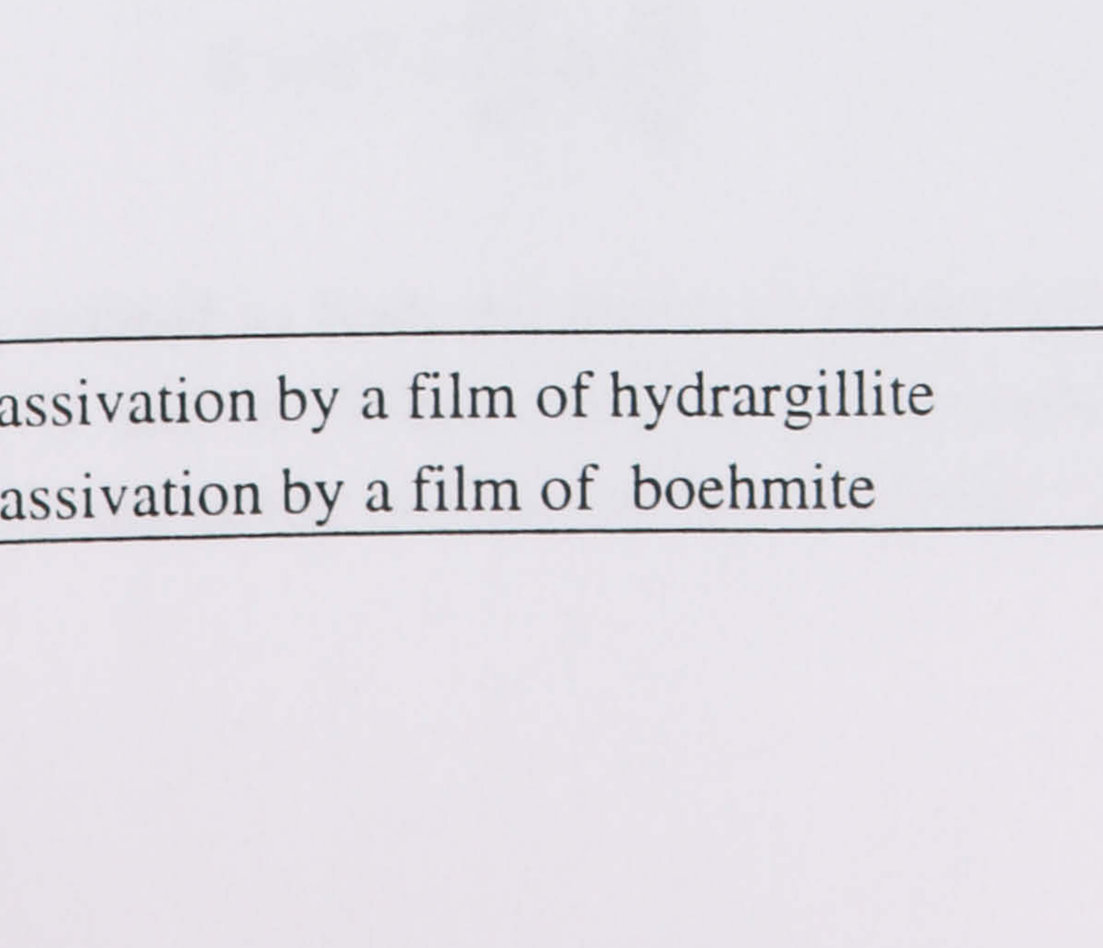

Fig. 1.2(a) Passivation by a film of hydrargillite
Fig. 1.2(b) Passivation by a film of boehmite

1.3.5 Equilibrium Potential

For the purpose of the work carried out in this thesis it is important to distinguish between an *equilibrium* situation and a *steady state* situation.

For the reactions at a platinum electrode;

$$Fe^{3+} + e^- \rightarrow Fe^{2+}$$
$$Fe^{2+} \rightarrow Fe^{3+} + e^-$$

a steady state is reached at the rest potential, but the system is also considered to be in equilibrium as the process is reversible and there is no net flow of electrons. For a system such as aluminium in a water based electrolyte, where there is a slow but continual loss of the metal essentially due to the reactions;

$$Al \rightarrow Al^{3+} + 3e^-$$

$$e^- + H_2O \rightarrow \tfrac{1}{2}H_2 + OH^-$$

at the rest potential we refer to the system as being at steady state with zero flow of current, as opposed to an equilibrium which is also established with no net current flow.

1.3.6 The Nernst Equation

For a reversible electrode reaction at equilibrium,

$$O + ne^- = R$$

the equilibrium potential E may be represented by the Nernst equation:

$$E = E^0 + \frac{RT}{nF} \ln \frac{a_O^\sigma}{a_R^\sigma} \qquad (1.1)$$

E is directly related to both the standard electrode potential E^0 and the surface activities of O and R. When there is zero-current flow, no overall chemical change can be occurring and the surface activities will be equal to those in the

bulk of the solution. For the purpose of this work, concentrations are used rather than the activities.

1.4 General Principles in Relation to Aluminium Corrosion

1.4.1 Limitations Imposed by Thermodynamics

Aluminium is covered with a film of aluminium hydroxide or aluminium oxide when it is in contact with aqueous solution. The film on the metal surface may be formed by reaction of the metal with air (before immersion in the aqueous solution) or with water. It is convenient to consider the film as being one of the forms of $Al(OH)_3$. However the situation is essentially the same if we consider the surface film to be Al_2O_3.

$$2Al + 3H_2O \rightarrow Al_2O_3 + 3H_2\uparrow \qquad \Delta E = -864 \text{ kJ/mol}$$

$$H_2O + Al_2O_3 \leftrightarrow 2Al(OH)_3$$

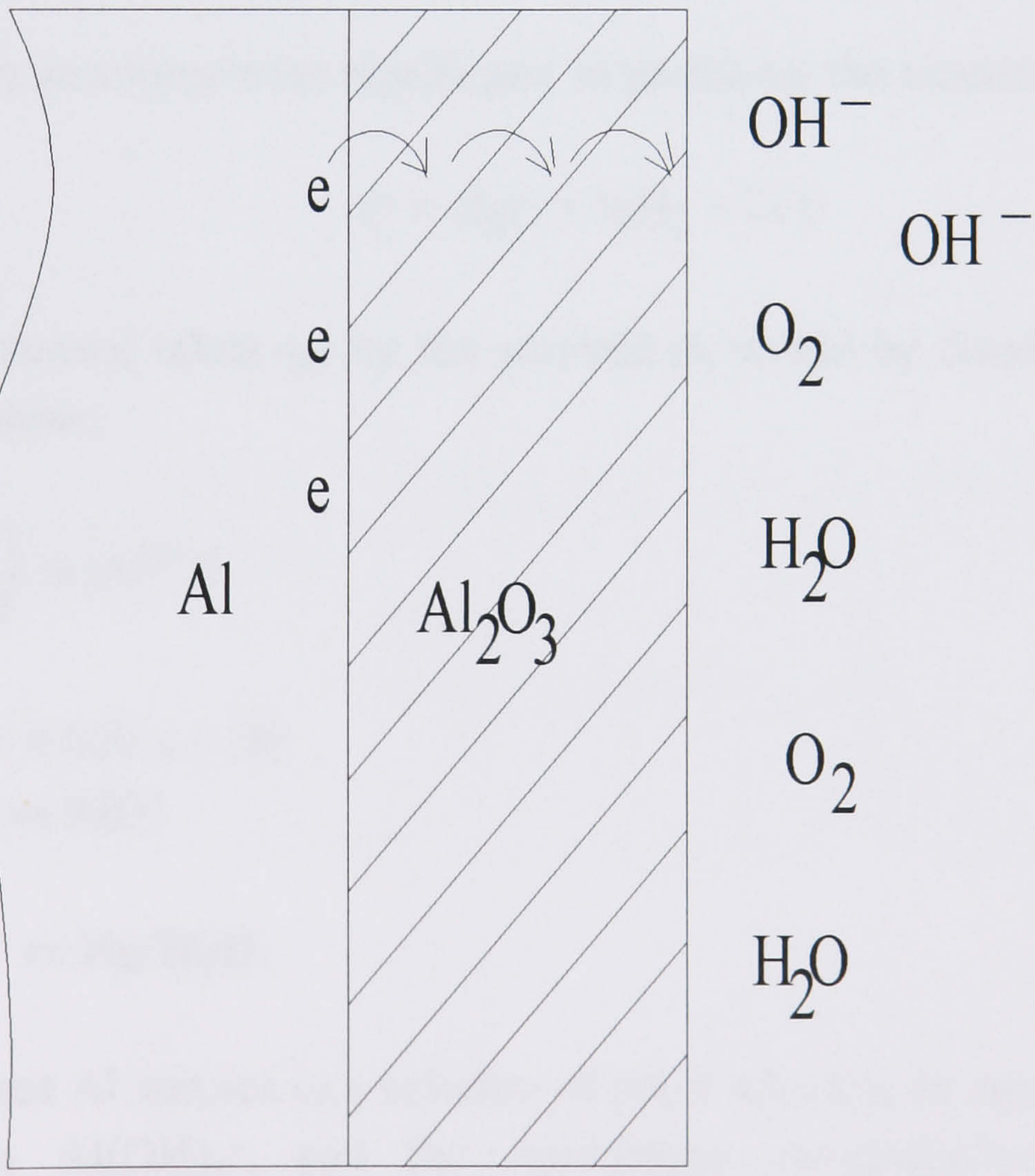

Fig. 1.3 Schematic - electron loss during Al corrosion in an aqueous solution

The standard electrode potential E^o for Al/Al^{3+} is -1.66V versus the standard hydrogen electrode (SHE), or -1.76V versus Hg/HgO.

The solubility product of $Al(OH)_3$ is approximately 1×10^{-33} mol^4 dm^{-12}. There are various forms of $Al(OH)_3$. The exact figures for the solubility product will depend on which form is being considered.

Therefore at pH 9, (where $[OH^-] = 10^{-5}$, and $K_{sp} = [Al^{3+}][OH^-]^3$), the Al^{3+} concentration in equilibrium with $Al(OH)_3$ is 10^{-18} M.

If, for the $Al/Al(OH)_3/H_20$ (pH 9, deoxygenated) system, the following equilibria are set up;

1. Al^{3+} in equilibrium between Al metal and $Al(OH)_3$,

2. Al^{3+} in equilibrium between $Al(OH)_3$ and the aqueous solution,

3. OH^- in equilibrium between $Al(OH)_3$ and the aqueous solution,

and no other reactions were significant, in particular the reaction;

$$e^- + H_2O = \tfrac{1}{2}H_2 + OH^-$$

then the potential taken up by the aluminium would be fixed and given by the Nernst equation;

$$E = E^0 + \frac{RT}{3F} \ln [Al^{3+}]$$

$$= -1.66 + 0.020 \text{ x } (-18)$$

$$= \mathbf{-2.02V \text{ vs SHE}}$$

$$= \mathbf{-2.12V \text{ vs Hg/HgO.}}$$

The dominant Al species in a solution of pH 9 which is in equilibrium with solid $Al(OH)_3$ is $Al(OH)_4^-$, and the equilibrium concentration of $Al(OH)_4^-$ is $3x10^{-6}$ M.

Thus if the system $Al/Al(OH)_3/H_20$ (pH 9, deoxygenated) were in equilibrium as described above, we would have $Al(OH)_4^-$ present at 3 x 10^{-6} M in the aqueous phase, and the Al will have a well defined potential of -2.12 V versus Hg/HgO. It may be expected that this situation would be found in cases where a thick film of $Al(OH)_3$ (or Al_2O_3) has been formed on the metal, either by reaction with oxygen or by anodic oxidation. Corrosion is minimised if the film prevents electron tunnelling.

From the solubility diagram in Fig. 3.6 it can be seen that aluminium oxide/hydroxide is soluble, dissolving as aluminate in aqueous solutions of neutral and alkaline pH. If the aqueous solution is constantly renewed the $Al(OH)_3$ will slowly dissolve and eventually disappear from the surface of the aluminium. If a fixed potential more positive to -2.12V were applied to the aluminium metal by use of a potentiostat, a current would pass and the $Al(OH)_3$ layer would thicken i.e. the reaction;

$$Al + 3OH^- = Al(OH)_3 + 3e^- \qquad (1.2)$$

would occur. The current would decrease with time but never reach zero with the $Al(OH)_3$ layer getting ever thicker. There is no steady state or equilibrium condition if the aqueous solution is constantly renewed so that the $Al(OH)_4^-$ concentration never reaches its equilibrium level. A steady state situation is possible where the rate of formation of $Al(OH)_3$ is the same as the rate of its dissolution.

A potential negative to -2.12V applied by a potentiostat would cause the film to be removed by the reaction;

$$Al(OH)_3 + 3e^- = Al + 3OH^-$$

The situation described above will not generally be found because of the reactions;

$$e^- + H_2O = \tfrac{1}{2} H_2 + OH^- \quad \text{and,} \quad O_2 + 4e^- + 4H^+ = 2H_2O$$

Even if these reactions occur, $Al(OH)_3$ still cannot be reduced electrochemically to aluminium unless the potential is negative to -2.12V (at a pH of 9). At all potentials positive to -2.12V (including open circuit conditions) the $Al(OH)_3$ film

will thicken (equation 1.2) above will occur. Thickening can only stop if the rate of dissolution of $Al(OH)_3$ in the electrolyte as $Al(OH)_4^-$, matches the rate of film formation.

The highest possible rate of dissolution of the film is given by the maximum rate of diffusion of aluminate from the surface, into the solution;

$$i = 3FD\frac{c}{\delta} \qquad (1.3)$$

where,

D = Diffusion coefficient (typically 10^{-5} cm^2 s^{-1})
F = Faraday constant (9.6485 x 10^4 C mol^{-1}),
c = concentration of aluminate at the electrode (mol cm^{-3})
δ = diffusion layer thickness (cm).

If the diffusion coefficient D, is taken as $10^{-5}cm^2$ s^{-1}, then the limiting current can be estimated from equation 1.3. For a pH of 9 and $\delta = 10^{-3}$ cm (vigorous gas bubbling);

$i = 3 \times 10^5 \times 10^{-5} \times 3 \times 10^{-9}/10^{-3}$
$= 9 \times 10^{-6}$ A cm^{-2}

Therefore, whenever the anodic current is greater than this value (either impressed by a potentiostat or on open circuit), the film must be thickening.

From these general considerations there is one further point. If aluminium corrosion is occurring because of the reactions (deoxygenated solution);

$$Al + 3OH^- = Al(OH)_3 + 3e^- \quad \text{and} \quad e^- + H_2O = \tfrac{1}{2}H_2 + OH^-$$

the potential of the electrode on open circuit must lie between the reversible potential for $Al/Al(OH)_3/H_20$ and that for H^+/H_2 i.e. between -2.12V and -0.64V. The nearer the potential is to -2.12V the more difficult it is for electrons to cross from the metal to the water molecules. The nearer potential is to -0.64V, the easier it is for electrons to cross from the metal to the water molecules. When oxygen reduction is included the potential must lie between -2.12V and +0.59V.

On open circuit with a potential positive to -2.12V, the film must slowly thicken. This will in turn cause the cathodic reactions to be inhibited so that the OCP will drift with time to more negative values.

1.4.2 Kinetics of Corrosion

This section outlines the kinetics of the corrosion process which provides us with information about the rate of reaction. The rate may be expressed in terms of a current density I (A cm^{-2}).

Theory of Electron Transfer - Tafel Analysis

For the electron transfer reactions,

$$Fe^{3+} + e^- \rightarrow Fe^{2+} \qquad (1.4)$$
$$Fe^{2+} \rightarrow Fe^{3+} + e^- \qquad (1.5)$$

both reactions occur at equal rates when $\eta=0$. Consider a situation in which we have 1mM Fe^{2+} and 1mM Fe^{3+} ions together in 1M $HClO_4$ solution. Species will move towards the electrode due to thermal agitation with approximately only 1 in 10^6 of the collisions leading to a reaction. This is due to the nature of the configuration of the hydration shells surrounding the respective ions i.e. At equilibrium, the interatomic distance for Fe^{3+}— O is shorter than Fe^{2+}— O due to the different polarisabilities of the cations. Since, according to the Franck-Condon principle, electron transfer is fast relative to changes in interatomic bond distances, the Fe — O bond distance is effectively frozen whilst electron transfer takes place. The configuration then that allows a reaction to take place at $\eta = 0$, must be such that the Fe — O distance is a non equilibrium value, Fig. 1.4.

At negative overpotentials, the number of reactions producing Fe^{2+} species will exceed the number of reactions producing Fe^{3+} species and there will result a net flow of current (cathodic current).

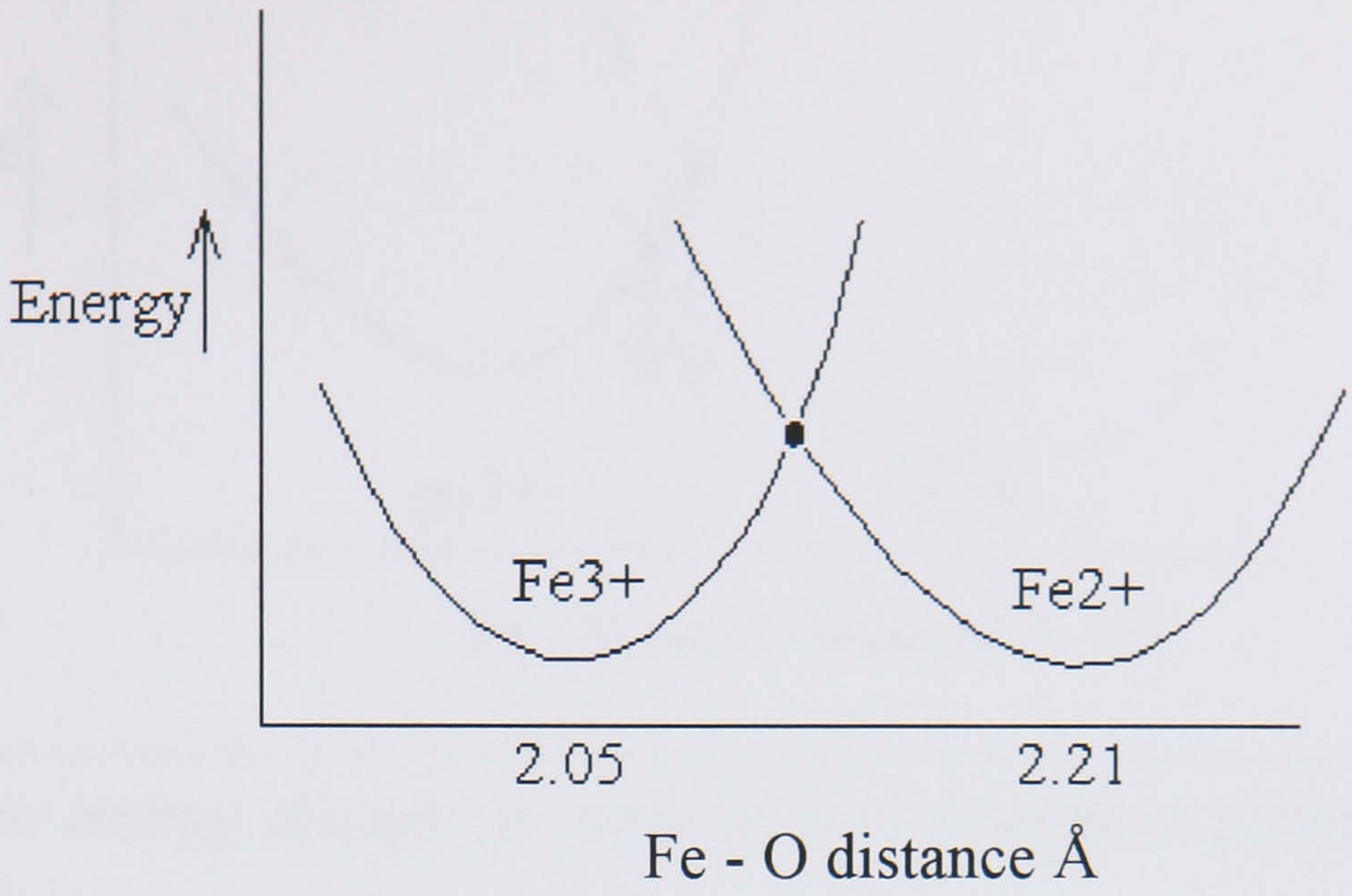

Fig. 1.4 Free energy curves of an Fe^{2+}/Fe^{3+} redox couple at equilibrium

For the reduction (equation 1.4) at $\eta = 0$,

$$i_o = nFZ \exp(-\Delta G^{\ddagger}/RT)$$

where,

n = number of electrons being transferred (3 for aluminium)

F = Faraday constant (9.6485×10^4 \C mol^{-1})

Z = collision frequency factor (the probability that any one collision will lead to electron transfer =$1x\ 10^6$ at $\eta = 0$)

$\Delta G^{\ddagger}$ = Free energy of activation

R = Gas Constant (8.314 J K^{-1} mol^{-1})

T = Temperature (K)

If the α is the factor by which the free energy changes (usually 0.5) then the change in the free energy of activation is,

$$= -\alpha nF\eta$$

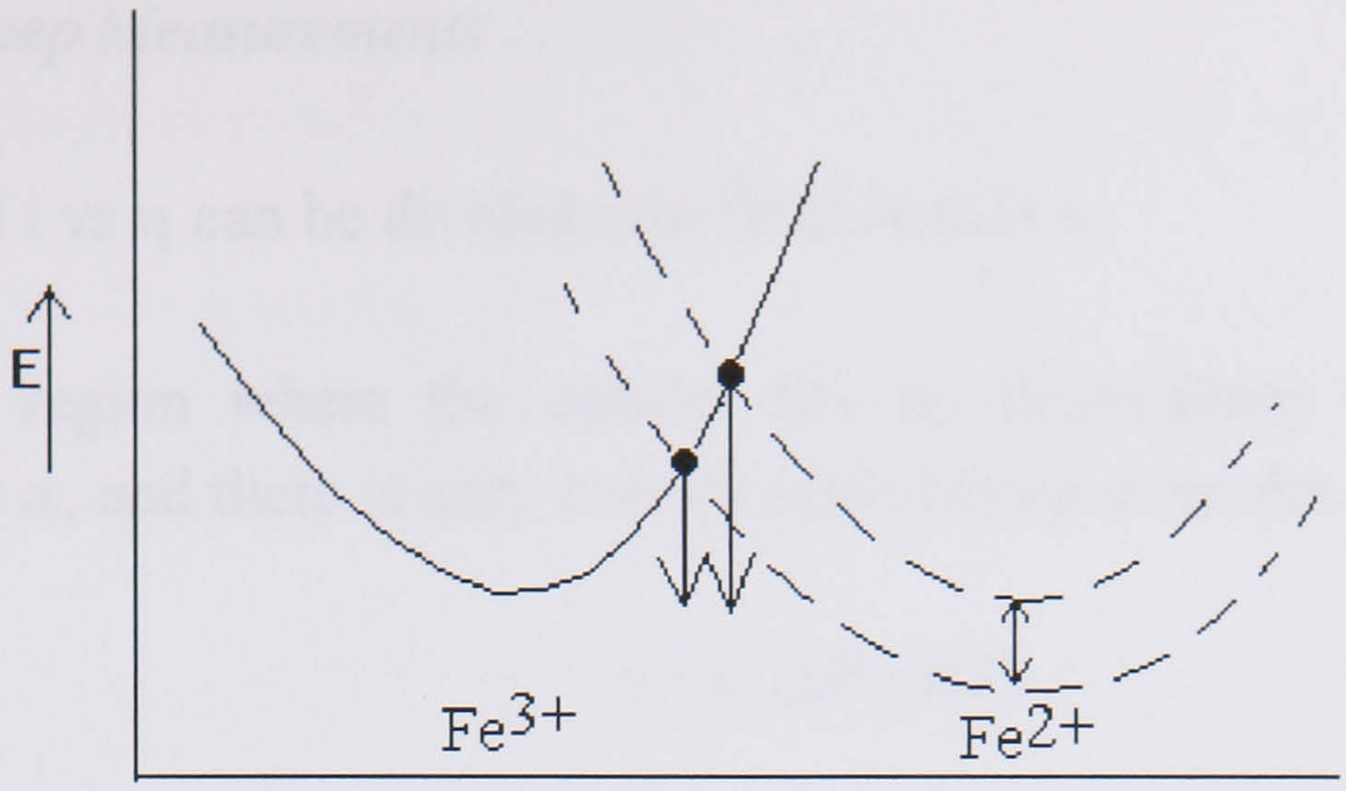

Fig. 1.5 Free energy change on application of a negative potential to a Fe^{2+}/Fe^{3+} redox couple.

$$i = nFZ \exp (\{-\Delta G^{\ddagger} + \alpha nF\eta\}/RT)$$

$$i/i_o = \exp (\alpha nF\eta/RT)$$

$$\ln (i/i_o) = \alpha nF\eta/RT$$

rearranging gives;

$$\eta = RT/\alpha nF \,.\, \ln i \;\; - \;\; RT/\alpha nF \,.\, \ln i_o$$

The Tafel equation is represented in the form;

$$\eta = \; - \; RT/\alpha nF \,.\, \ln i_o + \; 2.303 \; RT/\alpha nF \,.\, \log i \qquad (1.6)$$

or,

$$\eta = a + b \log i \qquad (1.7)$$

with the Tafel slope, $b = 2.303\ RT/\alpha nF$, and $a = -\ RT/\alpha nF \,.\, \ln i_o$

Linear Sweep Measurements

A graph of i vs η can be divided into three sections;

1) Linear region where the current has no dependency on the transmission coefficient α, and there is only a small perturbation from the rest potential where,

$$i = i_o (nF\eta/RT)$$

2) Exponential region or Tafel region where $\eta \neq 0$ and the current is anodically and cathodically dependant on α and 1- α respectively,

$$i = i_o \exp (\alpha nF\eta/RT) \qquad \text{(anodic)}$$

$$i = -i_o \exp (-[1-\alpha]nF\eta/RT) \qquad \text{(cathodic)}$$

3) Diffusion limited region where the current is limited by mass transfer effects.

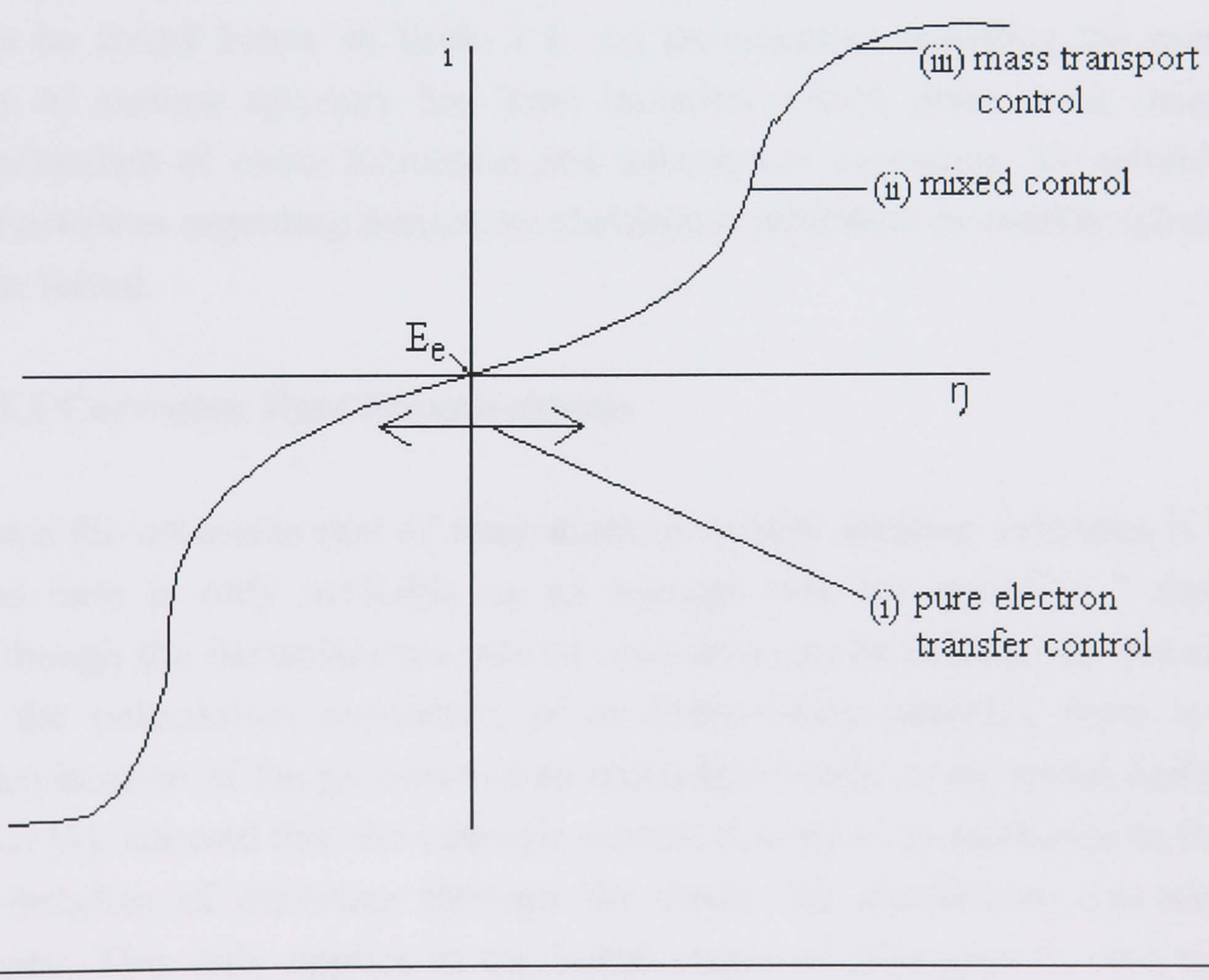

Fig. 1.6 I-E characteristics for an irreversible electron transfer reaction.

At small deviations from equilibrium, such that $\exp(x) \rightarrow x+1$, bearing in mind the overall current is the algebraic sum of the anodic and cathodic currents;

$$i = i_o \exp(\alpha n F \eta / RT) - i_o \exp(-[1-\alpha] n F \eta / RT)$$
$$i = i_o [(\alpha n F \eta / RT) + 1] - i_o [(1-[1-\alpha] n F \eta / RT)]$$
$$= i_o (n F \eta / RT)$$

At higher η, the approximation $\exp(x) \rightarrow x+1$ is no longer applicable and hence there is a dependence on α.

1.5 Previous Work on Aluminium

Information has been carefully selected from the literature relevant to the experimental work that has been carried out.

1.5.1 Introduction

A great deal of work has been carried out on aluminium in alkaline solutions in the pH range 7-11. A table summarising previous electrochemical measurements can be found below in Table 1.1. An introduction regarding the morphology of the Al surface structure has been included, which gives some insight into the mechanism of oxide formation and subsequent corrosion. No reliable source of information regarding amines as aluminium inhibitors in weakly alkaline solution was found.

1.5.2 Corrosion Rate Measurements

Since the corrosion rate of aluminium in weakly alkaline solutions is low, weight loss data is only available as an average rate for typically 7 days or more. Although the instantaneous rate of corrosion can be inferred by the measurement of the polarisation resistance, or by Stern-Geary analysis, there is always the complication of the presence of an oxide/hydroxide on the metal surface. Shimizu *et al* [9], showed that the cathodic current density is proportional to the tunnelling probability of electrons through the oxide for aluminium specimens of high purity. This only applies in the initial stages of film growth, and until the film approaches the limiting tunnelling thickness. In this section, corrosion rate measurements of aluminium in contact with aqueous solutions have been

summarised between pH values of 7-11. Corrosion rate measurements where inhibitors and chloride ions have been added can be found in the next section.

The most reliable recent measurements of corrosion rate based on weight change have been obtained by Tabrizi *et al* [10], who found that in solutions between pH 8-12 equilibrated with air there was a 10% increase in corrosion rate in going from pH 8→9 and an increase of a further 10% in going from pH 9→10. Between pH 10 and 11 they recorded a two fold increase in the corrosion rate. At pH 9 the corrosion rate was about 100g m^{-2} y^{-1} (equivalent to a corrosion current of 3.4μA cm^{-2} at 30°C). Earlier corrosion rate measurements using weight change are summarised by Tabrizi *et al* [10]. They show corrosion rate values between 22g m^{-2} y^{-1} and 45g m^{-2} y^{-1} at pH 9 (25°C), the lower values however were due to the lower temperature at which the measurements were taken.

Hurlen and Haug [11] used electrochemical measurements to estimate the corrosion rate in solutions of ammonium acetate + ammonia. They found that for reproducible behaviour to be approached at a chosen potential, a stabilisation period of about 20 hrs was necessary. This included the time needed to sweep at a rate of 1mV s^{-1}, and an initial conditioning period of 1-2 hrs at the OCP. For a deoxygenated solution at pH 8.9, the i_c value calculated from polarisation data was approximately 7μA cm^{-2} (25°C), and E_c = -1308 mV vs SHE. On going from a pH value of 8.9 to 9.9, the corrosion current increased by a factor of 5. Stirring was shown to have little effect below pH 9 but raised the passive current slightly at higher pH values. The potential independent stationary passive current was shown to depend strongly on pH, and went through a minimum at a pH of about 8. Here oxygen acted as a passivator by raising the corrosion potential, and lowering the corrosion rate slightly, especially at pH values above 9.

Schueller, Taylor and Hajcsar [12], found that the OCP in deaerated borate buffer was unpredictable from one test to the next, and unstable during a given test. A relatively stable value of -458 mV vs SHE was attained after exposure for 2.2 hrs, but extended studies showed that the potential was unstable dropping to -1100 mV after 14 hrs, and never attained a truly stable value. Experiments conducted in aerated borate buffer indicated some improvements in the reproducibility of these measurements.

Table 1 below summarises the data taken from reliable electrochemical sources as discussed above.

Table 1.1 Previous corrosion rate measurements of aluminium in weakly alkaline solutions.

Ref	Solution	pH	Exposure time	Temp °C	Weight loss $g/cm^2/s$	Corrosion current equivalent A/cm^2	OCP (vs SHE) mV
12	0.1M sodium borate / boric acid buffer.	7.0	2.2 hrs 14 hrs	-	- -	0.1×10^{-6} -	-458 -858
11	1M NH_4Ac +xM NH_3	8.9	20 hrs	25	-	7.0×10^{-6}	-1308
13	ethylene glycol/ water	-	-	-	-	0.6×10^{-6}	-338
10	NaOH	9	short term	25	6.98×10^{-11}	7.48×10^{-7}	-
10	NaOH	9	1 hr	25	1.43×10^{-10}	1.53×10^{-6}	-
10	NaOH	10	short term	25	8.88×10^{-10}	9.53×10^{-6}	-
10	NaOH	10	1 hr	25	1.13×10^{-9}	1.21×10^{-5}	-
10	NaOH	11	after 40 days exposure	30	3.49×10^{-10}	3.74×10^{-6}	-
10	NaOH	11	after 40 days exposure	30	8.56×10^{-10}	9.18×10^{-6}	-

1.6 Nature of the Surface Structure

The dominant Al species in a solution of pH 9 which is in equilibrium with solid $Al(OH)_3$ is $Al(OH)_4^-$, at a concentration of 3×10^{-6} M. The exact conditions of hydrolysis (such as the composition of the solutions that are combined, the rate at which they are combined, the amount of agitation, and the temperature) will determine the nature and quantity of the species formed.

Two crystalline forms of the hydroxide are known, α-$Al(OH)_3$ (gibbsite) and γ-$Al(OH)_3$ (bayerite), gibbsite being the stable form at room temperature. Both can be formed by precipitation from alkaline aluminate solutions. At higher temperatures two dehydrated forms appear namely α-Al(OH) (diaspore) and γ-AlO(OH) (boehmite) [14].

In α-Al_2O_3 the oxide ions form a close packed array and the aluminium ions are distributed symmetrically along the octahedral interstices. The γ-Al_2O_3 structure is regarded as being a defect spinel structure with a deficit of cations. The Al_2O_3 that is formed on the surface of the metal has another structure, namely a defect rock salt structure. This is an arrangement of Al and O ions in the rock salt ordering with every third Al ion missing. There are several important hydrated forms of alumina corresponding to the stoichiometries AlO.OH and $Al(OH)_3$.

The hydroxides are amphoteric;

$$3H^+ + Al(OH)_3\ (s) = Al^{3+} + 3H_2O$$

$$OH^- + Al(OH)_3\ (s) = Al(OH)_4^-$$

For the aluminium system between pH 8 and 12, the main species appears to be a polymer with octahedral Al and OH bridges but at higher pH values above 13, a tetrahedral ion exists.

Takahashi [15] prepared composite oxide films by immersing pure aluminium specimens in boiling water and then anodising galvanostatically in a neutral borate solution at different temperatures. These were then analysed using electron microscopy. He reported to have found the presence of two layers; a crystalline oxide layer (outer layer), and an amorphous oxide layer (inner layer). A high

concentration of voids were observed in the crystalline oxide layer close to the amorphous layer.

Similarly, Hurlen and Haug [11] showed using capacitance data, that the oxide film formed on aluminium in weakly alkaline solution is duplex, having an inner barrier part and an outer non-barrier part. The non-barrier part is almost absent in weakly acidic solution, but increases in thickness with increasing pH in alkaline solution. The metal/oxide interface became rather rough, and it is thought that small fragments of metal may have become embedded in the oxide film during its formation.

Transmission electron microscopy and electron diffraction analysis performed by Kobayashi and Shimizu [16] have shown that the films consists of amorphous, γ'' - alumina and γ - alumina. The presence of a thin layer of thermal oxide on the surface of the aluminium promoted the growth of γ'' - alumina during subsequent oxidation. The thermal oxide may or may not have contained γ - alumina crystals, a factor which depended on the growth conditions.

Shimizu, Thompson and Wood [9], exposed aluminium sections to an ammonium pentaborate solution for 10 minutes. They showed that the inner layer was approximately 215 nm thick and composed of almost pure crystalline Al_2O_3 next to the metal. The non crystalline outer layer about 144nm thick, was doped with borate species being adjacent to the electrolyte.

Exposure to aqueous borate solutions was shown by Schueller, Taylor and Hajcscar [12] to result in aluminium oxide thickening, and borate ion incorporation into the oxide when potentials of 50mV or more are applied. Exposure near to the OCP resulted in no borate ion incorporation. Additionally, they found that the layer could easily be removed by rinsing the sample with water after immersion, indicating that near to the OCP borate ions protect the surface by adsorption. XPS analysis of 99.999% purity aluminium samples after various times of exposure to an aerated electrolyte, revealed that the average oxide thickness was approximately 300nm.

1.7 Electrochemical Impedance Spectroscopy (EIS)

To determine the thickness of insulating layers formed on the aluminium surface in various environments, a spectroscopic impedance technique was employed.

This enabled measurements of thickness of the oxide layer on the aluminium surface in contact with a range of alkaline solutions to be made. The extent of corrosion in each electrolyte could then be studied.

The theory of impedance is only briefly discussed in this section. There are, however, many standard works available for reference on this subject [17-19].

1.7.1 Theory

The electrode interface can be considered as being made up of a number of components that comprise of a number of resistors and capacitors. The impedance of such an interface can be analysed with reference to an equivalent circuit which is intended to represent the reaction taking place at the interface.

The current flowing across a metal/solution interface can be divided into two parts,

(i) Faradaic part - charge transfer process when the current is part of the electrochemical reaction. A charge transfer resistance or Polarisation resistance is set up - Rct

(ii) Non Faradaic part which establishes a charged interface consisting of a double layer, since there is no transfer of charged particles across it. This is equivalent of the Capacitance C in the electronic circuit.

In principle, 3 basic pieces of information may be obtained from the system.

1. $\mathbf{C_{dl}}$, the Metal Interfacial (Double Layer) Capacitance. This is the capacitance formed by electrolyte contact with the substrate metal.

2. $\mathbf{R_{ct}}$, the Charge Transfer Resistance. This corresponds to the charge transfer resistance of the Faradaic process occurring at the metal surface. If R_{ct} is measured at the corrosion potential of the metal then it may also be considered as the Polarisation Resistance of the metal, R_p.

3. $\mathbf{R_{sol}}$, the solution resistance between the working and reference electrodes.

By definition,

$$C = \frac{Q}{V}$$

C = Capacitance /F
Q = Charge /C
V = Potential /V

The capacitance depends upon the size and separation of the plates, and on the permittivity of the material (dielectric) between the plates.

For a parallel plate capacitor,

$$C = \frac{\in A}{d} \qquad (1.8)$$

A = Area of each plate
d = distance between the plates
$\in$ = the permittivity of the dielectric

where, $\in = \in_0 \in_r$

$\in_0$= the permittivity of free space
$\in_r$= the relative permittivity (dielectric constant)

The relative permittivity of free space is unity by definition.

From Gauss's theorem the field strength between the plates of a parallel plate capacitor is given by,

$$E = \sigma/\in$$

where, σ is the charge density and E is the field strength (strictly for an infinitely conducting plate)

$$C = \frac{A\sigma}{V}$$

therefore,

$$C = \frac{\in EA}{V}$$

but, $E = V/d$ this assumes the field is uniform

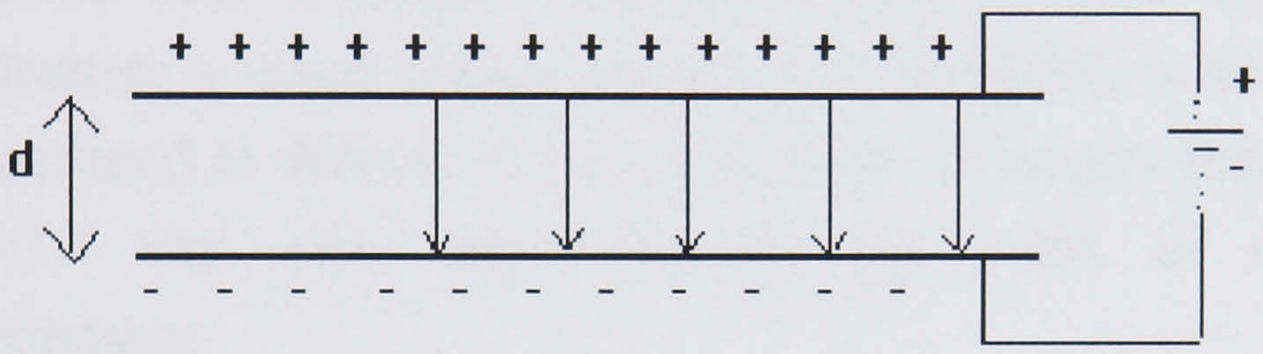

Fig. 1.7 Uniform field between the plates of a parallel plate capacitor

Except at the edges the field between the plates is uniform and therefore the potential gradient at all parts between A and B are the same,

$$\mathbf{C} = \frac{\in VA}{dV} = \frac{\in_0 \in_r \mathbf{A}}{\mathbf{d}} \qquad (1.9)$$

This is the fundamental equation from which the thickness of the surface oxide layer formed on the aluminium was estimated.

1.8 Aluminium Alloys

Some of the work carried out in this thesis has involved the corrosion and staining of aluminium alloys. It is therefore of interest to study some of the background on aluminium alloys.

1.8.1 Introduction

Pure aluminium is soft and mechanically weak, which limits its applications in industry. By alloying with certain other metals, the strength of aluminium can be greatly increased. However, the addition of some alloying elements can severely reduce the corrosion resistance of the alloy compared to that of pure aluminium.

1.8.2 Previous Work on Aluminium Alloys

Exposure of aluminium to the atmosphere results in corrosion, to give an unsightly rough oxide layer which protects the underlying metal. In the case of aluminium therefore the action of rain washing over the metal is actually beneficial. In an industrial environment, the corrosion rate of aluminium, averaged over a six year period, is between 2 and 5 μm per year [3]. Although the corrosion rate averaged over the whole surface is so low, the rate of local penetration is much higher because the corrosion is confined to a number of small pits initiated at defects in the oxide film. Typically these pits may reach a depth of 0.25-0.5 mm after approximately six years of exposure to an industrial environment.

The statue of Eros in Piccadilly Circus has stood for over 50 yrs and is still in excellent condition although cast in a low purity (98%) aluminium. Tests lasting over 20 years at marine and industrial sites in the US, have shown that the majority of attack takes place in the first year, and that a low rate of attack is maintained thereafter [2].

In an experiment carried out by Bombara and Bernabai [21], weight losses after 24 hrs were measured as a function of inhibitor concentration in demineralised water. The results showed that an inhibitor concentration of 0.6% appeared to accelerate the corrosion of an aluminium alloy by two orders of magnitude by the untreated water. The variation of the pH shown in the same diagram helped to clarify the mechanism. At low concentrations, the commercial inhibitor worked only as an alkaline buffering agent, and did not promote the growth of a protective film on the aluminium surface. This resulted in defective oxide formation.

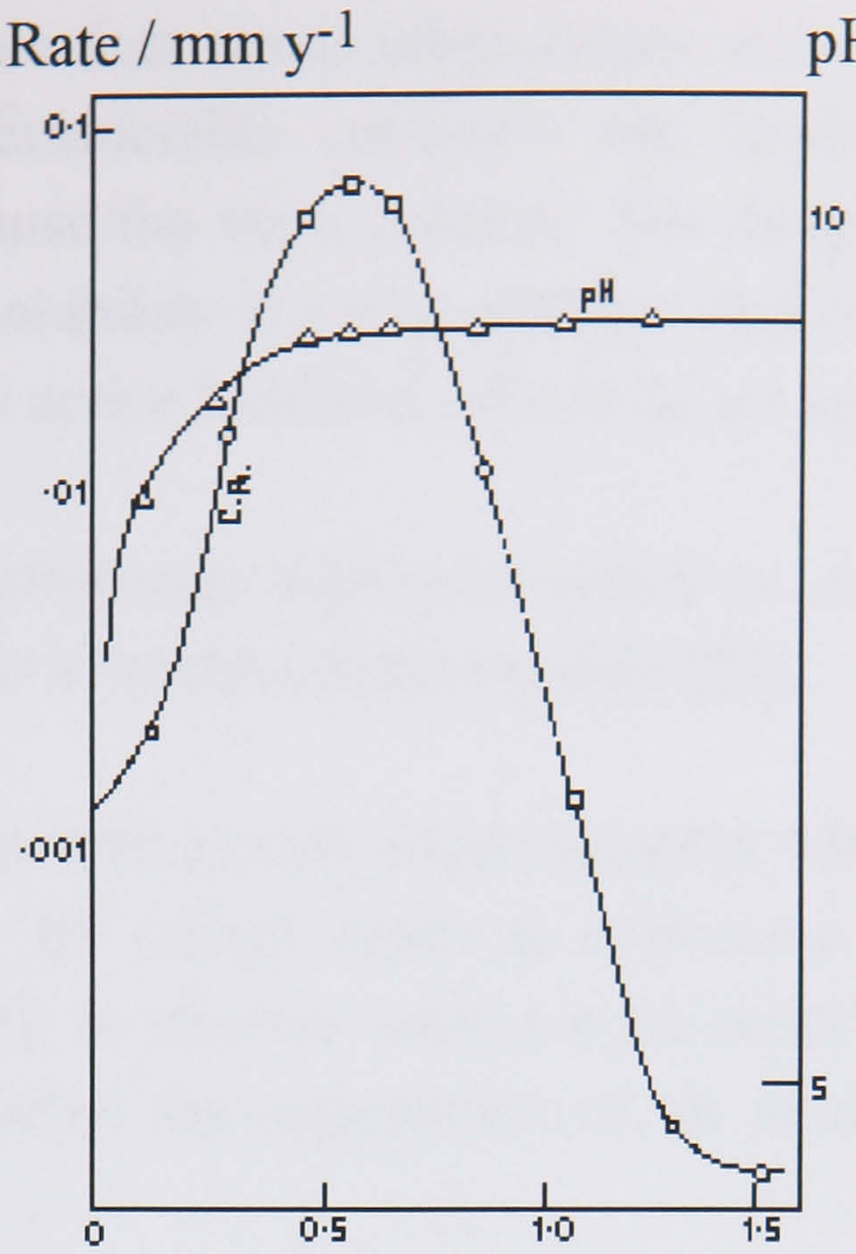

Fig. 1.8 Inhibitor concentration vs. pH and corrosion rate profiles for aluminium alloys in contact with demineralised water [21].

They concluded that alkaline-buffered inhibitive mixtures for alloys must be regarded as extremely dangerous inhibitors for aluminium, since they act as strong corrodents or highly efficient inhibitors for this metal, depending on their concentration.

Pengfei *et al* [22], explain that the uniform distribution of alloying elements is an essential factor for lowering the corrosion rate of an alloy. They have described the development of aluminium alloys by the process of combining electrochemical measurements with micro morphological analysis as determined by scanning electron microscopy (SEM). They concluded that whilst the addition of some alloying elements to aluminium improved the anodic dissolution behaviour, excessive amounts of the additives are not recommended. This would result in the formation of a secondary phase which provides cathodic sites for hydrogen evolution and therefore promotes the corrosion of aluminium. Lowering or avoiding the accumulation of alloying elements will significantly reduce the corrosion rate of aluminium.

Aluminium is less noble than many other metals and when joined to them in a suitable electrolyte, considerable corrosion can result. In practice, copper or copper based alloys cause the most concern. The danger from copper is greatly increased as its slight solubility in many solutions and subsequent redeposition on aluminium causes very active localised cells to be set up.

It is known that aluminium may accelerate attack on zinc alloys, but in alkaline solutions the aluminium is preferentially attacked [23].

Experiments carried out with anions which complex with copper ions resulted in an increased solubility for copper oxide or hydroxide which helped to form a copper free surface [24]. In alkaline solutions the oxide film was found to be no longer stable, but assumed the appearance of an incoherent and non-adherent layer of white alumina.

1.9 Scanning Electron Microscopy (SEM)

SEM images of the surface of some aluminium alloy surfaces were obtained after exposure to various electrolytes.

The fact that interactions occur between the electrons and the nucleus within the atom forms the fundamental basis upon which SEM is based. Sharing of electrons that are within close proximity of each other causes some of the outer electrons to be emitted from the atom. Within the microscope electrons are excited and focused into a beam and accelerated towards the specimen to the examined. To avoid scattering by gas molecules the system is evacuated [25].

When the electron collides with the sample surface, the energy of the incident beam may be dissipated as secondary emissions. Some of the electrons are backscattered. Any radiation from the specimen provides a signal each as a result of a particular interaction between the specimen and incident electron.

As the secondary electrons are emitted they are detected by a phosphor scintillator which emits light which is detected and converted to pulses of electrons which are amplified. An image is built up during the scan which can be displayed on a computer monitor.

1.10 Energy Dispersive Analysis of X-Rays (EDAX)

In order to determine the nature of the stain material on the surface of each alloy, some metal samples were prepared for examination by EDAX.

The detector and emitter make up the EDAX machine which is controlled by computer. The detector is held in position in the line of the sample, so that as many X-rays as possible are emitted from the sample as are detected [26].

The emitter emits a steady stream of electrons which are accelerated and made to strike the sample. At this point an X-ray of characteristic wavelength is emitted from the sample exciting a number of electrons in the conduction band on the detector. As a voltage is applied across the detector a current flows as each X-ray is absorbed by the detector, the magnitude of which is directly related to the energy of the X-ray.

A histogram for the energies of all the X-rays arriving at the detector are displayed on a VDU. It is possible to identify where a line for a particular element should occur on the spectrum but due to poor energy resolution, the X-rays are not often detected as sharp lines.

EDAX allows rapid qualitative and quantitative analysis of the surface of a sample i.e. which elements are present, and the number of X-rays emitted per second. This technique stores the energies of X-rays from a wide range of elements, but will not detect elements lighter than sodium.

1.11 Cutting Fluids

The experimental work that was carried out has involved monitoring the corrosion of aluminium and aluminium alloys in the presence of specified experimental and propriety metal working fluid emulsions. It is necessary therefore to consider the composition and properties of such fluids.

This section is intended to promote a better understanding of the contribution made by cutting fluids in the usage of machine tools. Machine tools occupy a key position in industry and contribute to the production of most goods and services that are required by society today.

1.11.1 Background

In view of the unique machining requirements of aluminium and its alloys and the growth in the use of the metal in industry, it was proposed and agreed that a range of products should be formulated and promoted for aluminium and aluminium alloy machining. Castrol Alusol B (formulation A, Table 1.2) is the first member of this series, and is the premium Castrol grade for aluminium machining [27].

This research project is partly funded by Castrol International, Whitchurch Hill, Pangbourne, Berkshire RG8 7QR UK. Work has been carried out on the short term corrosive nature of aluminium and aluminium alloys in contact with some of the metalworking fluids (MWFs) that they supply for use in metalworking processes.

1.11.2 Classification

Most metal cutting operations require the use of a cutting fluid. They introduce a means of automatic swarf control, and allow for great improvement in tool life expectation. Also, a higher standard of metal surface refinement may be achieved.

There are three main types of metalworking oils;

- **Soluble oils** These can either be an emulsion or a synthetic solution. These are the best cooling oils especially for grinding operations because of their high water content.

• **Neat oils** Neat oils are best for lubrication purposes. They are used mainly in heavy duty cutting operations.

• **Heat treatment or quenching oils** These oils are used because of their cooling characteristics. They give a good finish to the metal surface and improve the metals 'hardness'.

The choice of metal cutting fluid depends very much upon the type of application for which they are in use. The effect of using a cutting fluid in machining operations depends not only upon the properties of the fluid, but also to a large extent on the machining conditions (such as the tool and work materials, tool geometry and the speed of machining). Work has been carried out on soluble oils used for machining aluminium alloys. For example, cutting aerospace alloys and drilling alloy engine blocks. According to their formulae, soluble oils give either opaque, semi-clear or fully clear mixtures with water. This characteristic is influenced by the particular mineral salts present in the water supply and the degree of 'mechanical working' to which the mixture is subjected during the cutting operation. There is a potential risk of corrosion of the machine parts primarily composed of steel, as well as corrosion of the aluminium work piece.

1.11.3 Composition

Metal working fluids are composed of oils and/or chemicals stabilised in water and have been developed over many years due to the technological advances in high speed metal cutting and grinding applications [28-30]. Generally, these fluids consist of fatty acid or petroleum oil soaps and additional additives such as anti-foam agents, coupling agents, biocides and corrosion inhibitors. Work was carried out on amines added to the water phase of the concentrate for use as intended aluminium corrosion inhibitors.

The fluids are marketed in the form of an oil concentrate which is diluted with water typically to between 3% and 10%, depending upon the type of fluid and application. A diluted oil concentrate is called an emulsion. Upon dilution, the emulsion can be stored in small or larger tanks (containing 10 litres - 1000 gallons).

Table 1.2 Composition of propriety oil concentrate 'A' as produced by Castrol International.

%	Component
A	
10.4	Water
2.4	Triethanolamine
4.3	Monoethanolamine
5.0	Boric Acid
3.0	Low temperature stability coupler
0.8	Copper corrosion inhibitor
48.7	Refined mineral oil and natural vegetable oil
17.0	Emulsifiers
3.0	Biocide
0.4	Fungicide
4.5	Alcoholic couplers
0.5	Antifoam agents

The distilled water acts a carrier for all the water phase components including triethanolamine and monoethanolamine. These are included as aluminium corrosion inhibitors but it appears that the exact corrosion inhibiting mechanism is not fully understood. It may be possible to exclude these amines altogether and hence increase the cost effectiveness and simplicity of the working fluid, that is, providing an alternative solution which is stable and also maintains the pH at around 9 can be found. The amines also provide some buffering capacity, forming a salt with the boric acid i.e. $R\text{-}NH_3^+H_2BO_3^-$, H_3BO_3. Boric acid also has some resistive bacterial properties required to create what is known as a 'biostable fluid'.

In the oil phase, mineral and vegetable oils act as the carrier for the oil phase components. Lubrication is one of the key requirements of the fluid for machining purposes. Long chained hydrocarbons and a distilled oil, act as emulsifying agents and are required to bring the oil and water phases together as an emulsion. Bacterial preventatives are added which work by releasing formaldehyde, consequently killing any bacteria or fungus present.

Emulsions require preparation in a specified manner to ensure a stable mixture (refer to experimental section 2.8.1). The correct ratio of oil to water should be selected. Ideally the water used for emulsification purposes should be soft, but

many oils will accept hard waters without any obvious separation. Even slight hardness tends to weaken the emulsion and reduce its cutting efficiency. Ions in the water may react with concentrate constituents and produce an unsightly deposit on the metal surface. This should not be confused with any of the products of corrosion.

1.11.4 Function Of Metal Cutting Fluids

The four main functions of the fluid are cooling, lubrication, physio-chemical effects (such as corrosion protection of the machined component) and mechanical swarf removal. Cutting fluids are used in industry to improve efficiency of machining operations in terms of the following criteria:

i) increased tool life
ii) improved surface finish
iii) reduced power consumption

A soluble oil is the main class of fluid used in metal cutting, they emulsify better, remain more stable in use and are far less likely to cause machine tool staining if they maintain an alkaline condition around pH 9. They are also effective, adaptable, and low in cost. Most applications make full use of the superior cooling properties of an emulsion and in addition, a lubricating effect is conveyed to the cutting action to ensure a reduction in the rate of tool wear. They also help to produce an acceptable surface finish for a wide range of material surfaces [31].

In general, wet machining offers these advantages:

1) Higher cutting speeds
2) Improved surface finish
3) Longer tool life
4) Reduced power consumption
5) Instantaneous 'starting' of the tools
6) Positive removal of finer swarf from tooling area
7) As frictional heat is quenched by the oil stream, tools give a better performance, and dimensional accuracy of components is more easily maintained

A requirement exists for the development of a cutting fluid which is compatable with aerospace alloys. Mono and diethanolamine can cause staining of aluminium and are aggressive towards some additives rendering them ineffective.

1.12 Deterioration of Metal Cutting Fluids and Microbiological Corrosion

One of the major causes of fluid deterioration is microbial contamination. Most concentrates are practically free of bacteria and/or fungi and can be stored for several months without undergoing any appreciable deterioration.

1.12.1 Microbial Growth

The elemental requirements for bacterial reproduction at the oil water interface are water, carbon, hydrogen, oxygen, nitrogen, sulphur, and phosphorus.

Removing the nitrogen containing components from the formulation will maximise the inhibition of bacterial growth, that is if the buffering capacity of the water phase in the concentrate is strong enough to maintain a stable pH over a period of time. This is the basis from which formulation B (a variation of the standard oil concentrate formulation) was prepared. It was proposed that it may be possible to eliminate the biocides and fungicides also from the formulation and reduce the overall fluid costs further. A1-D1 (Table 2.1) are concentrate formulations with and without inclusion of biocides and fungicides. 5% emulsions of A1 - D1 were tested for long term growth of bacteria and their effect on the short term corrosion rate of aluminium.

1.12.2 Problems Caused by Contamination

On dilution with water to the usage concentration, the emulsion/solution is susceptible to microbial attack and can quickly become contaminated. An emulsion/solution which is contaminated can contain in excess of 100 million organisms per ml of fluid. Even cleaning and recharging the system with fresh fluid can only have a temporary effect.

Microbial growth can lead to degradation of chemical structures within the fluid causing discolouration and the build up of foul smelling gases and eventually to a gradual decomposition of the emulsion. The emulsion eventually 'inverts' and becomes a water-in-oil mixture lacking stability and is rendered useless for machining purposes. Evaporation or other water loss may cause this condition, also when water softening chemicals such as soda ash (or any other form of concentrated alkaline species) are added to the water prior to emulsification.

Problems caused by contamination;

1/ Metabolic by-products of degradation - production of acids e.g. citric, sulphuric, acetic
2/ Degradation of amines - TEA → DEA → MEA → $NH_3\uparrow$ Production of ammonia gives an unacceptable emanation
3/ Loss of emulsification - increased droplet size → separation of phases

It should be noted also that *C.resinae* produces citric, isocitric, cis-aconitic and ketoglutaric acids derived from metabolic oxidation of kerosene [32]. Odourless kerosene is included in the original formulation as an anti-foam agent, but it is thought to be present at sufficiently low levels for the effect to be negligible.

1.13 Previous Work on Inhibitors and Cutting Fluids

Work on various anions and cations as inhibitors for aluminium corrosion has been fairly extensive [24, 33-40]. However, little electrochemical research has been carried out in non-chloride containing solutions in the pH range 8-10.

Vujicic and Lovrecek [41] used measurements of weight loss and polarisation resistance to estimate corrosion rates. They used solutions of 10^{-4}M KCl and 10^{-4}M KCl + 10^{-3}M ethylenediamine and found that there was no clear evidence for any inhibition of aluminium corrosion at pH values greater than 7. Their results imply a corrosion rate of 3μA cm^{-2}. Talati and Joshi [33] have examined the effects of inhibitors in contact with a number of aluminium alloys. However, they have not distinguished between pH changes caused by the addition of amines to the solutions and the amines themselves. It is therefore difficult to use the data for any quantitative assessment of the use of amines.

Improved products can only be developed efficiently from greater understanding of corrosion and inhibition mechanisms. The mechanism of amines as corrosion inhibitors has been reported by Mehta [42]. This report is not specific to any metal or solution. He suggests that hydrocarbon soluble amines form a hydrophobic film or 'repellent barrier' on the metal surface which prevents 'water and water soluble corroding agents' from reaching the surface.

1.14 Previous Work on Mechanical Wear

There several reasons why the mechanical cutting of a metal surface may cause the electrochemical properties of that surface to change. A number of these were discussed by Tomashov and Vershinina [43] who investigated the effect of

mechanically abrading the electrode. They found that in some situations e.g. hydrogen evolution on a Pb electrode, that there was little difference between the behaviour of abraded and non-abraded electrodes. In the case of Ti abrading the surface caused a considerable change in the i-E characteristics due to removal of the passive layer. Similarly, in the case of aluminium we would expect continuous removal of the oxide/hydroxide layer (which is always present when aluminium is in contact with an aqueous solution) to be very important. In the past, cathodic reduction of the metal has been used as a method of removing the surface layer, but it is not considered to be an acceptable method now for several reasons. There may be some variation in the surface composition of alloys during and after reduction, and the extent of reduction of the pre existing film is not known. Recognition of these difficulties has led to a variety of techniques designed to remove the pre oxidised surface mechanically.

A technique has recently been described by Burstein and Cinderey [44,45] which allows measurement of the transient electrochemical processes occurring on freshly cut metal surfaces *in situ*. Their technique provided a means of measuring the potential of a freshly generated 'bare' aluminium electrode surface and its subsequent evolution with time, both on open circuit and under galvanostatically applied current. The nature of their experiments allowed recovery of the electrode surface to be analysed in the first few milliseconds after cutting with a boron nitride edge. In the case of aluminium in contact with aqueous solutions in the pH range 7-10, they found that over a period of 1ms to 1s after cutting, the OCP was cathodic to its normal value and initially increased linearly with log(t).

References

[1] Corrosion Education Manual, prepared by the Working Party on Corrosion Education of the European Federation of Corrosion, 2nd Edition, Swedish Corrosion Institute, Stockholm, (1974)□.

[2] *Principles of Corrosion*, edited by L. L. Shreir, **1** pp.1:3-1:9, Newnes-Butterworths, London.

[3] D. Harrop, *Chemical Inhibitors for Corrosion Control*, edited by B. G. Clubley, pp. 1-20, Manchester.

[4] A. D. Mercer, 'Corrosion Inhibitor Testing : Principles and Practices', *Chemical Inhibitors for Corrosion Control*, edited by B. G. Clubley, ISO 8044 (1986) pp.46-56.

[5] J. A. Haslegrave W. M. Hedges, H. T. R. Montgomerie, and T. M. O'Brien, 'The Development of Corrosion Inhibitors with Low-Environmental Toxicity', Exxon Chemical Ltd., Soc. of Petroleum Engineers, SPE 24846, (1992).

[6] J. E. Donham, 'The design of corrosion inhibitors to meet specific requirements for oilfield applications', *Chemical Inhibitors for Corrosion Control*, edited by B. G. Clubley, (1986) pp.21-45

[7] *Corrosion*, Metals Handbook Ninth Edition, **13** pp.8-10.

[8] Marcel Pourbaix, 'Atlas of electrochemical equilibria in aqueous solutions', 2nd Edition, Cebelcor, Texas, (1974) pp.171-172 NACE.

[9] K. Shimizu, G. E. Thompson and G. C. Wood, 'The duplex nature of anodic barrier films formed on aluminium in aqueous borate and borate-glycol solutions', *Thin Solid Films*, **85** (1981) pp.53-59.

[10] M. R. Tabrizi, S. B. Lyon, G. E. Thompson and J. M. Ferguson, 'The long term corrosion of aluminium in alkaline media', *Corr. Sci.*, **32** (1991) pp.733-742.

[11] T. Hurlen and A. T. Haug, 'Corrosion and passive behaviour of aluminium in weakly alkaline solution', *Electrochim. Acta*, **29** (1984) pp.1133-1138.

[12] G. R. T. Schueller, S. R. Taylor and E. E. Hajcscar, 'Evaluation of natural oxides on aluminium in neutral borate electrolyte' *J. Electrochem. Soc.*, **139** (1992) pp.2799-2805.

[13] R. R. Wiggle, V. Hospadaruk, and E. A. Styloglou, 'The effectiveness of automotive engine coolant inhibitors for aluminium', *Materials Performance*, NACE (1981) pp.13-18.

[14] F. A. Cotton and G. Wilkinson, *Advanced Inorganic Chemistry*, 4th Edition, J.Wiley, New York, pp.328-335.

[15] Hideaki Takahashi, 'Structure of anodic films on aluminium - Composite oxide films', *J. of Electron Microscopy*, **39** (1990) p.134.

[16] K. Kobayashi and K. Shimizu, 'Influence of γ-alumina on the structure of barrier anodic oxide films on aluminium', *J. Electrochem Soc.*, **135** (1988) pp.908-910.

[17] W. I. Archer, and R. D. Armstrong, *Electrochemistry*, Vol.7, (1980), The Royal Soc., London.

[18] Southampton Electrochemistry Group, *Instrumental Methods in Electrochemistry*, Ellis-Horwood, (1985).

[19] A. J. Bard, and L. R. Faulkner, *Electrochemical Methods*, Wiley and Sons.

[20] I. J. Polmear, *Metallurgy of the Light Metals*, 2nd Edition, E. Arnold, New York, pp.18-33.

[21] G. Bombara and U. Bernabai, 'Corrosion of aluminium in multimetal water systems', *Br. Corros. J.*, **11** (1976) pp.25-30.

[22] S. Pengfei Y. Geping, X. Baojia, and L. Guoqi, Short Communication, *Corr. Sci.*, (1992) pp.106-109.

[23] *Aluminium and Aluminium Alloys*, Anti-corrosion manual, 5th Edition, Corrosion prevention and control.

[24] M. G. A. Khedr and A. M. S. Lashien, 'The role of metal cations in the corrosion and corrosion inhibition of aluminium in aqueous solutions', *Corr. Sci.*, **33** (1992) pp.137-151.

[25] P. J. Goodhew and F. J. Humphreys, *Electron microscopy and analysis* 2nd Edition, Taylor and Francis Ltd., UK (1988).

[26] C. A. Hall, University of Newcastle upon Tyne, Ph.D thesis (1994).

[27] G. C. J. Morris, 'Preparation and Assessment of Hydrolytic Stability of Boric Acid/Alkanolamine Condensates and Boric Acid/Alkanolamine/Fatty Acid Condensates for Use in Methal Cutting Fluids', Wolverhampton Polytechnic (1992).

[28] D. Kirkpatrick, 'Present and Future Trends in Soluble Oil Formulations', Castrol International, Pangbourne, Reading.

[29] M. P. Duncan, 'Chemistry of Lubricant Additives', Keil Chemical Division, Ferro Corporation (1993).

[30] 'Castrol Alusol B, Soluble Oil for Aluminium', Marketing Support Manual, Pub. International Industrial Marketing, Castrol Ltd., Swindon, Wiltshire.

[31] *Talking About Cutting Fluids*, 8th Edition, Feb. (1975), Castrol International, Pangbourne, Reading.

[32] R. C. Salvarezza, M. F. L. de Mele and H. A. Videla, 'Redox potential and the microbiological corrosion of aluminium and it's alloys in fuel/water systems', *Br. Corros. J.*, **16** (1981) pp.162-168.

[33] J. D. Talati and N. H. Joshi, 'Corrosion of Aluminium in aliphatic amines and its inhibition by some dyes', *Werstoffe und Korrosion*, **31** (1980) pp.926-933.

[34] P. J. Zanzucchi and J. H. Thomas, 'Corrosion inhibitors for aluminum films', *J. Electrochem. Soc.*, **135** (1988) 1370-1375.

[35] M. G. A. Khedr and A. M. S. Lashien, 'Corrosion behavior of aluminum in the presence of accelarating metal cations and inhibition', *J. Electrochem. Soc.*, **136** (1989) pp.968-972.

[36] H. Scholl and M. D. Jimenez, 'The application of 1-hydroxyimidazole-3-N-oxides as aluminum corrosion inhibitors in alkaline solutions', *Corr. Sci.*, **33** (1992) pp.1967-1978.

[37] D. L. Hallam, C. D. Adams, D. C. Creagh, S. A. Holt, E. J. Wanless, T. J. Senden and G. A. Heath, 'Petroleum Sulphonate Corrosion Inhibitors', *Optilube Australasia*, Aviation Pangb'n.

[38] A. K. Sarkar, A. Dasgupta and N. Kurmaiah, 'Rubeanic acid as a corrosion inhibitor for aluminium alloys in sodium hydroxide solution', *Bulletin of Electrochemistry*, **10** (1994) pp.150-153.

[39] L. Gnana Sahaya Rosilda, M. Ganesan, M. Anbu Kulandainathan and V. Kapali, 'Influence of inhibitors on corrosion and behaviour of different grades of aluminium in alkaline media', *Journal of Power Sources*, **50** (1994) pp.321-329.

[40] D. M. Brasher, 'Corrosion Inhibitors', pp.288-292

[41] V. Vujicic and B. Lovrecek, 'A study of the influence of pH on the corrosion rate of aluminium', *Surface Technology*, **25** (1985) pp.49-57.

[42] M. J. Mehta, 'Amines as corrosion inhibitors', CEW, **27** (1992) pp.67-71.

[43] N. D. Tomashov and L. P. Vershinina, 'Kinetics of some electrode processes on a continuously renewed surface of solid metal', *Electrochim. Acta*, **15** (1970) pp.501-517.

[44] G. T. Burstein and R. J. Cinderey, 'The potential of freshly generated metal surfaces determined from the guillotined electrode - A new technique', *Corros. Sci.* **32** (1991) p.1195.

[45] G. T. Burstein and C. Liu, 'Time resolved electrochemical impedance of the guillotined aluminium electrode', *Electrochim. Acta*, **39** (1994) p.873.

CHAPTER 2

EXPERIMENTAL

2.0 Experimental

This chapter provides a detailed explanation of the apparatus used for the purpose of the work that has been carried out. The solution compositions and methods of preparation, and finally the experimental procedures that were followed are outlined.

2.1 Apparatus

2.1.1 Electrochemical Measurements

Impedance and linear sweep polarisation measurements were made in a three-electrode glass cell (Fig.2.1).

A separate reference electrode compartment with a three way tap was connected to the main compartment via a spherical joint and a fine Luggin capillary. This allowed the working and counter electrodes to be immersed in buffer solutions whilst the reference electrode compartment was filled with 1M NaOH solution. A mercury/mercuric oxide (in 1M NaOH) reference electrode was used (Hg | HgO, +100mV *vs* SHE) and unless otherwise stated, all potentials are quoted relative to this reference electrode. The counter electrode was a ring of platinum foil supported by glass, and held in position directly below the working electrode in the main compartment. A glass tube introduced gases from the bottom of the cell, and a bubbler socket prevented gases from the atmosphere entering into the cell from outside.

The cell was cleaned by coating the inside surfaces with concentrated nitric acid and leaving overnight, followed by rinsing in Purite water.

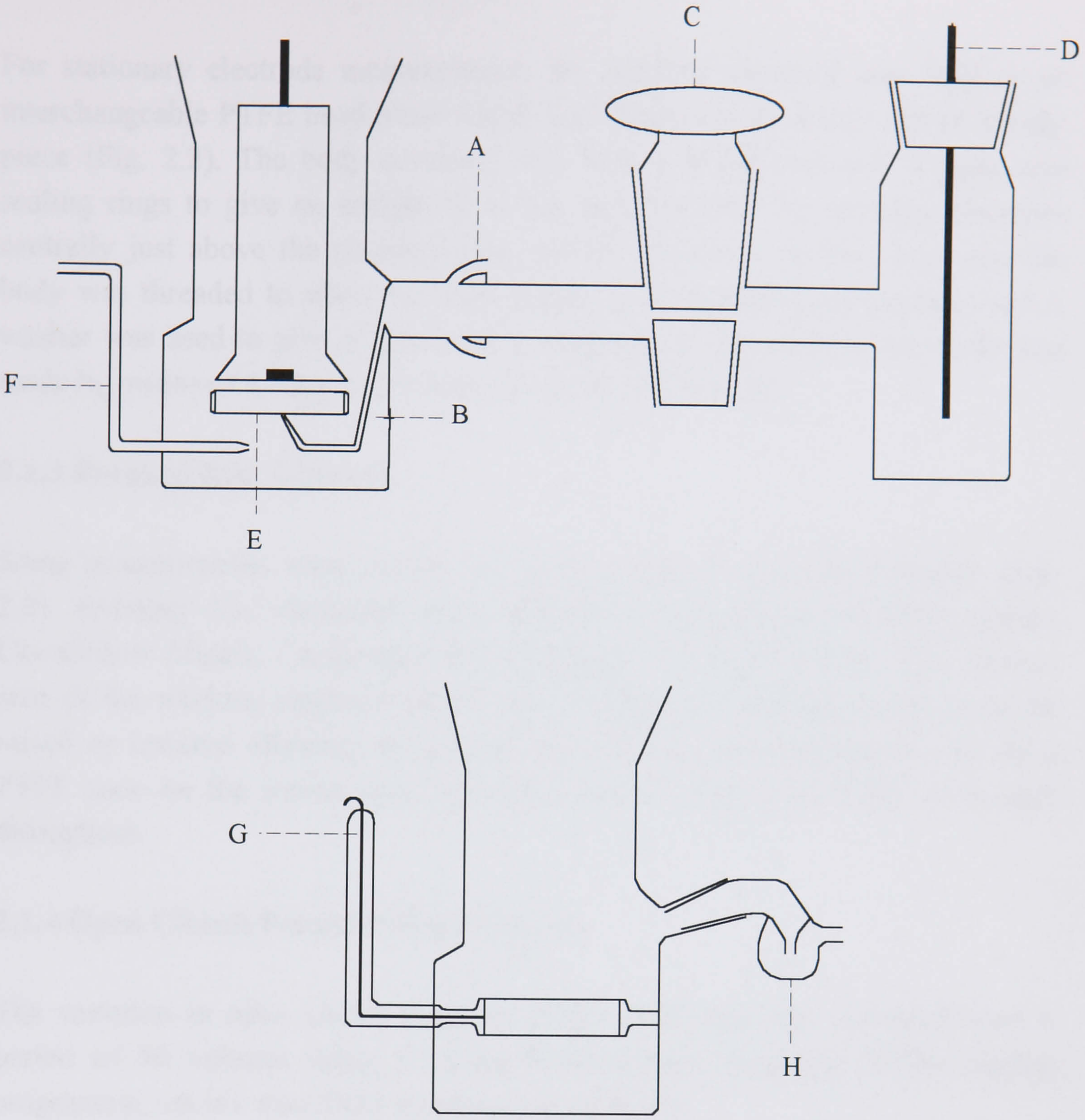

Fig. 2.1 Three electrode glass cell used for corrosion rate measurements in Newcastle.

A - Glass Joint

B - Luggin Capillary

C - 3 - Way Tap

D - Reference Electrode

E - Platinum Counter Electrode

F - Gas Inlet

G - Counter Electrode

H - Gas Outlet

2.1.2 Stationary Electrode Assembly

For stationary electrode measurements, the working electrode was held in an interchangeable PTFE head piece which was fitted into the lower end of a body piece (Fig. 2.2). The body consisted of a hollow PTFE rod with a bung and sealing rings to give an airtight fit to the cell and hold the working electrode centrally just above the platinum ring counter electrode. At the lower end the body was threaded to allow the head pieces to be screwed into position and a washer was used to give a good seal. Connection to the working electrode was made by means of a copper rod down the centre of the body.

2.1.3 Rotating Disc Electrode

Some measurements were carried out using a rotating electrode assembly (Fig. 2.3). Rotating disc electrodes were made from aluminium (99.999% purity, Goodfellow Metals, Cambridge) and embedded in Teflon holders. The surface area of the working electrode was 0.126cm^2. The electrode assembly could be raised or lowered allowing an airtight seal with the electrochemical cell via a PTFE cone on the rotator unit. Rotation rates of either 5 or 40Hz were used throughout.

2.1.4 Open Circuit Potential Measurements

The variation in open circuit potential (OCP) with time was measured over a period of 50 minutes using a Linear Potentiostatic Response (LPR) logging programme, via the AutoTafel instrument potentiostat.

Results were recorded immediately after initial immersion of the electrode into the electrolyte solution.

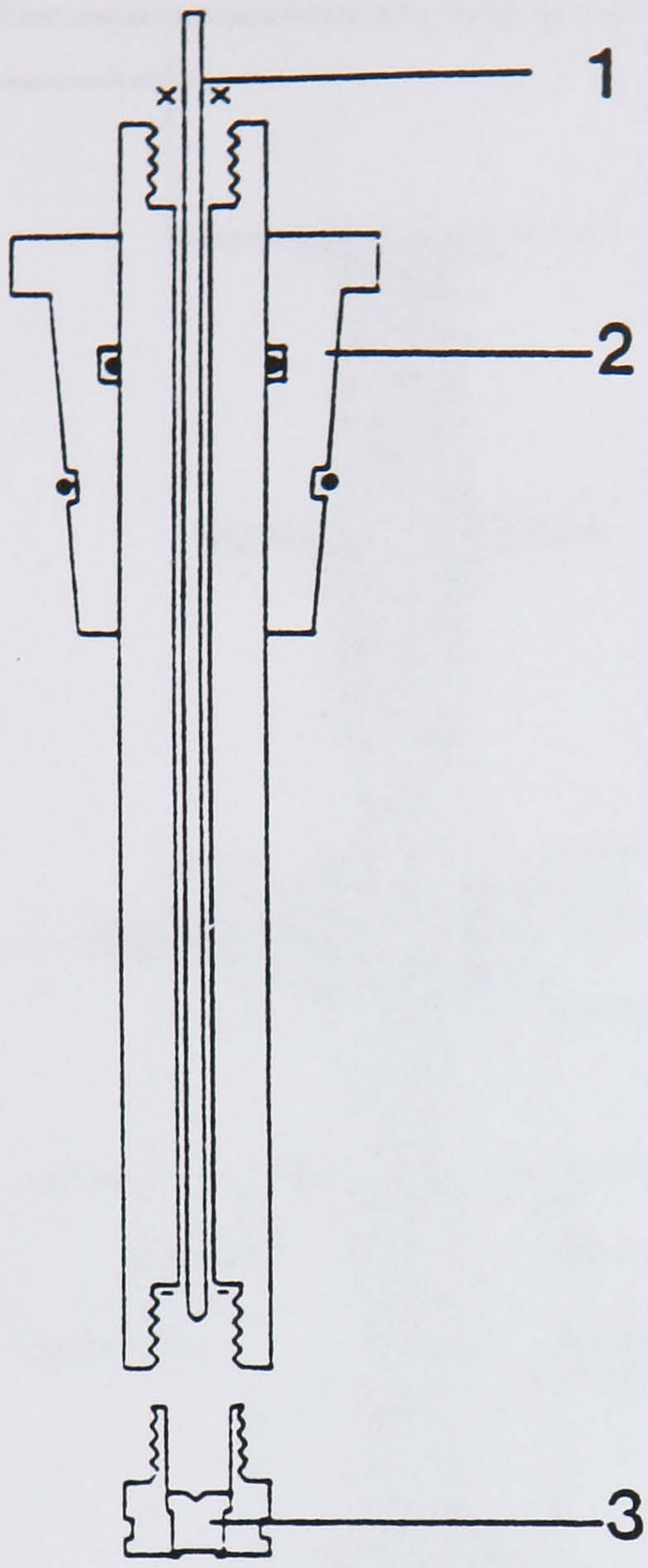

1 - Copper contact rod

2 - PTFE cone with rubber 'O' rings

3 - Aluminium metal head piece

Fig. 2.2 Stationary Working Electrode Assembly

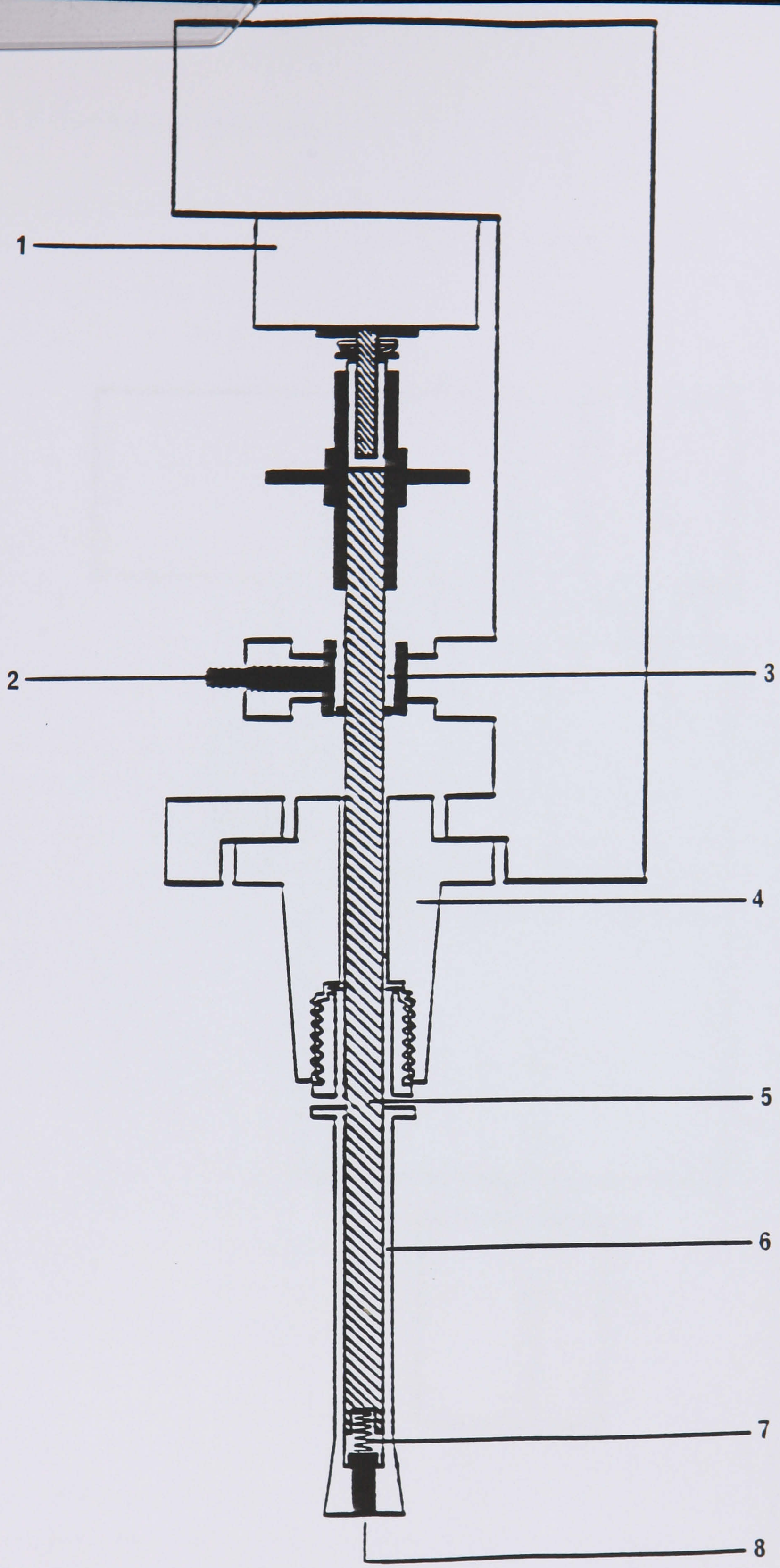

Fig. 2.3 Rotating Disc Electrode Assembly

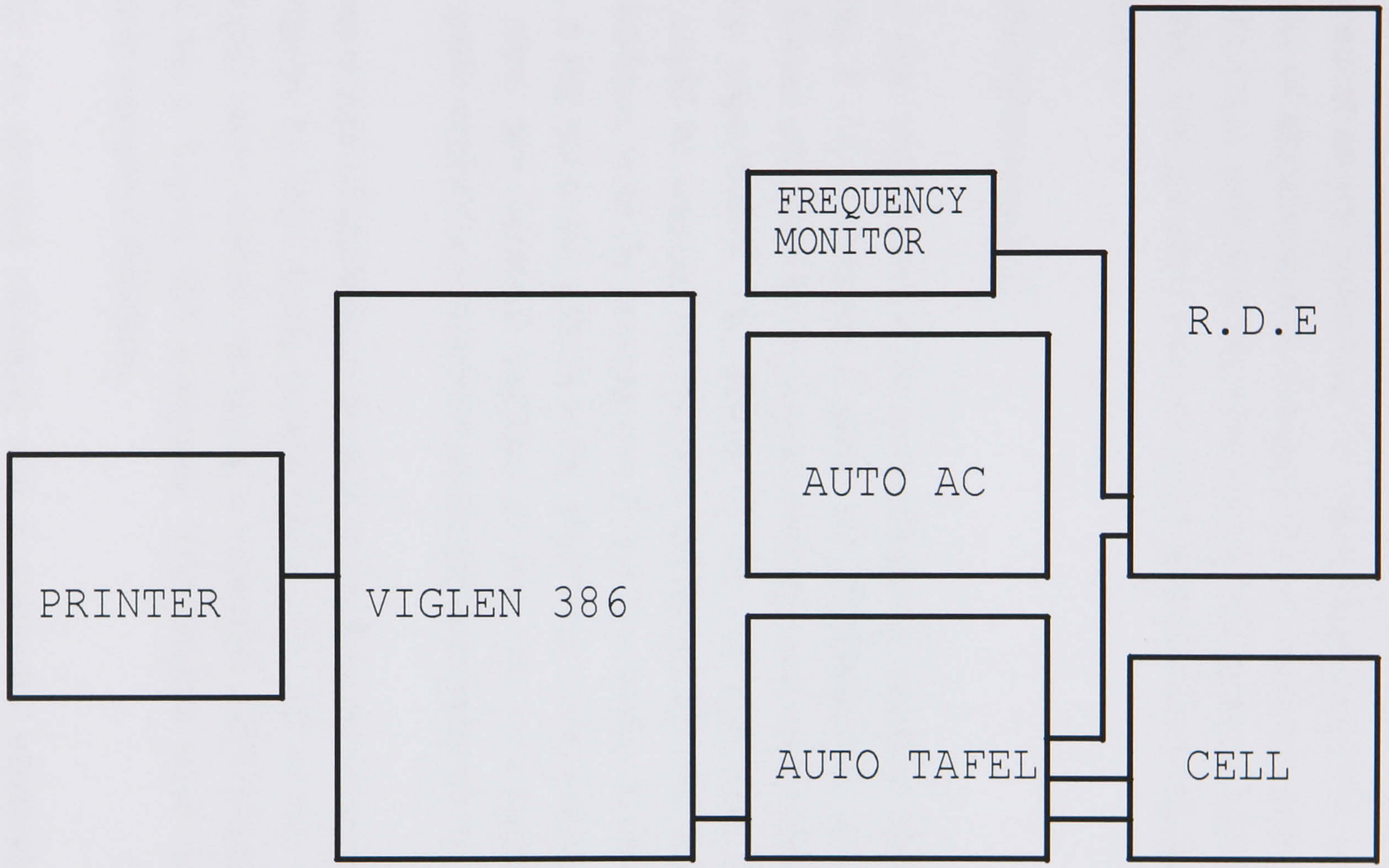

Fig 2.4 Instrumentation used for impedance and corrosion rate measurements in Newcastle.

2.1.5 Mechanical Abrasion

For pure aluminium, results are reported for a chemically pre treated surface with immersion in 1M NaOH for 10 minutes. This however, is not representative of the real system where a bare aluminium metal surface is created by a mechanical action such as drilling. Because the grain structure of the surface is dependent on the way in which the oxide layer is removed, we can expect the initial rates of corrosion also to be dependent on pre treatment. An experimental method was devised whereby a rotating disc of aluminium was lowered onto a stationary glass frit, situated beneath it (Fig. 2.5). Once sufficient time had elapsed for a fresh aluminium surface to have been created, the pressure was released and electrochemical measurements were made *in situ*.

Steady State Measurements

Corrosion rate measurements on a continuously abraded aluminium surface were made using a cell containing a glass frit. Rotating disc electrodes (surface area $0.126cm^2$) were prepared from pure aluminium rods, embedded in Teflon holders as in previous experiments. The design of the cell was such that the rotating disc electrode could be abraded on the glass frit (Fig.2.5). The cell was placed on one side of a balance, with the rotating disc fixed in position. With the disc rotating (100 rads/sec), a 2kg mass was placed at the other side of the balance so that the frit was raised to meet the electrode surface. In this way electrochemical measurements could be made whilst the aluminium electrode was being abraded.

The corrosion rate of aluminium in each electrolyte was determined by measuring i-E relationships by slow linear sweep ($5mV\ s^{-1}$). All of the steady state abrasion measurements were carried out using a Solartron 1286 Electrochemical Interface, controlled by a Viglen 486 computer. The sweeps were initiated at -2.0V and proceeded in a positive direction.

Results for an abraded electrode and a stationary electrode are reported. This enabled the results for a mechanically pre treated surface to be compared to those of a chemically pre treated electrode. Logi-E characteristics for the electrodes were determined whilst the electrode was rotating on the glass frit for an abraded surface, and without abrasion, after 15 minutes in the electrolyte after abrasion.

The effect of electrolyte solutions (pH 9.2 and pH 10.0) was investigated in the presence and absence of oxygen. All measurements were made at room temperature (21±2°C).

Oxide Recovery

A potential transient from which information about the rate of recovery could be deduced was obtained by plotting E/V vs log(t/s). The slope of the linear section of the profile was recorded and used as a parameter for the rate of recovery of the oxide film on the surface of the aluminium. A series of measurements were made, although information about the initial repassivation of the surface within milli seconds of generating a bare aluminium surface as in the guillotined electrode method [1,2], could not be obtained.

Data is presented for the behaviour of pure aluminium in contact with aqueous solutions of varying pH and 5% cutting fluid emulsions in the absence and presence of oxygen. Measurements were initiated 3 seconds before the abrading electrode was released from the frit.

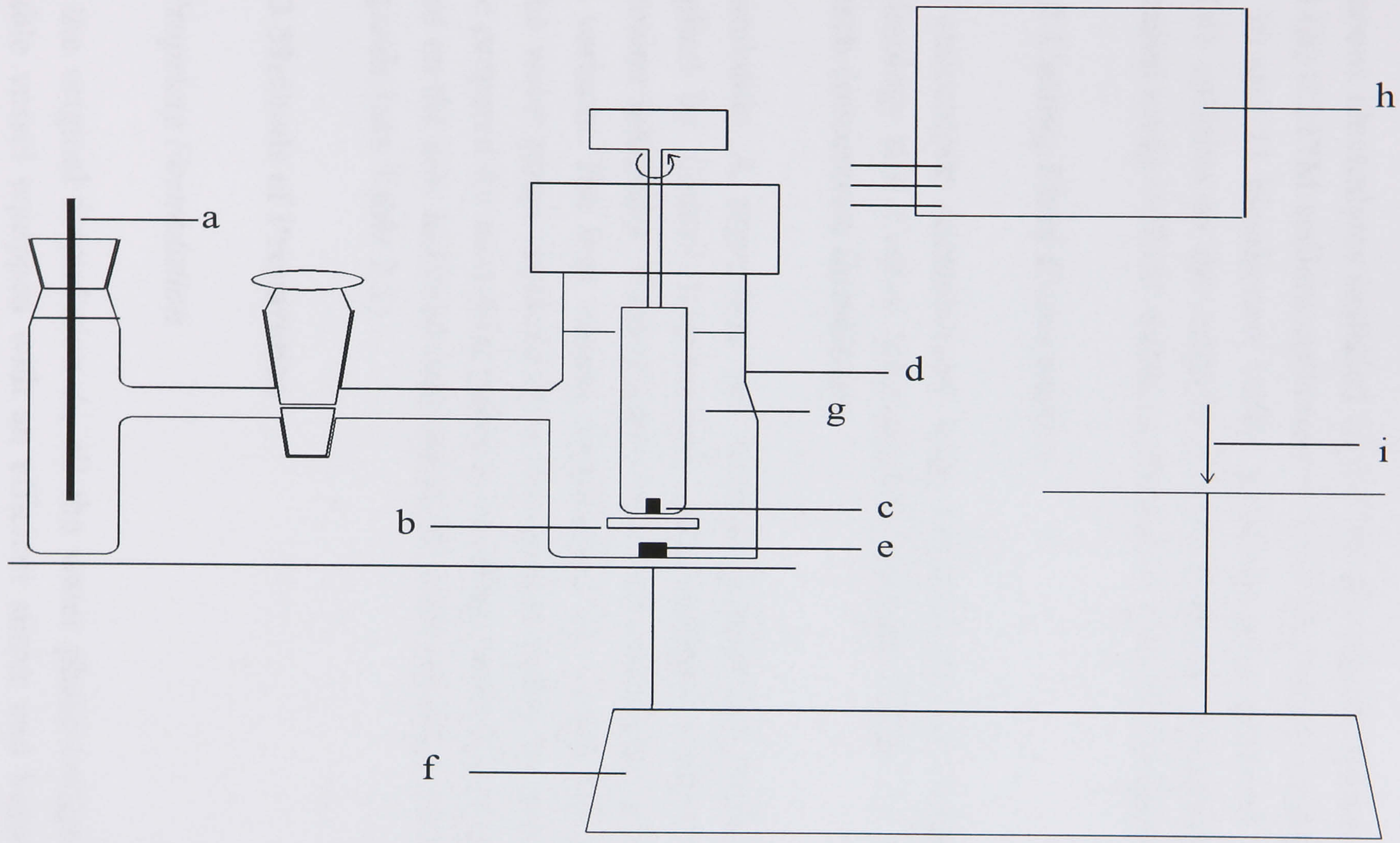

a- Reference Electrode, **b-** Platinum Counter Electrode, **c-** Working Electrode, **d-** Electrochemical Glass Cell, **e-** Glass Frit, **f-** Harvard Trip Balance, **g-** Electrolyte Solution, **h-** Computer Controlled Potentiostat, **i-** 2Kg Mass.

Fig. 2.5 Apparatus for measuring the corrosion rate of an abraded aluminium surface *in situ* with the electrolyte.

2.2 Solutions

All solutions were prepared from AnalaR® grade reagents and high purity de-ionised water (Purite Still*plus* HP).

2.2.1 Aqueous Solutions

Aqueous electrolytes included (i) 0.05M di-sodium tetraborate (pH 9.2 and pH 10), and (ii) 0.217M sodium carbonate + 0.821M sodium hydrogen carbonate (pH 9.2). pH 10 and 11 bicarbonate buffer solutions were prepared with the addition of 1M NaOH solution to the original pH 9.2 solution. Bicarbonate buffer, pH 8.0 was prepared using 0.022M sodium carbonate + 0.821M sodium hydrogen carbonate.

2.2.2 Cutting Fluid Concentrates

Oil concentrate formulations were prepared at the Production Engineering and Technology site, Castrol International, Reading. Table 2.1 outlines the composition of each concentrate formulation.

Formulation A represents the original concentrate blend named 'Alusol B', as supplied by Castrol International, and includes amines as intended aluminium corrosion inhibitors. Formulatory work was carried out in order to produce amine-free variants. The first variant, formulation 'B', simply has the original components in the water phase replaced by a bicarbonate buffer system. Formulations A1 - D1 were prepared for microbial stability challenge testing (see section 2.3.4). They were based on the new buffered concentrate B, with varying concentrations of biocide and fungicide (see Table 2.1).

2.2.3 Methods of Preparation

(i) *Propriety Formulation*

For the original formulation A, all the water phase components were placed in a suitable vessel equipped with an efficient stirrer and heated to 50°C until all the solid material had dissolved. Similarly, the oil phase components bar the biocide, decouplers and anti-foam agents were mixed and heated until homogeneous in a separate vessel. The aqueous phase was then added to the oil phase and cooled to less than 30°C while mixing. The concentrate emulsion at this stage is yellow and

opaque, and alcohol decouplers are required to help the emulsification process. These are added until the concentrate is clear and generally 'aesthetically pleasing', but at a level not greater than 1% due to the tendency to evaporate off at higher temperatures. Export of the product to warm countries means that this factor is a practical consideration. The emulsion was then sampled to the laboratory before the anti-foam agents were added. Any air gaps forming in the emulsion would reduce the lubricity and result in a loss of emulsification.

(ii) *New Sample Concentrates B and A1 - D1*

The bicarbonate and borax buffer solutions were prepared to maximum solubility 69.0 g/dm^{-3} and 20.1 g/dm^{-3} respectively, and the pH was adjusted to 10.2 using a concentrated sodium hydroxide solution. This ensured that the pH of the final emulsion was the same as that of the original formulation. This water phase was then added to a mixture of the oil phase at 50°C for 2 to 3 hrs, with stirring, and left to cool to room temperature.

Different combinations of the hydrogen carbonate/carbonate ratio were tested and also different proportions of the buffer were used, with formulation B giving the most stable and clear final concentrate.

Anti-foaming agents were omitted in the new samples.

(iii) *Preparation of Emulsions*

Oil in water emulsions were prepared from oil concentrates (formulations A and B), by diluting with distilled water by a factor of 1:20 by volume, (5%). The soluble oil concentrate should be poured gradually into the full volume of water, and not vice-versa, to ensure thorough mixing of the two phases.

Table 2.1 Composition of Oil Concentrates

% wt A	% wt B	Component	% wt A1	% wt B1	% wt C1	% wt D1
	26.0	Bicarbonate buffer, pH 10.2	27.5	27.2	26.4	26.0
10.4	-	Water	-	-	-	-
2.4	-	Triethanolamine	-	-	-	-
4.3	-	Monoethanolamine	-	-	-	-
5.0	-	Boric Acid	-	-	-	-
3.0	-	Low temperature stability coupler	-	-	-	-
0.8	-	Copper corrosion inhibitor	-	-	-	-
48.7	50.7	Refined mineral oil and natural vegetable oil	53.5	53.0	51.5	50.7
17.0	17.7	Emulsifiers	18.7	18.7	18.2	17.7
3.0	3.1	Biocide	-	-	3.1	3.1
0.4	0.4	Fungicide	-	0.4	-	0.4
4.5	2.1	Alcoholic couplers	0.4	0.7	0.6	2.1
0.5	-	Antifoam agents	-	-	-	-

2.2.4 Water Classification

Corrosion rate measurements as described were carried out on aluminium in contact with 5% emulsions prepared using three different types of water. These were (i) tap water, (ii) distilled water, and (iii) Purite.

Staining experiments were carried out on 10% emulsions prepared from hard waters with $CaCO_3$ concentrations of 200ppm and 400ppm.

2.2.5 Concentration Effects

The effects of concentration on the corrosion rate of aluminium were studied with 2.5%, 5%, and 10% emulsions.

Amine Concentrations

In the original concentrate formulation A, monoethanolamine is present at 0.7M and triethanolamine at 0.16M. This corresponds to concentrations of 0.035M and 0.008M respectively for a 5% emulsion i.e. 20 parts water : 1 part oil concentrate, giving a total amine concentration of 0.043M in the emulsion. (These concentrations are calculated assuming that the volume of formulatory components is approximately 100ml). Corrosion rate measurements were carried out on aluminium in contact with aqueous solutions containing double the concentration of amines compared to that found in the standard emulsions.

Table 2.2 Amine concentrations in 0.05 M borax solutions.

Sol^n	**Composition**	**Concentration of Amine**
1	4.30g monoethanolamine	0.07M
2	5.25g diethanolamine	0.05M
3	2.40g triethanolamine	0.016M
4	4.30g monoethanolamine + 2.40g triethanolamine + 3.0g monoethylene glycol	0.086M

N.B The pH of amine solutions was adjusted to pH 9.2 with boric acid solution.

After confirming that the amines had no short term corrosion inhibiting effect at these concentrations, solutions were made up of near saturation concentration e.g.

1M monoethanolamine and triethanolamine to determine whether there was any inhibiting effect found at these levels. The pH of the solutions was maintained at 9.15 with boric acid powder using the following criteria:

Quantity of boric acid required to maintain pH 9.15;

For boric acid we have ;

$$[H^+]\,[H_2BO_3^-] / [H_3BO_3] = 1x10^{-9.15}$$

Therefore if $[H^+] = 10^{-9.15}$ then, $[H_2BO_3^-] = [H_3BO_3]$.

For 1M triethanolamine we have,

$$[H^+][A] / [HA^+] = 10^{-7.77}$$

with $[H^+] = 10^{-9.15}$, and, $[A] / [HA^+] = 24$

Therefore, 1 mol of amine at pH 9.15 has 1/24 mol present as HA^+ i.e. 0.04 mol. This requires 2 x 0.04 mol of boric acid i.e. 0.08 mol.

2.3 Experimental Procedures

The new concentrates under went various tests in order to determine how they performed in comparison with the original formulation. Preliminary electrochemical measurements were carried out on aqueous solutions, in order to determine some information about the aluminium corrosion mechanism itself.

2.3.1 Electrode Pre treatment

Electrodes with varying thicknesses of oxide present on the surface prior to immersion in the solution were found to give irreproducible results. The working electrode was chemically pre treated by immersing in 1M NaOH solution for approximately 5-8 minutes with stirring to optimise the reproducibility. Prior to every electrochemical experiment the working electrode was exposed to the electrolyte for approximately 20 minutes for a steady state condition to be achieved. All measurements were made at room temperature (21± 2°C).

2.3.2 Corrosion Rate Measurements

An ACM computer controlled potentiostat (ACM Instruments, Heywood, Lancashire), with AutoTafel Analysis software was used to make potentiostatic measurements on the cell, in order to determine the rates of corrosion in the various solutions. The built in potentiostat enabled the potential to be swept through the desired limits, whilst measuring the current output. The corrosion rate in each electrolyte was estimated by measuring the E-logi relationship by slow linear sweep (1mV s^{-1}). A straight line was fitted to the cathodic part of the E-logi curve as indicated in Fig. 2.6 below. This line was then extrapolated to the OCP.

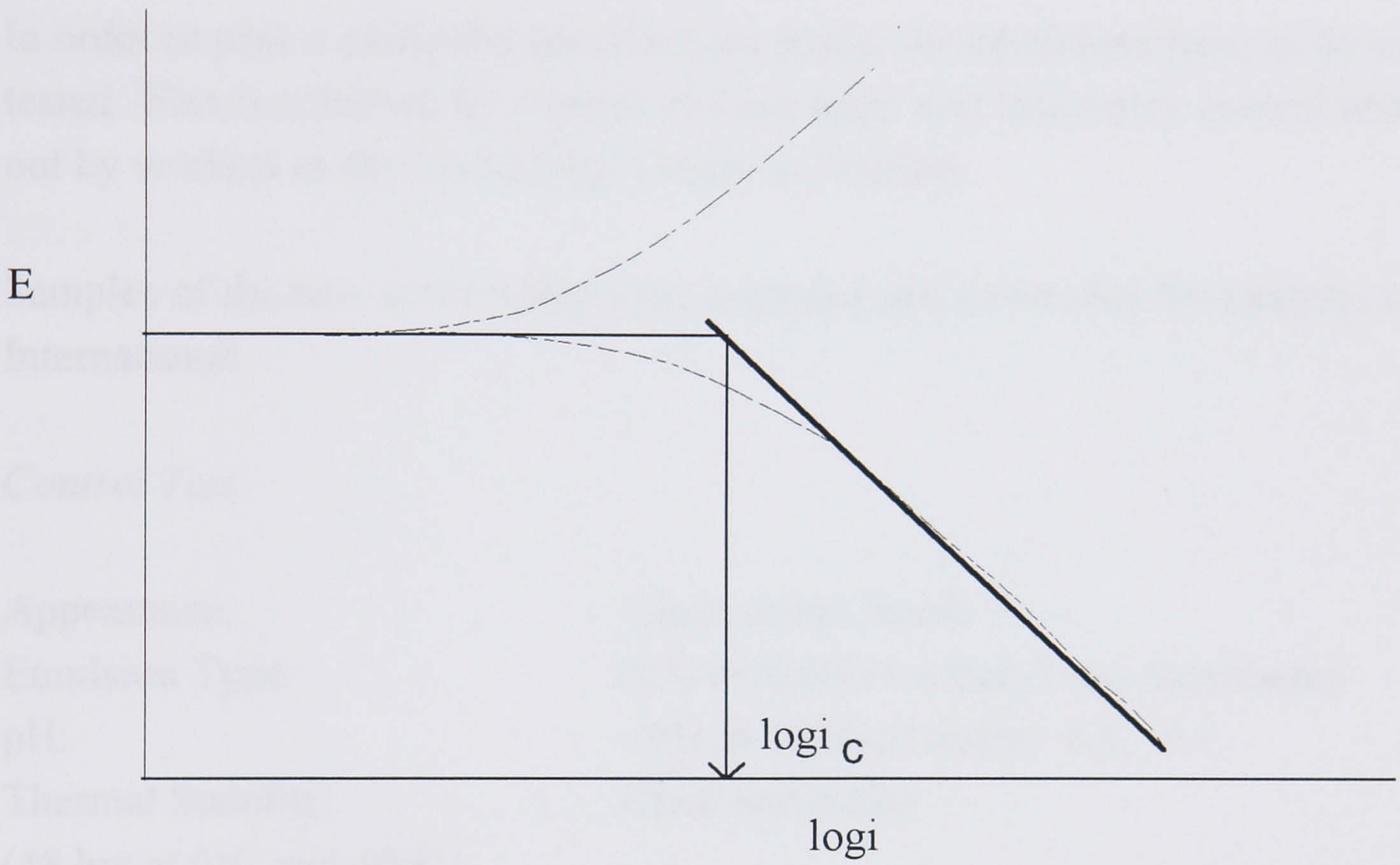

Fig. 2.6 Method used for estimating the corrosion rate by extrapolation of the cathodic Tafel slope to the corrosion potential.

Runs were initiated 300mV negative to the potential measured on open circuit, and proceeded in a positive direction. For measurements involving careful analysis of the anodic and cathodic Tafel slopes, runs were initiated at approximately -1800mV using a slower sweep speed of 10mV min^{-1}.

Measurements were controlled by a 386 Viglen computer.

Emulsions

Corrosion rate measurements were made using Tafel analysis on aluminium in contact with aerated emulsions of concentrate A, with the usual electrode pre treatment in 1M NaOH. Rotation at 5Hz was applied for all measurements to ensure there was no static build up of molecular aggregates at the metal oxide\solution interface. Measurements were made after 20 minutes of metal exposure to the solution, and again after 24 hrs.

2.3.3 Control Tests and Thermal Stability.

In order to pass a particular specification grade, the emulsions have to be vigorously tested. This is achieved by a range of field trials and laboratory control tests carried out by workers at the Technology Centre in Reading.

Samples of the new concentrate were prepared and forwarded for analysis to Castrol International.

Control Test

Appearance:	Clear amber liquid
Emulsion Type:	(5% in distilled water) Semi-translucent
pH:	(5% in distilled water) 8.6 - 9.1
Thermal Stability:	Clear and stable
(48 hrs at 0°C and 40°C)	
Defoam:	Must defoam rapidly without scumming
Aluminium Staining Test:	No stain
(5% in distilled water for 24 hrs)	

Thermal Stability

This test is simply an appraisal of a products ability to remain homogeneous under extremes of temperature, as a guide to its storage stability. 50mls of a sample is placed in a clean, dry stoppered glass container and put into an oven, or refrigerator and examined after the stipulated time interval has elapsed.

Details of the emulsion stability test are outlined in the Burmah analytical method no.189 [3]

2.3.4 Microbial Stability Challenge Test

2.5% and 5.0% solutions were prepared in 100ml mineral salts in 250ml conical flasks. Solutions were subsequently challenged daily with *Cephalosporium sp. and Pseudomonas aeruginosa*. The initial pH of each solution was recorded and adjusted where necessary to pH 9.0, using 0.5 M HCl and/or 0.1 M NaOH. The pH of the solution was measured again at the end of the test.

Dry weights were obtained for fungal challenge tests, using the standard method 1/PE/146 (see Appendix A).

These analysis tests were carried out by the Industrial and Marine group at Castrol International, Reading.

2.3.5 Buffering Capacity

An acid-base titration was carried out in order to determine the relative buffering capacities of the standard emulsion, and the new concentrate formulation B. Distilled water was used as the control. 0.1M HCl was added dropwise to 100ml of solution with constant stirring, and the change in pH at room temperature was recorded. Time in between adding the acid increments was left in order for a stable pH reading to be reached.

2.3.6 Electrochemical Impedance Spectroscopy (EIS)

Impedance analysis was carried out on aluminium in contact with 5% aerated oil in water emulsions using the procedure described below.

Estimates of the varying thicknesses of oxide on metal surfaces were made by measuring the impedance at the metal/solution interface. The electrode impedance was measured after the metal had been polarised at the start potential for 2 minutes. All measurements were carried out on an ACM Instruments potentiostat (Heywood, England) using AutoAC impedance software, controlled by a Viglen 486 computer. In most cases, 7 frequency measurements per decade were made. The frequency was scanned from 1 - 10000 Hz (scanning to the highest frequency 55kHz, was found to give artefacts caused by the capacitance of the leads). The RMS amplitude was 10mV, and the d.c. offset was set to test at the rest potential of the cell. The electrode was pre treated as in previous experiments in 1M NaOH for approximately

8 minutes with vigorous stirring. Impedance measurements were made in order to determine the thickness of the oxide layer formed on the metal surface.

Analysis of capacitance results using the ACM analysis programme software proved unsatisfactory after a run was performed on a dummy cell of known capacitance. Instead, a Boukamp [4] analysis programme was employed which proved to be a more accurate method of analysis. Resistance and capacitance values were given, the programme having taken all the relevant data points into account.

In order to obtain a thick surface layer on the metal surface, the electrode was immersed in a borax buffer electrolyte pH 9, after the same pre treatment as previously described. The EIS logging programme was run in order to attain the impedance characteristics of the system. A constant current unit was used to maintain a potential of approximately 250V and the impedance programme was run to confirm that a thick layer had formed on the surface. The anodic potential was pulsed on for 15 mins and off for 10 mins. This pulse was applied until there was little or no current flow which was an indication that the film had reached maximum thickness.

After forming the thick oxide layer as described, the system was discharged by holding the electrode at negative potentials, sweeping between 0 and -1.5V.

2.3.7 Aluminium Alloy Corrosion and Staining

Two aluminium alloys namely 2024 and 7075, were studied. The compositions of the alloys are shown below.

Table 2.3 The compositions of selected aluminium casting alloys 2024 and 7075 [5].

	Al	Cu	Zn	Fe	Mn	Mg	Cr	Ti	Si	Other
2024	main	3.80-4.90	0.25	0.50	/	1.20-1.80	0.10	0.15	0.50	0.15
7075	main	1.20-2.00	5.10-6.40	-	-	2.10-2.90	0.10-0.25	0.20	/	/

Compositions are in % maximum by weight

/ denotes element is present in trace amounts

Copper and zinc are the main alloying elements in aluminium alloys 2024 and 7075 respectively.

6" by 4" photographs of the stained aluminium alloy surfaces after immersion in various electrolytes were obtained from the Audio Visual department at the University of Newcastle upon Tyne.

For corrosion rate measurements, the same electrochemical cell as used in previous experiments was used, with a mercury/mercuric oxide reference electrode. Pre treatment of the electrode surface prior to each electrochemical measurement, involved abrasion with coarse (180C) waterproof paper to remove any stain already present. Brief exposure to 1M NaOH solution was then made before rinsing in purite water.

The corrosion rate was determined by measuring logi-E relationships by slow linear sweep (10mV min^{-1}) as previously described. Runs were initiated at approximately 500mV negative to the OCP and proceeded in a positive direction.

2.3.8 Rate of Stain Formation

An experiment was designed to determine the time taken for the surface of the alloy to change colour when in contact with aqueous solutions of increasing pH. Samples of both aluminium alloys were polished using coarse (180C) waterproof paper and immersed in aqueous solutions of varying pH. The time was noted before the alloy was completely covered in stain material. Where no significant staining was seen, the metal was polarised both anodically and cathodically, and the colour of the electrode was analysed visually after each sweep.

Potential sweeps of approximately 500mV were made at a rate of 1mV s^{-1}. They were initiated 100mV in a positive direction from the OCP for an anodic sweep, and 100mV in a negative direction from the OCP for a cathodic sweep.

2.3.9 Scanning Electron Microscopy (SEM)

Sample Preparation

In this work SEM was used as a technique for looking at the nature of the aluminium oxide layer, after exposure to different aqueous solutions and emulsions. Electron

micrographs were obtained on an S-2400 Hitachi Scanning Electron Microscope at the University of Newcastle upon Tyne under ultra high vacuum. Aluminium squares 1.5cm^2, were pre-treated in 1M NaOH for 8 minutes without stirring, washed with water and dried in air before being sputtered with gold by vapour deposition, in order to facilitate emission of electrons from the surface.

2.3.10 Energy Dispersive Analysis of X-rays (EDAX)

Aluminium/aluminium alloy metal samples were prepared for EDAX analysis. Results were obtained on a Links QX2000 instrument at the University of Newcastle upon Tyne. This enabled accurate determination of the elemental distribution of metal species at the surface after various metal pre treatments. This is known as micro characterisation.

Samples of pure aluminium and aluminium alloys, 2024 and 7075 were prepared in order to determine the differences in elemental surface composition when exposed to various conditions; (i) mechanical and chemical pre treatment, (ii) purite water, (iii) water containing 400ppm $CaCO_3$ and (iv) 10% emulsion. Samples were left immersed in the test solutions for approximately 100 hrs at room temperature before rinsing in purite water and drying in air.

References

[1] G. T. Burstein and R. J. Cinderey, 'The potential of freshly generated metal surfaces determined from the guillotined electrode - A new technique', *Corros. Sci.*, **32** (1991) p.1195.

[2] G. T. Burstein and R. J. Cinderey, 'Evolution of the corrosion potential of repassivating aluminium surfaces', *Corros. Sci.*, **33** (1992) p.475.

[3] 'Emulsion Stability Test for Soluble Oils', Burmah Analytical Method No.189, revised 11/5/93, Castrol International, Industrial and Marine Group, Pangbourne.

[4] Bernard A Boukamp, 'Equivalent Circuit Users Manual', 2nd revised edition, (1988) University of Twente.

[5] I. J. Polmear, *Light Alloys*, *Metallurgy of the Light Metals*, E. Arnold, New York (1989).

CHAPTER 3

CORROSION OF ALUMINIUM IN AQUEOUS SOLUTIONS

3.0 Corrosion of Pure Aluminium in Aqueous Solutions

The results of corrosion rate measurements as described in the experimental section 2.5 are presented and discussed in this chapter. Linear sweep and impedance measurements have been made on pure aluminium electrodes, immersed in alkaline aqueous solutions of varying pH, in the presence and absence of oxygen.

3.1 Results

Repeatability

The open circuit potential (OCP) was very unstable during the first few minutes of contact with the electrolyte solution. A relatively stable value was reached after approximately 20 minutes. Electrode pre treatment ensured that the electrochemical measurements were repeatable. The linear sweeps shown below are for pure aluminium in contact with a borax buffer solution pH 9, and give some indication of the repeatability of the system.

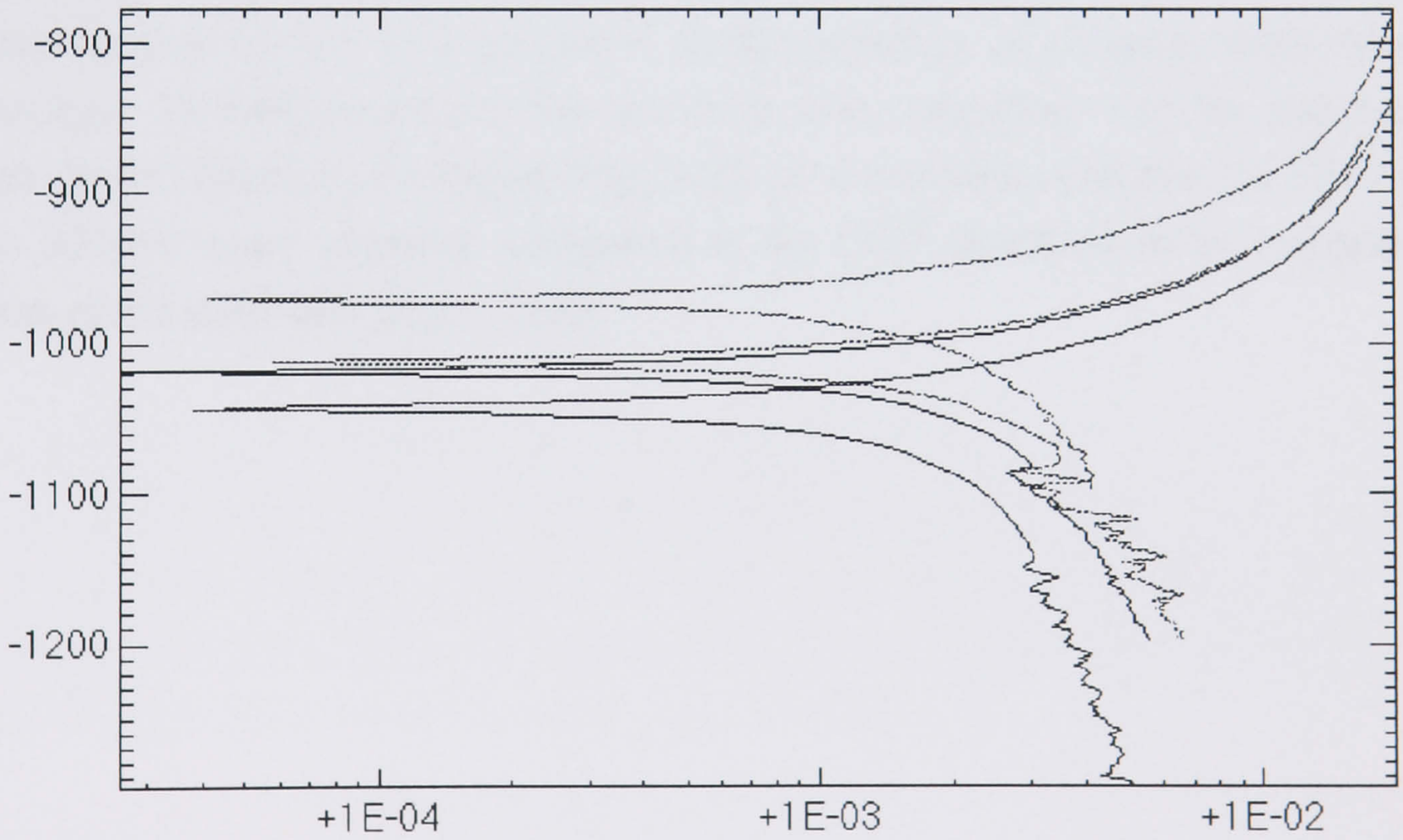

Fig. 3.1 Repeatability of Tafel plots for a pure aluminium electrode in an oxygenated borax buffer solution pH 9.2, rotation speed 5Hz.

OCP values were found to be reproducible to ±0.1V and Average values for corrosion currents are presented with a 30% error margin

3.1.1 Corrosion Rate Measurements

Corrosion of Aluminium in the Presence and Absence of Oxygen

Tafel plots were obtained for pure aluminium in a borax electrolyte, in the absence and presence of oxygen. Runs were initiated 300mV negative to the potential measured on open circuit, and proceeded in a positive direction. The corrosion currents in Table 3.1 were estimated by extrapolating the cathodic Tafel lines to the rest potential.

Table 3.1 Corrosion rate measurements of aluminium immersed in a borax buffer electrolyte solution in the absence and presence of oxygen at pH 8.2.

Solution	pH	Gas	Estimated Corrosion Current ($\mu A\ cm^{-2}$)	OCP /mV
Borax	8.2	N_2	0.07 ± 0.02	-1150
Borax	8.2	O_2	0.6 ± 0.2	-900

The corrosion rate of aluminium in a borax buffer solution of pH 8.2 saturated with nitrogen is $0.07 \pm 0.02\ \mu A\ cm^{-2}$. In the presence of oxygen, there was an approximate 10 fold increase in the corrosion rate compared to in the absence of oxygen. In the absence of oxygen (Fig. 3.2(b)), it was observed that the OCP was 200 to 300mV more negative, compared to the OCP observed in an oxygenated solution at the same pH (Fig. 3.2(a)).

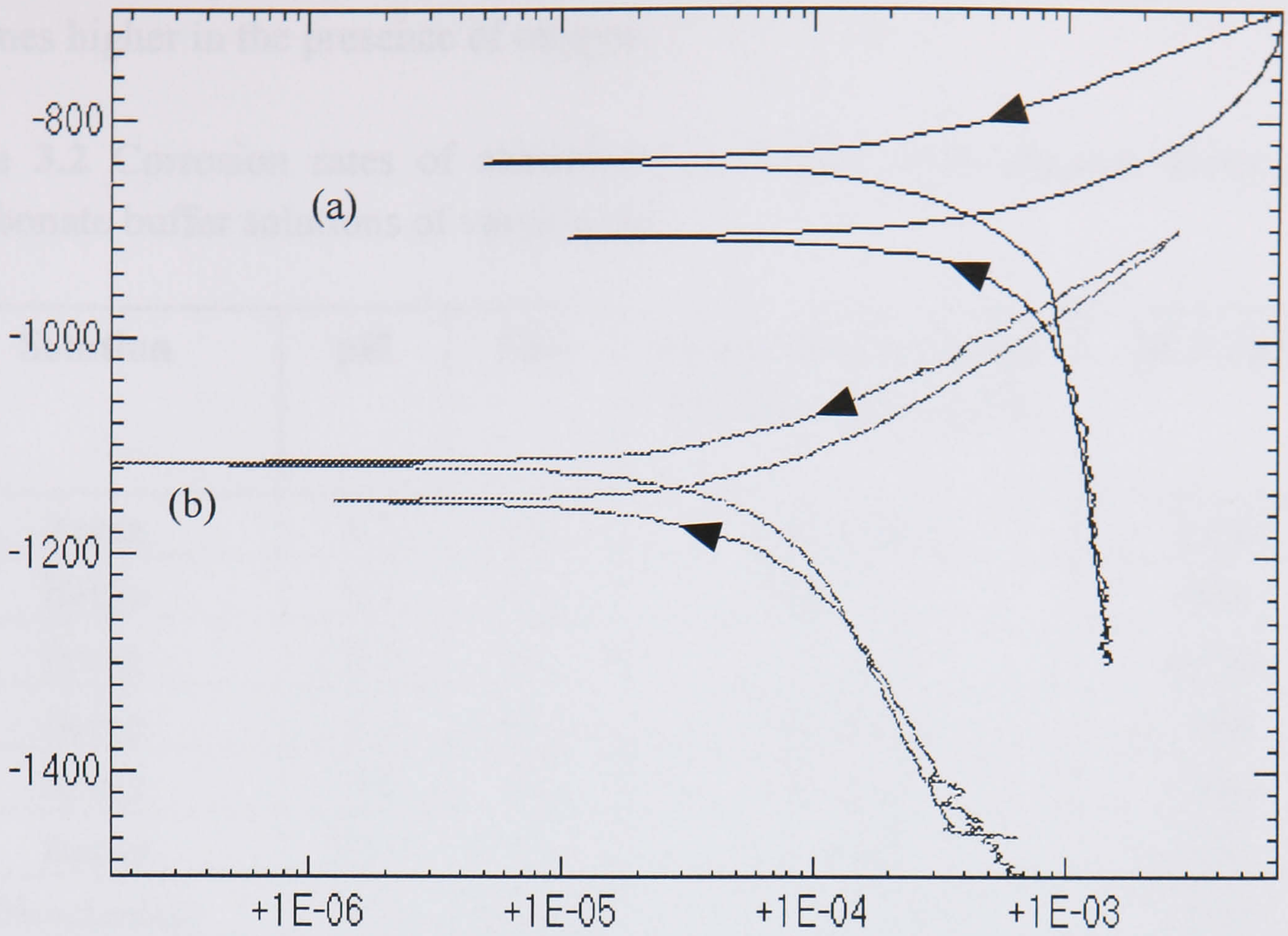

Fig. 3.2 Cyclic potential sweeps for aluminium in contact with a 0.05M borax buffer solution, pH 8.2 (a) oxygenated, (b) deoxygenated, sweep rate 1mV s^{-1}.

The profiles above are not retraced exactly. If the potential is swept too rapidly, the oxide layer does not have time to adapt to its steady state thickness, giving rise to anodic currents that are lower than predicted.

The corrosion rates were found to be only slightly dependent on the rotation speed of the electrode. For example in oxygenated solution there was an increase in the corrosion rate by a factor of only 1.2 when the rotation speed was increased from 5Hz to 40Hz. On rotation of the electrode at 40Hz under nitrogen, there is no significant change in the rate of corrosion.

Effect of pH

Corrosion rate values were obtained for aluminium in contact with aqueous borax and bicarbonate buffer solutions of pH 8.2, 9.2, 10.0, and 11.0. Each unit increase of pH between 8.2 and 11 was found to give an approximate 10 fold increase in the corrosion current. There is an approximate 3 fold increase in the corrosion rate in the presence of oxygen compared to in its absence at pH values

9.2 and 10.0. At pH 8.2, however, the increase in corrosion rate is approximately 10 times higher in the presence of oxygen.

Table 3.2 Corrosion rates of aluminium in contact with aqueous borax and bicarbonate buffer solutions of varying pH.

Solution	**pH**	**Gas**	**Estimated Corrosion Current ($\mu A\ cm^{-2}$)**	**OCP /mV**
Borax	8.2	N_2	0.07 ± 0.02	-1150
Borax	8.2	O_2	0.6 ± 0.2	-900
Borax	9.2	N_2	1.3 ± 0.1	-1250
Borax	9.2	O_2	4.0 ± 1.2	-1000
Borax	10.0	N_2	15 ± 4.5	-1400
Borax	10.0	O_2	51 ± 15.3	-1200
Bicarbonate	9.2	aerated	1.2 ± 0.4	-1000

The logi-E relationships obtained by slow linear sweep, at a rate of 10mV min^{-1} for a number of bicarbonate based solutions of varying pH, are shown in Fig. 3.3. Each sweep took approximately 3 hours to measure.

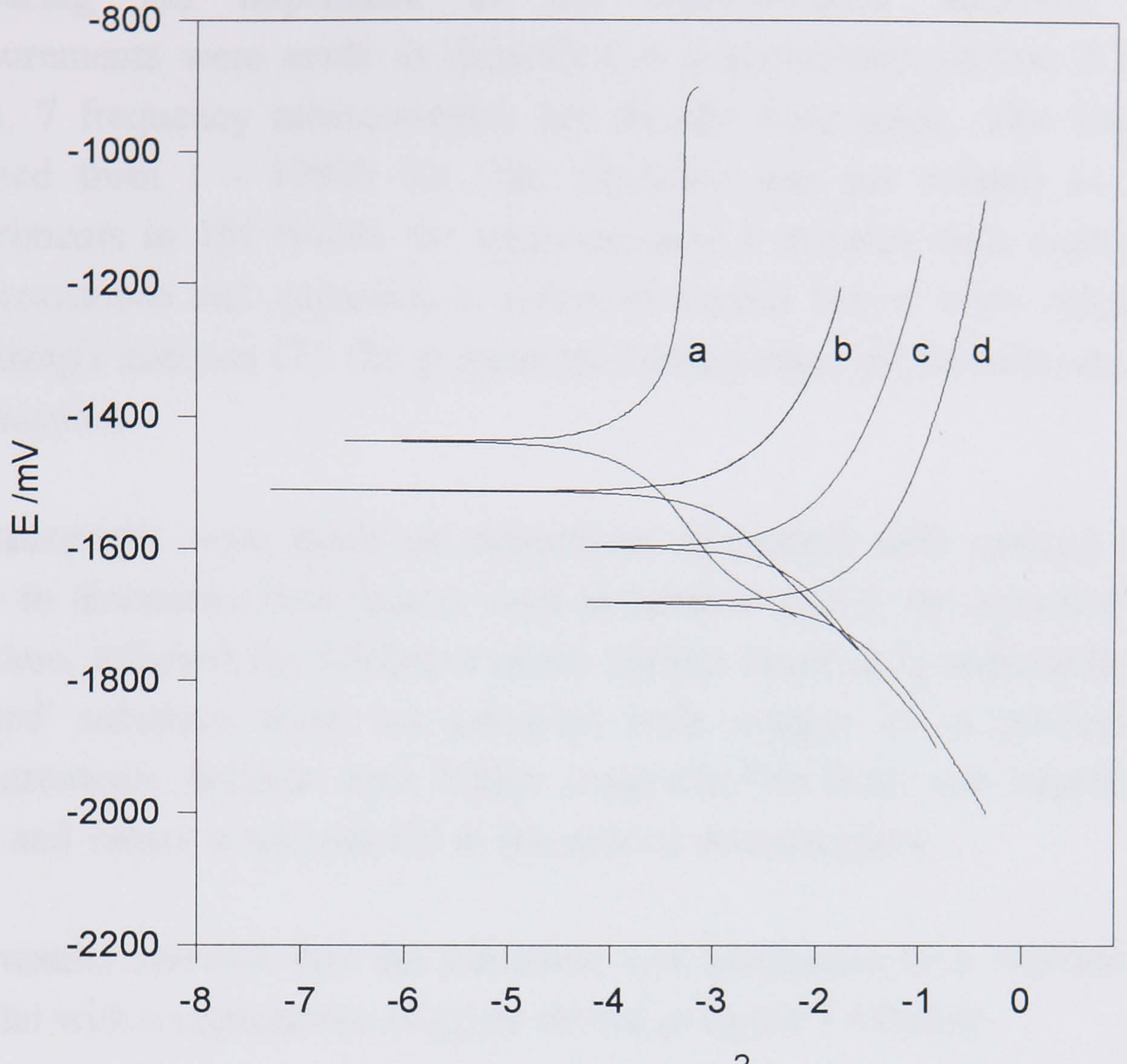

Fig. 3.3 Graph to show the effect of pH on the corrosion rate of pure aluminium in contact with an aerated aqueous bicarbonate buffer solution (a) pH 8.2, (b) pH 9.2, (c) pH 10.0 and (d) pH 11.0, sweep rate 10mV min^{-1}.

The anodic dissolution currents increased systematically by a factor of approximately 10 with each unit increase in pH. The current due to the cathodic reaction showed a Tafel dependence on the potential, and was the same within experimental error at a given potential for all solutions. It was therefore independent of pH. The Tafel slope of the cathodic line is approximately 0.169V $decade^{-1}$. This was found to be independent of the rotation speed.

The results reported here are in many respects similar to those found by Burstein and Liu [1] and are consistent with the work of Hurlen and Haug [2]. In particular the cathodic current is independent of anodic film thickness and pH, and depends only on the potential of the metal.

3.1.2 Impedance Measurements

Estimates of the varying thicknesses of oxide on the metal surface were made by measuring the impedance at the metal/solution interface. Impedance measurements were made as described in experimental section 2.3.6. In most cases, 7 frequency measurements per decade were made. The frequency was scanned from 1 - 10000 Hz. The electrode was pre treated as in previous experiments in 1M NaOH for approximately 8 minutes with vigorous stirring. The resistance and capacitance values presented below were calculated using Boukamp's analysis [3], the programme having taken all the relevant data points into account.

Measurements were made on aluminium in contact with various solutions in order to determine how factors such as rotation speed, the presence of oxygen, and time, affected the thickness of the surface layer. It is important to note that 'aerated' solutions were not saturated with oxygen as in previous electrode measurements. Results were highly irreproducible from one experiment to the next, and values were rounded to the nearest decimal place.

The results showed that the electrode was analogous to a resistance (R_{ct}) in parallel with a capacitance (C_{dl}) as shown in figure 3.4 below.

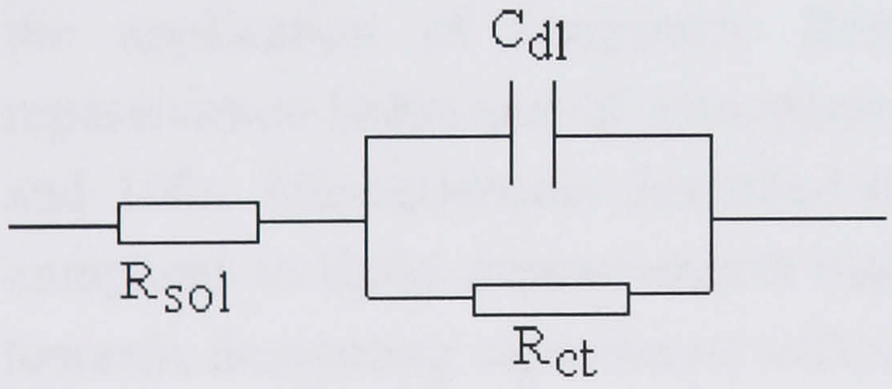

R_{sol} - Solution resistance between reference and working electrodes
R_{ct} - Charge transfer resistance of surface layer
C_{dl} - Double layer capacitance

Fig. 3.4 Circuit equivalent of a passive aluminium electrode surface showing a resistor in parallel with a capacitor.

Table 3.3 Impedance and corrosion current data measured at rotation speeds of 10 and 40Hz after 20 minutes and 16 hours exposure to; i) an aerated borax electrolyte pH 9.2 and, ii) a deoxygenated borax electrolyte pH 9.2 .

Solution	**t=30mins**				**t=16hrs**	
	10Hz		**40Hz**		**10Hz**	
	i_c	**C_{dl}**	**i_c**	**C_{dl}**	**i_c**	**C_{dl}**
Aerated borax pH 9.2	3.4	7.4	4.3	8.2	2.3	5.8
Deoxygenated borax pH 9.2	1.3	11.4	1.4	9.3	0.9	6.9

Units; $i_c/\mu A\ cm^{-2}$, $C_{dl}/\mu F\ cm^{-2}$

The capacitance values indicated a very thin surface film in all cases, comparable to one monolayer thickness. The thickness of the oxide layer on the aluminium surface in contact with aqueous solution at the rest potential was estimated using equation (1.9). The rotation speed was found to have no significant effect upon the corrosion rate or capacitance values. In the presence of oxygen i.e. in an aerated solution, capacitance values systematically decreased in all cases compared to results obtained in the absence of oxygen, at 10 and 40Hz, and after 30 minutes and 16 hrs.

With time the capacitance values decreased, indicating an increasing thickness of oxide layer on the surface. Correspondingly, the corrosion rate values decreased slightly after 16 hrs of exposure to the electrolyte. Burstein and Liu [4] describe the application of Frequency Response Analysis (FRA) to the transient repassivation behaviour of aluminium in a 0.3M phosphate solution after 1s, 10s and 100s. Measurements described in this work were made over a longer time compared to those measurements made by Burstein, but showed a similar trend towards decreasing capacitance with time.

The capacitance and charge transfer resistance values are shown in Table 3.4 below. They were obtained for an aluminium working electrode which was held at progressively increasing potentials, positive to the OCP.

Table 3.4 Impedance elements for pure aluminium in contact with a 0.05M borax solution in the absence of O_2, pH 9.2.

Potential /mV	**Capacitance /μF cm^{-2}**	**Charge Transfer Resistance /10^{4}Ω cm^2**
Open circuit	14.0 ± 1.0	0.52
+ 300*	12.0 ± 1.0	1.0
+ 800*	8.50 ±1.0	1.9
+1200*	3.8 ± 0.7	5.1

*Polarising potentials are quoted with respect to the rest potential

Table 3.5. Impedance elements for pure aluminium in contact with aerated aqueous bicarbonate buffer solutions, pH 9.2, 10.0 and 11.0 at potentials positive and negative to the rest potential, rotation speeds 5 and 40Hz.

pH	**Potential /mV**	**Rotation Speed /Hz**	**C_{dl}/μF cm^{-2}**	**R_{ct}/Ω cm^{2}x10^2**
9.2	-1800	5	55	4.2
9.2	OCP	5	13	6.1
9.2	-1100	5	8	9.3
9.2	-1800	40	55	4.2
9.2	OCP	40	24	-
9.2	-1100	40	11	17.0
10.0	-1800	5 + 40	134	1.6
10.0	-1100	5 + 40	31	2.7
11.0	-1800	5 + 40	189	1.4
11.0	-1100	5 + 40	58	1.6

Capacitance values were found to decrease with increasing positive polarisation from the rest potential. The charge transfer resistance increased, as expected for an insulating layer of increasing thickness. It is important to note that there is no significant rotation speed dependence on the capacitance or resistance of the surface layer.

The graphs shown below (Figures 3.5 (a) and (b)), were obtained using a three electrode glass cell. An alternating potential of well defined frequency and amplitude was applied between the aluminium working electrode and the

reference electrode, and the vector ratio of alternating potential to alternating current was measured i.e. the impedance. Aqueous bicarbonate buffer solutions of varying pH were aerated and in contact with the working electrode.

Impedance measurements (Figures 3.5(a), 3.5(b), and Table 3.5) suggest that the thickness of oxide layer changes with pH at given constant potential, becoming significantly thinner with increasing pH.

Constant Current Method

A pre treated aluminium electrode was immersed in a borax buffer electrolyte pH 9.2. After high anodic polarisation of the metal electrode as described in experimental section 2.3.6, the EIS logging programme was run in order to attain the impedance characteristics of the system. After the electrode had been left to discharge on its own in the borax solution for 24 hrs, the potential had only fallen to -54mV. After 40 hrs the rest potential had fallen to -296mV. The system was then discharged by holding the electrode at negative potentials, and performing a potential sweep between 0.0 and -1.5V. After discharging the electrode by performing a Tafel sweep, only a small current flowed as predicted. The rest potential fell to -1525mV, and impedance analysis gave a capacitance of 8.65 x 10^{-10}F cm^{-2}.

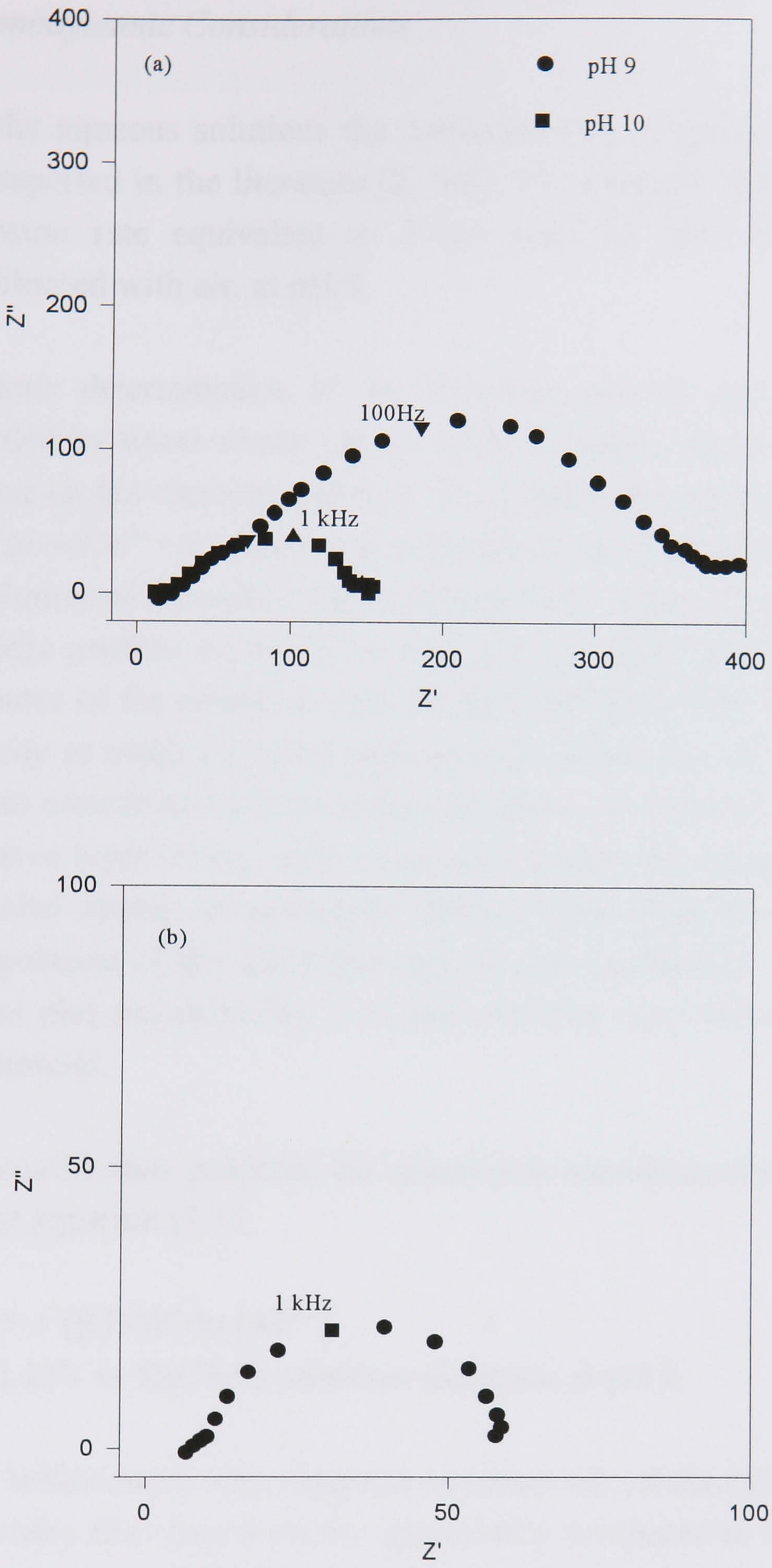

Fig. 3.5 The thickness of oxide on an aluminium surface becomes thinner with increasing pH. Impedance spectra are shown for the frequency range 1 - 10000 Hz (7 frequency points per decade), for pure aluminium in aerated bicarbonate buffer solutions, (a) pH 9 and 10, (b) pH 11.

3.2 Discussion

Thermodynamic Considerations

For the aqueous solutions the corrosion rate of pure aluminium was similar to that reported in the literature [2, 5-8]. For example Thompson *et al* [9], report a corrosion rate equivalent to 3.4μA cm^{-2} at 30°C for a solution of NaOH equilibrated with air, at pH 9.

Accurate determination of the corrosion rate by use of logi-E measurements recorded by linear sweep can be difficult when a metal oxide/hydroxide layer is present on the electrode surface. For a metal directly in contact with its solution e.g. $Cu \rightarrow Cu^{+} + e^{-}$, there is a well defined cell rest potential corresponding to the dissolution of the metal. The resulting Tafel slopes (the slopes of the anodic and cathodic profiles on the E vs logi plot) are also well defined so that accurate estimates of the corrosion rate can be made [10]. The Tafel slopes deviate from linearity at small potential perturbations either side of the OCP. This is due to current contributions from equal and opposite electrode reactions. When there is a passive layer on the surface of a metal electrode, deviations from a linear Tafel line also appear at potentials further away from the OCP. As a result, the extrapolation of the Tafel line may become ambiguous, as can be seen from the typical plot shown in Fig. 3.1, and corrosion rate values can only be considered as estimates.

The equilibrium potential for aluminium/aluminium hydroxide is given by the Nernst equation (1.1),

$$E = E^{o} + (RT/3F) \ln [Al^{3+}]$$
$$= -2.12V \text{ vs } Hg/HgO \text{ reference electrode at pH 9.}$$

Tafel behaviour is only expected on either side of the OCP, when the thickness of the anodic film does not vary appreciably compared to its value on open circuit, before the start of the linear sweep. It is reasonable to assume that this is the case at potentials between the OCP, and -2.12V.

Anodising the electrode causes the oxide layer to thicken. The electrode surface is said to be 'passive', with an insulating barrier layer forming in the early stages of nucleation and growth of the film [11]. By sufficiently thickening the oxide layer, the water reduction reaction can in theory be prevented from occurring. In this case, we can expect the potential to approach that of the calculated equilibrium potential measured at the OCP. This is as opposed to the more

positive rest potential that is observed when the system is corroding when there is a relatively thin protective oxide layer on the metal surface.

The results obtained substantiate these suggestions, although the water reduction reaction cannot have totally been prevented as the OCP value did not fall to -2.12V. A thick film formed after the electrode was held anodically at approximately +250V for some time (constant current method, experimental section 2.3.6). The rest potential fell to -1525mV, and impedance analysis gave a capacitance of 8.647×10^{-10}F cm^{-2}. This corresponds to a thickness of 1264nm.

The reversible potential for H^+/H_2 vs Hg/HgO is -0.64V. Therefore, in terms of thermodynamics in the absence of oxygen, we should expect the OCP for aluminium in solution to lie between -0.64V and -2.12V, as is observed. All of the OCP values are considerably positive to the calculated equilibrium potential, and in correspondence a layer of oxide or hydroxide is found on the surface of the aluminium metal in all of the solutions that have been explored here. The majority of Al(III) species formed in the corrosion reaction are $Al(OH)_4^-$ at pH values greater than 7.5.

The 10 fold increase in corrosion current that is observed with unit increase in pH be explained by looking at the degree of solubility of the oxide layer at various pH values on the graph below [12].

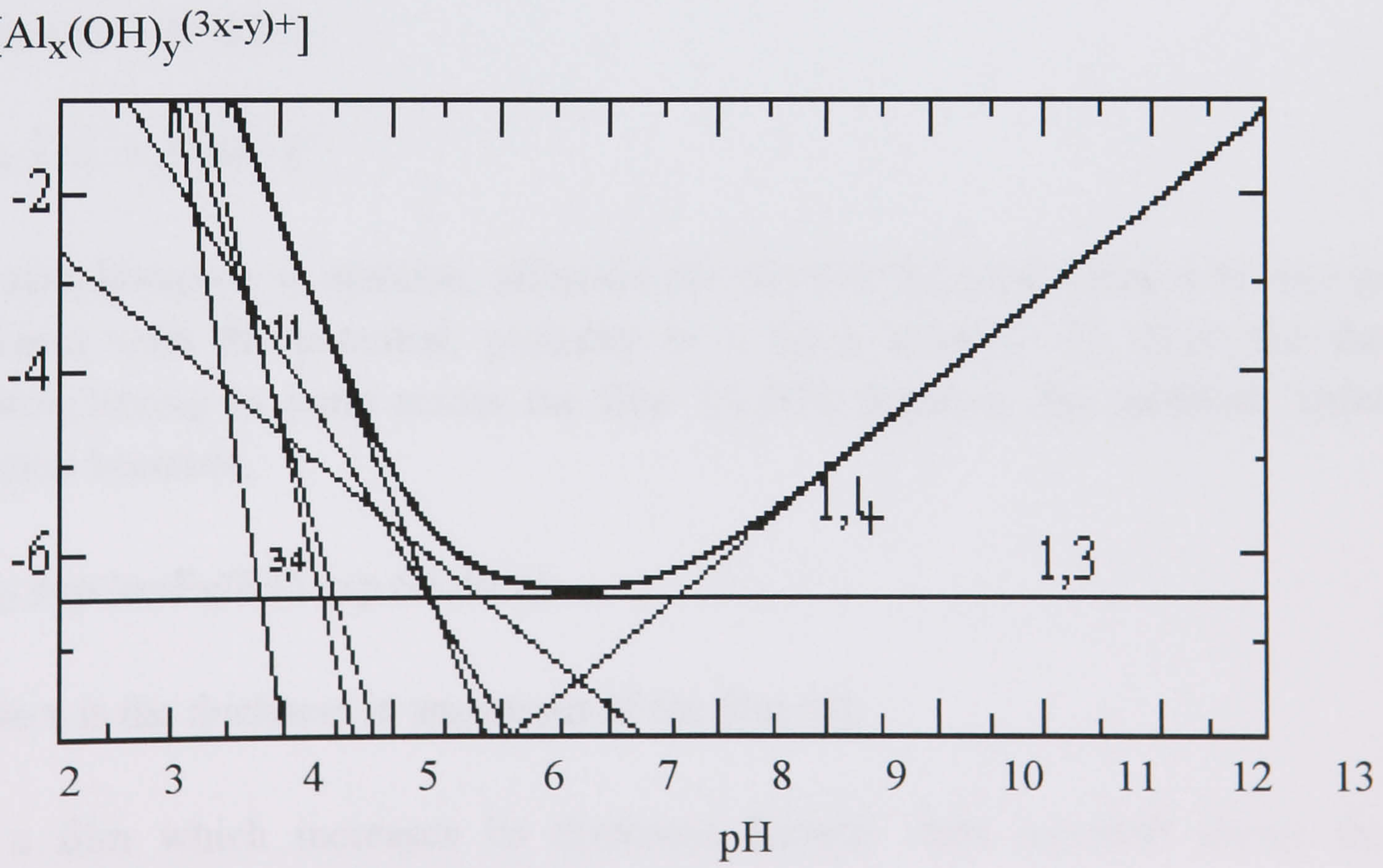

Fig. 3.6 Distribution of hydrolysis products (x,y) at 25°C in solutions saturated with α-$Al(OH)_3$. The heavy curve is the total concentration of Al(III) [12].

From the solubility diagram in Fig. 3.6 it can be seen that aluminium oxide/hydroxide is approximately 10 times more soluble at pH 10, than it is at pH 9. Aluminium exposed to aqueous solutions of pH 10 would therefore be expected to have a thinner protective layer on the surface, due to the greater extent of aluminium dissolution as aluminate into the solution. With a thinner oxide layer present on the metal surface, the corrosion rate is observed to increase in proportion with the rate of solubility of the oxide/hydroxide i.e. there is a 10 fold increase in corrosion rate for unit increase in pH.

3.2.1 The Cathodic Reaction on Aluminium in Weakly Alkaline Solutions

Predictions

We would expect the Tafel equation to be obeyed for the reaction,

$$e^- + H_2O = \tfrac{1}{2}H_2 + OH^-$$

if the hydroxide/oxide layer were of constant thickness over the potential region of interest. For a Tafel slope of 0.12V decade^{-1} (on the assumption that the slow step in the reaction is $e^- + H_2O = H_{ads} + OH^-$).

We have,

$$i = -i_o \exp(\alpha n F \eta / RT)$$

with, $|\eta| = -0.64 - E$

We must however, in addition, allow for the fact that the anodic film will vary in thickness with the potential, probably in a linear manner. To allow for the electron having to jump across the film 1/1.40Å distance, the modified Tafel equation becomes,

$$i = i_o \exp(\alpha n F \eta / RT) \exp(-1.40\ x)$$

where x is the thickness in angstroms of the film [4].

For a film which increases its thickness linearly with potential above the reversible oxide/hydroxide potential

$$x = \beta (1.76 + E)$$

Substituting these values gives;

$$i = i_o \exp(\alpha nF(-0.63 - E)/RT) \exp(-1.40\,\beta\,(1.76 + E))$$

Thus, Tafel behaviour is expected i.e. a linear dependence of E on logi, but with a Tafel slope which is not 0.12V decade^{-1}, but less than this value.

Considering the cathodic current at E = -1.00V and at -1.12V; because of the simple Tafel behaviour the current will be ten times higher at -1.12V compared with that at -1.00V. However, the film thickness will be (0.64/0.76) its thickness at -1.12V compared with that at -1.00V. Therefore this will increase the current by a factor of exp(γ 0.76/0.64), with the value of γ unknown. Therefore the total increase in cathodic current is not 10 but more than 10.

Predicted E - logi for different rotation speeds ***Note: The Tafel slopes are arbitary***

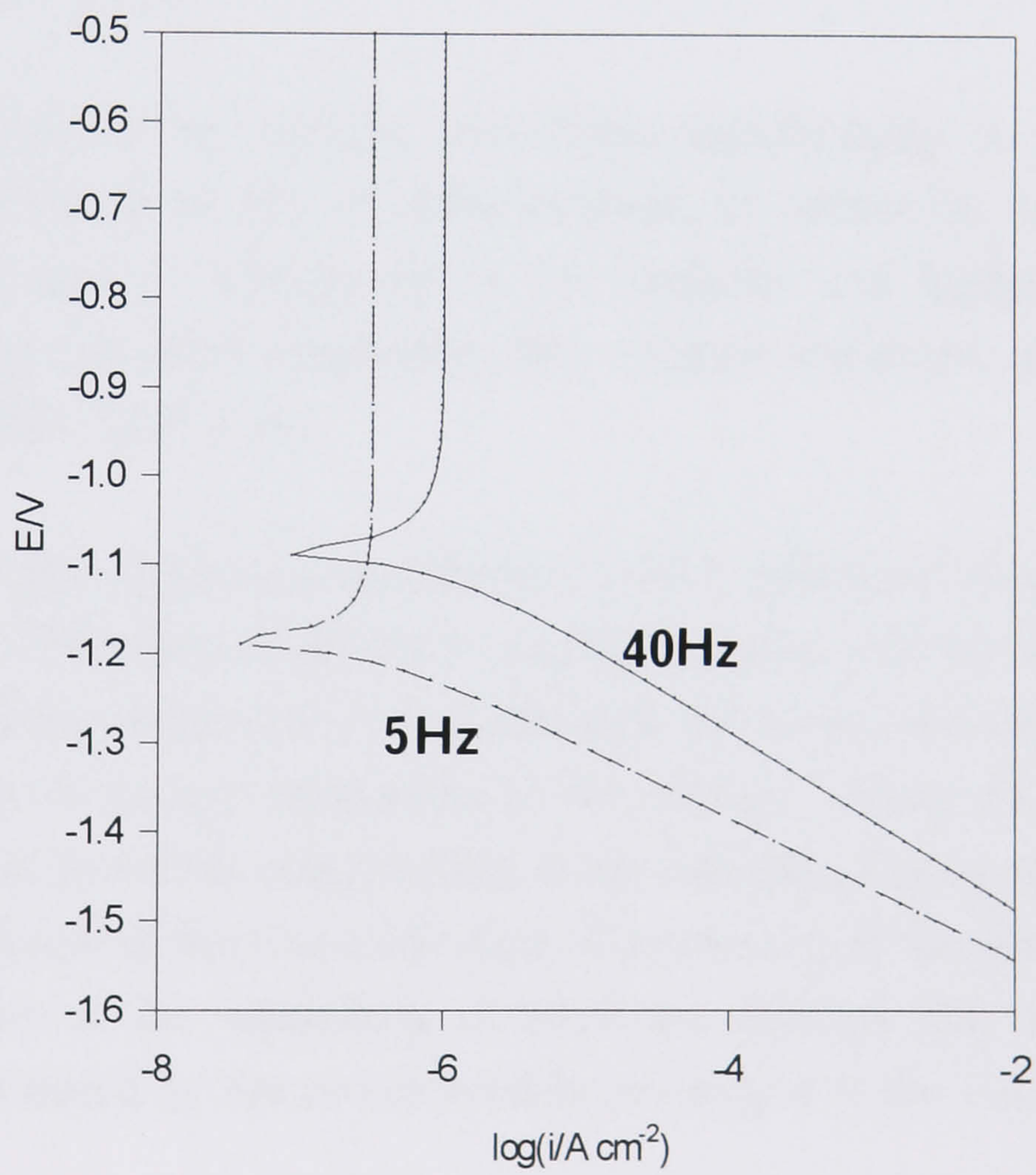

Fig. 3.7 Predicted E - logi graph for different rotation speeds, 5 and 40 Hz. The Tafel slopes are arbitrary and less than 0.12V dec^{-1}

The Tafel slope then becomes less than 0.12V decade^{-1}. It could perhaps fall to 0.09V decade^{-1}.

Oxygen Reduction Reaction Mechanism

In this system, at the surface of the oxide layer, the activation energy for the reduction of oxygen is lower than that required for the reduction of water. So, although the oxygen concentration is only 1mM in solution at saturation, it is reduced in preference to the water. In the absence of oxygen, the cathodic reaction involves release of hydrogen, formed from the reduction of water,

$$H_2O + e^- \rightarrow 1/2\ H_2 + OH^- \qquad (3.1)$$

In the presence of oxygen there is also the reaction,

$$O_2 + 4e^- + 2H_2O \rightarrow 4OH^- \qquad (3.2)$$

as well as the reduction of water. Hence, the corrosion rate in the presence of oxygen is greater then when in its absence, (since the anodic current must balance that of the cathodic).

At pH 8.2, the reduction of oxygen contributes significantly to the corrosion current. This is reflected in the 10 fold increase in corrosion current that is observed when oxygen is introduced to the solution. At higher pH values, hydroxide dissolution is more important than oxygen reduction in determining the corrosion rate (see Table 3.2).

If the slow step of the reduction mechanism is the diffusion of oxygen to the surface of the oxide then the reduction of surface species will be independent of the number of electrons waiting to tunnel through the layer, and dependent upon the rate of diffusion of oxygen molecules to the surface. There should therefore be a current which is potential independent in the cathodic region, and dependent upon the rotation speed of the electrode disc. Conversely, if the slow step in the corrosion mechanism is the tunnelling of electrons through the layer, then the current will not be limited by the concentration of oxygen at the surface.

Using the Levich equation (3.3), it is possible to calculate the maximum current output that is expected in the oxygen diffusion controlled case. The diffusion layer thickness δ is given by;

$$\delta = 0.643\ \upsilon^{1/6} D^{1/3} \omega^{-1/2} \qquad (3.3)$$

where,

δ - Diffusion layer thickness, cm

ω- Rotation speed, Hz

υ - Kinematic viscosity of water = 10^{-2} cm^2 s^{-1}
D - Diffusion coefficient = 10^{-5} cm^2 s^{-1}

δ = 0.643/6.32 x 0.464 x 0.022
δ = **1.03 x 10^{-3} cm**

According to Fick's first law of diffusion,

$$i_d = nAFDc_b/\delta \qquad (3.4)$$

where,

i_d- Diffusion limited current, A
A - Surface area = 0.126 cm^2
n- Number of electrons being transferred (= 4 for O_2 reduction)
F- Faraday constant = 9.6484 x 10^4 C mol^{-1}
D- Diffusion coefficient = $10^{-5}cm^2$ s^{-1}
c_b- concentration of oxygen = 1x10^{-6} mol cm^{-3}
δ- diffusion layer thickness, cm.

i_d = 0.496 x 10^{-3} A
= 3.9 mA cm^{-2}

This current, however, is not of the same magnitude as the experimental value found at 40Hz under oxygen, which is of the order of μA. This suggests that the reduction of oxygen is not limited by its diffusion to the surface, but by electron tunnelling through the oxide layer.

From equations (3.3) and (3.4) we can show that,

$i_{d1}/i_{d2} = \delta_2/\delta_1 = (\omega_1/\omega_2)^{1/2}$
$= (40/5)^{1/2}$
= 2.9

One would therefore expect an increase in the current output by a factor of 2.9 in the diffusion limited case. On increasing the rotation rate from 5 - 40Hz however, this is not the case. The increase in corrosion current observed when the rotation speed is increased from 5 - 40Hz, is a factor of 1.2. Therefore, the results indicate that the system is only slightly dependent on rotation speed i.e. the concentration of oxygen at the surface of the electrode is comparable to that in the bulk solution.

Water Reduction Reaction Mechanism

For a bare metal such as gold, the reduction of water produces a cathodic Tafel slope of 0.12V dec^{-1}. In the case of aluminium however there is a passive surface layer which gives rise to deviations from this value depending on the layer thickness. The magnitude of the cathodic slope found here is less than that found by Burstein and Liu [4], and the observed corrosion currents are approximately 2 orders of magnitude lower than those reported by Burstein. This difference may be associated with the nature of the different surface pre treatments in the two experiments.

It is surprising that the current due to the cathodic reaction is independent of pH since there is strong evidence from the impedance measurements (see Figs 3.5 (a) and (b)), that the steady state thickness of the anodic film at a fixed potential decreases with increasing pH. Therefore, if the cathodic current had involved electron tunnelling across the anodic film, it should have increased at a constant potential with increasing pH, just as a systematic increase in the number of hydroalkylthiol monolayers on electrodes for the reduction of $[Fe(CN)_6]^{3-}$, results in a systematic decrease in the heterogeneous electron transfer rate [13].

The pH independence observed for the cathodic current on pure aluminium is analogous to that of lead used in lead acid batteries. The lead forms an oxide layer on its surface and the cathodic current becomes pH independent. This is thought to be due to the accummulation of hydroxide ions in the vicinity of the oxide layer following the reduction of water and/or oxygen molecules incorporated within the layer. The hydroxide concentration in this region can reach pH 11 and is independent of the surrounding electrolyte pH which remains weakly alkaline.

The mechanism of the cathodic reaction must be one of the following:

1. Electron transfer at the aluminium surface to water molecules which are present in the passive layer.

2. Electron transfer to water molecules from the surface of the passivating layer which contacts the solution. This is improbable since it is expected that the potential (ϕF) of the surface of the anodic film will change systematically with solution pH. This would cause the rate of the electron transfer reaction to change with pH, (if the OH^- ion were in equilibrium between the film and the solution, ϕ F would decrease by 60mV for an increase of the solution pH by one pH unit).

3. Electron tunnelling through the passive layer. This seems unlikely since the rate of the cathodic reaction is independent of the thickness of the passive layer.

Only explanation 1 above is consistent with the results reported here and those of Burstein and Liu [4]. The difficulties with explanation 1 are that;

(a) the water content of the passive layer must be approximately the same in all experiments

(b) the impedance data indicates that the passive layer is only approximately one monolayer thick at negative potentials.

3.2.2 The Kinetics of the Anodic Reaction in the Corrosion of Aluminium

Two cases are presented for possible anodic reaction mechanisms. Case 1 suggests that aluminium hydroxide is in equilibrium with aluminate at the oxide/solution interface, and the corrosion rate determining step is diffusion of aluminate into the bulk solution. Case 2 speculates that aluminium hydroxide is not in equilibrium with aluminate and that the slow step is the formation of aluminate.

*P*redictions

For 'case 1' the concentration profiles are shown in the first figure below.

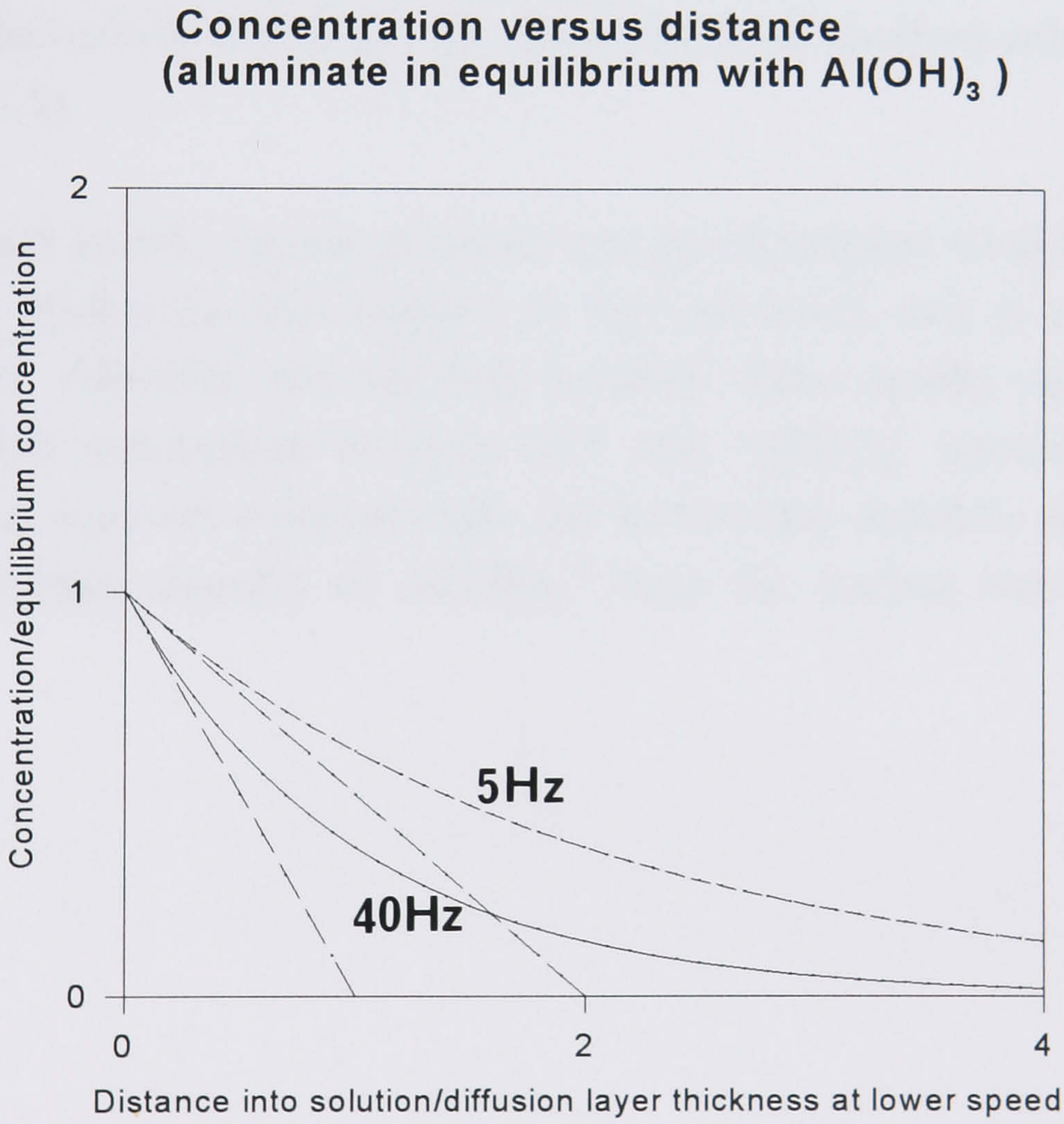

Fig. 3.8 Concentration versus distance profiles for 'case 1' (aluminate in equilibrium with $Al(OH)_3$) at 5 and 40 Hz.

The corrosion rate is given by,

$$i = 3AFDc_E / \delta \qquad (3.5)$$

where,

A = electrode area,
D = diffusion coefficient of aluminate,
c_E = equilibrium concentration of aluminate and δ is the thickness of the Nernst diffusion layer.

If this 'case 1' model is correct we would expect to find;

a) an anodic current which is independent of potential at low sweep speeds
b) an anodic current which increases with the square root of rotation speed
c) an anodic current which increases linearly with $[OH^-]$
d) an anodic current which can be calculated from standard solubility data using equation (3.5).

An increased anodic current at higher speeds of rotation would suggest that the aluminium hydroxide dissolution rate has increased, and is controlled by the diffusion of $Al(OH)_4^-$ into the bulk solution. These results would indicate that the corrosion mechanism involves OH^- and $Al(OH)_4^-$ species in equilibrium between the aqueous solution/oxide (or hydroxide) interface and that the slow step is the mass transfer of $Al(OH)_4^-$ from the surface into the bulk of the solution.

For 'case 2' the concentration profiles are shown in the second figure below.

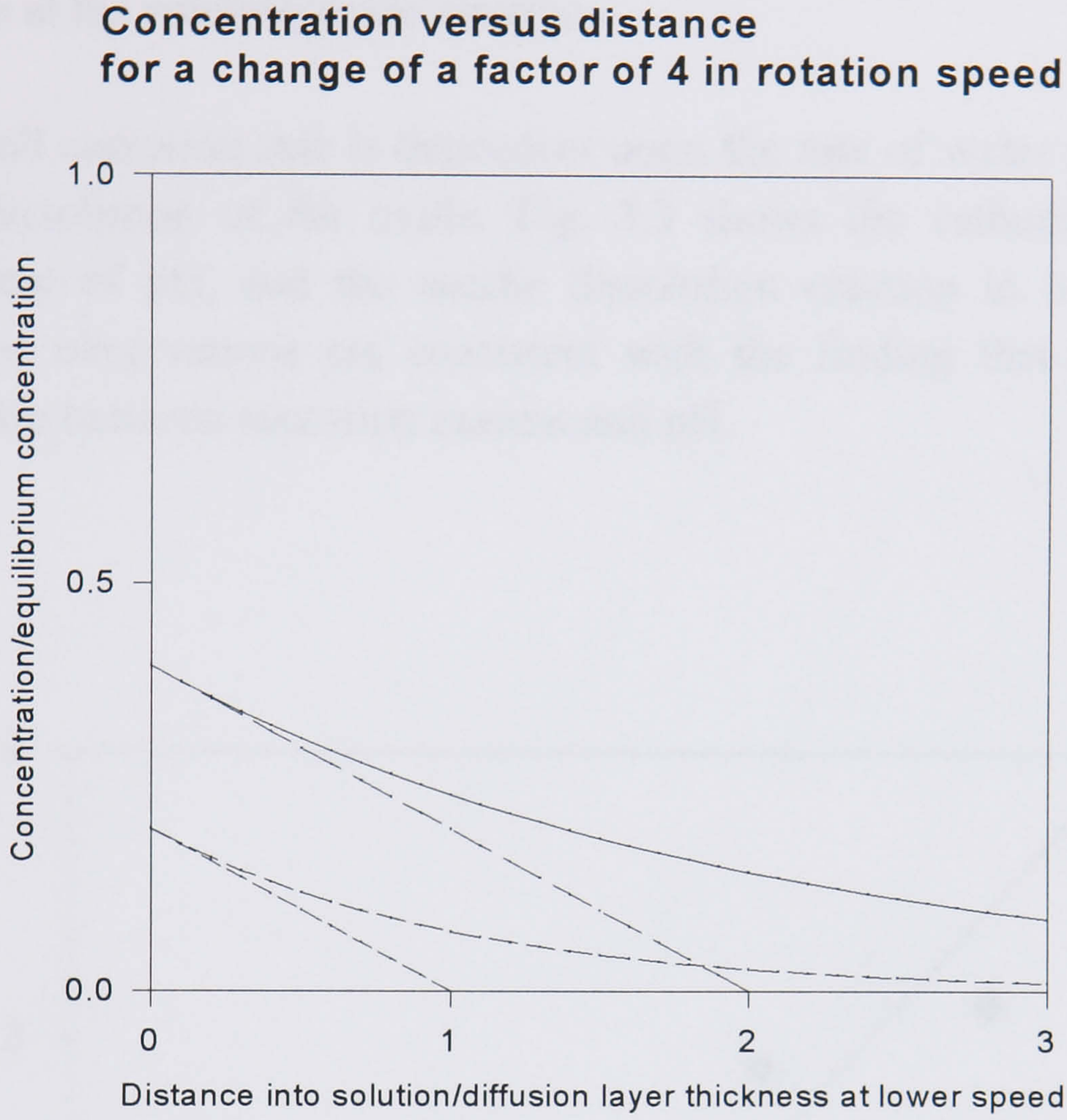

Fig 3.9 Concentration versus distance profiles for 'case 2' with a change of a factor of 4 in rotation speed.

If this model is correct we would expect to find;

a) an anodic current which is independent of potential at low sweep speeds
b) an anodic current which is independent of rotation speed
c) an anodic current which increases with $[OH^-]$
d) an anodic current which is less than that which can be calculated from standard solubility data using equation (3.5).

If the mechanism of oxide/hydroxide loss by the formation and subsequent dissolution of aluminate ions is correct, then in theory the driving force for

corrosion could be prevented if the electrolyte solution was saturated with aluminate ions. In this case a much lower corrosion current would be observed. Saturation of the solutions with sodium aluminate at pH 9 and 10 however, gave no significant decrease in the anodic or cathodic currents. This is further evidence to suggest that the slow step in the anodic reaction is the formation of aluminate at the solution/oxide interface.

The overall corrosion rate is dependent upon the rate of water reduction and the rate of dissolution of the oxide. Fig. 3.3 shows the cathodic reaction to be independent of pH, and the anodic dissolution reaction to be pH dependent. These two observations are consistent with the finding that there is a linear relationship between corrosion current and pH.

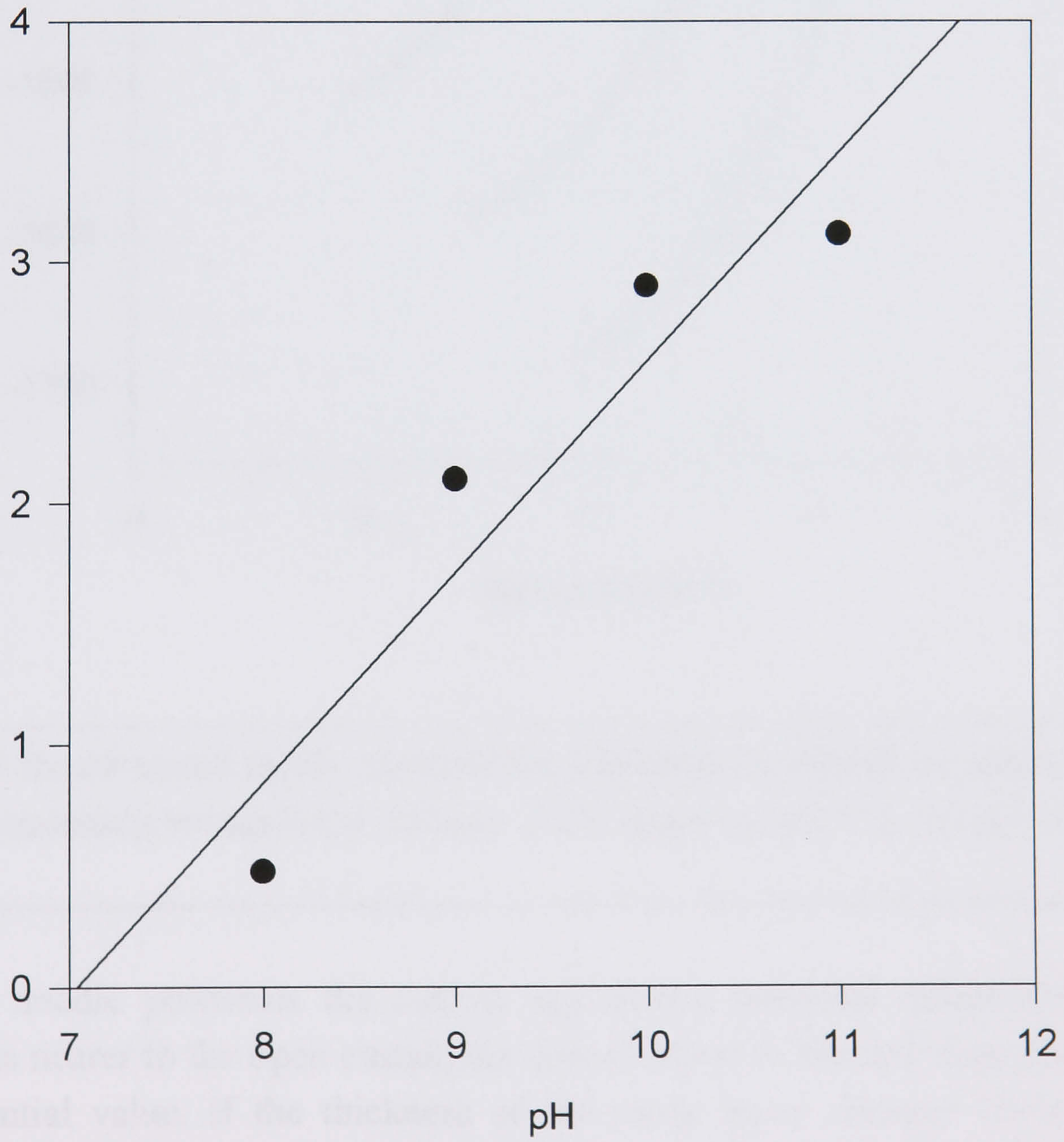

Fig. 3.10 Graph to illustrate the linear relationship between pH and corrosion current for pure aluminium in aqueous bicarbonate solutions.

Recalculated values for the anodic dissolution currents were obtained by extrapolating the cathodic hydrogen evolution Tafel line, positive to the OCP, and subsequently adding the two currents together at a specified potential. This is illustrated below in Fig. 3.11.

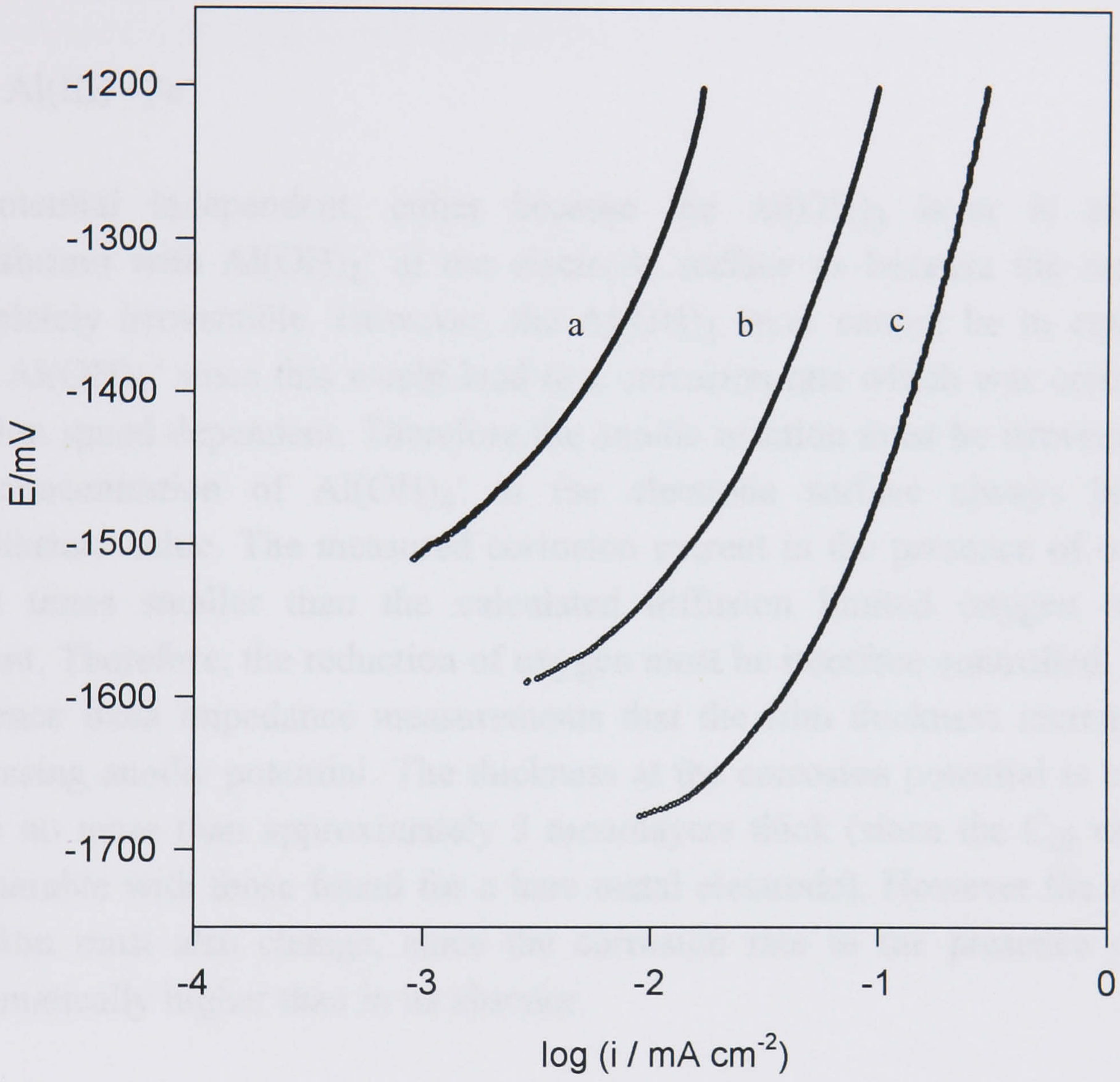

Fig. 3.11 Recalculated anodic currents for aluminium, obtained by subtraction of the corresponding extrapolated cathodic Tafel slope (a) pH 9.2, (b) pH 10,(c) pH 11.

At high anodic potentials the current approaches potential independence. At potentials nearer to the open circuit, the current starts to become dependent upon the potential value. If the thickness of the oxide layer changed linearly with potential then we would expect the anodic current to be independent of potential. However, this is not the case near to the OCP, although the anodic current becomes potential independent at high anodic potentials. This behaviour suggests that when the anodic film is very thin (near and cathodic to the OCP) it behaves

like a film of varying composition, whereas when it is comparatively thick it behaves as a film of constant composition.

The simplest model for a film of $Al(OH)_3$ on an electrode surface is one in which the hydroxide ions in the film are in equilibrium with the hydroxide in the solution, this equilibrium determining the potential at the film surface. This requires that the film thickness increases linearly with increasing anodic potential and that the rate of the anodic reaction,

$Al = Al(III) + 3e^-$

is potential independent, either because the $Al(OH)_3$ layer is always in equilibrium with $Al(OH)_4^-$ at the electrode surface or because the reaction is completely irreversible. However, the $Al(OH)_3$ layer cannot be in equilibrium with $Al(OH)_4^-$ since this would lead to a corrosion rate which was considerably rotation speed dependent. Therefore the anodic reaction must be irreversible and the concentration of $Al(OH)_4^-$ at the electrode surface always below its equilibrium value. The measured corrosion current in the presence of oxygen is 1000 times smaller than the calculated diffusion limited oxygen reduction current. Therefore, the reduction of oxygen must be interface controlled. There is evidence from impedance measurements that the film thickness increases with increasing anodic potential. The thickness at the corrosion potential is estimated to be no more than approximately 3 monolayers thick (since the C_{dl} values are comparable with those found for a bare metal electrode). However the nature of the film must also change, since the corrosion rate in the presence of O_2 is systematically higher than in its absence.

Summary

1. The rate of the cathodic reaction which occurs when aluminium corrodes in weakly alkaline solution i.e.

$H_2O + e^- = \frac{1}{2}H_2 + OH^-$

is a function of electrode potential but not of pH.

2. Since the thickness of the anodic film on aluminium varies with pH the reaction rate is independent of film thickness .

3. The observations are consistent with a mechanism in which the electrons react with water at the surface of the metal and water molecules incorporated within the anodic film.

4. The slow step in the anodic reaction,

$$Al + 4OH^- = Al(OH)4^- + 3e^-$$

is the formation of aluminate from the anodic film on the electrode surface.

References

[1] G. T. Burstein and C. Liu, 'Time resolved electrochemical impedance of the guillotined aluminium electrode', *Electrochim. Acta*, **39** (1994) p.873.

[2] T. Hurlen and A. T. Haug, 'Corrosion and passive behaviour of aluminium in weakly alkaline solution', *Electrochim. Acta*, **29** (1984) pp.1133-1138.

[3] B. A. Boukamp, 'Equivalent Circuit Users Manual', 2nd revised edition (1989).

[4] G. T. Burstein and C. Liu, 'The cathodic reaction during repassivation of aluminium in open circuit', *Corros. Sci.*, **37** (1995) pp.1151-1162.

[5] G. R. T. Schueller, S. R. Taylor and E. E. Hajcscar, 'Evaluation of natural oxides on aluminium in neutral borate electrolyte', *J. Electrochem. Soc.*, **139** (1992) pp.2799-2805.

[6] K. Kobayashi and K. Shimizu, 'Influence of γ-alumina on the structure of barrier anodic oxide films on aluminium', *J. Electrochem. Soc.*, **135** (1988) p.908-910.

[7] V. Vujicic and B. Lovrecek, 'A study of the influence of pH on the corrosion rate of aluminium', *Surface Technology*, **25** (1985) pp.49-57.

[8] R. R. Wiggle, V. Hospadaruk and E. A. Styloglou, 'The effectiveness of automotive engine coolant inhibitors for aluminium', *Materials Performance*, NACE, (1981) pp.13-18.

[9] K. Shimizu, G. E. Thompson and G. C. Wood, 'The duplex nature of anodic barrier films formed on aluminium in aqueous borate and borate-glycol solutions', *Thin Solid Films*, **85** (1981) pp.53-59.

[10] M. Fleishmann and H. R. Thirsk, *Advances in electrochemistry and electrochemical engineering*, edited by Gerischer and Delahey, Vol. 3, p.162.

[11] Southampton Electrochemistry Group, *Instrumental Methods in Electrochemistry*, Ellis-Horwood, (1985), p.313.

[12] C. F. Baes Jr., and R. E. Mesmer, The *Hydrolysis of Cations*, (1976) p.122, Wiley, New York.

[13] Israel Rubinstein, *Physical Chemistry, Principles, Methods, and Applications*, edited by Allen J. Bard, p.58, Dekker, New York.

CHAPTER 4

METAL WORKING FLUID CONCENTRATES AND EMULSIONS

4.0 Metal Working Fluid Concentrates and Emulsions

Work in this chapter includes corrosion rate measurements made on pure aluminium in contact with oil in water emulsions. The results were compared to those of aluminium in contact with an aqueous buffer solution of the same pH. Results are also reported with respect to the long term stability of the emulsion. Corrosion rates could not easily be determined for oxygenated or nitrogen saturated emulsions due to the foaming nature of the fluid brought about by continuous bubbling of gas through the cell, and measurements were made for aluminium in contact with aerated emulsions. Electron micrographs of the metal surface after various treatments were also obtained.

4.1 Corrosion of Pure Aluminium in Emulsions

The aluminium corrosion rate was approximately 10 times lower when the metal was in contact with a typical metal working fluid compared to when in contact with an aqueous borax buffer of the same pH (Tables 4.5 and 4.6). Over a longer period of time (24 hrs), the corrosion appears to be non-uniform.

Corrosion in the Presence of Amines

Average values for corrosion currents from repeated experiments are shown in table 4.1 again with a 30% error margin to allow for the irreproducibility of the system.

Table 4.1 Corrosion currents for pure aluminium in contact with aqueous solutions pH 9.2, rotation speed 5 Hz, sweep rate 1mV s^{-1}

Solution	pH	Gas	Estimated Corrosion Current ($\mu A\ cm^{-2}$)	OCP /mV
Borax	9.2	N_2	1.3 ± 0.4	-1250
Borax	9.2	O_2	4.0 ± 1.2	-1000
Borax + Amines*	9.2	N_2	2.4 ± 0.7	-1300
Borax + Amines*	9.2	O_2	3.0 ± 0.9	-1050

*0.05M borax, with amines in the following concentrations: 0.07M monoethanolamine + 0.016M triethanolamine, (the pH was adjusted to 9.2 with boric acid).

In an aqueous solution, the presence of amines does not significantly change the corrosion rate of aluminium when compared to that measured in the absence of amines at the same pH.

Measurements were made on aqueous solutions containing double the concentration of amines compared to that found in the standard emulsions.

Table 4.2 Amine concentrations in 0.05M borax solutions.

Solution	Composition	Concentration of Amine M
1	4.30g monoethanolamine	0.070
2	5.25g diethanolamine	0.050
3	2.40g triethanolamine	0.016
4	4.30g monoethanolamine + 2.40g triethanolamine + 3.0g monoethylene glycol	0.086

N.B The pH of the amine solutions above was adjusted to pH 9.2 with boric acid solution.

Monoethylene glycol was included in solution 4, because it is included in the water phase of the original oil concentrate as an intended anti freeze.

Table 4.3 Corrosion rates of pure aluminium in contact with aqueous amine solutions pH 9.2, rotation speed 5Hz.

Solution	pH	Gas N_2/O_2	Estimated Corrosion Current /μA cm^{-2}	OCP /mV
Borax	9.2	N_2	1.7 ± 0.5	-1237
"	9.2	O_2	4.0 ± 1.2	-1011
"	10.0	N_2	15.0 ± 4.5	-1412
"	10.0	O_2	51.0 ±15.3	-1190
Sol^n. 1	9.2	N_2	1.6 ± 0.5	-1182
"	9.2	O_2	4.5 ± 1.4	-886
Sol^n. 2	9.2	N_2	1.9 ± 0.6	-1071
"	9.2	O_2	5.1 ± 1.5	-772
Sol^n. 3	9.2	N_2	0.8 ± 0.2	-1135
"	9.2	O_2	2.7 ± 0.8	-879
Sol^n. 4	9.2	N_2	2.4 ± 0.7	-1288
"	9.2	O_2	3.0 ± 0.9	-1058

N.B. For the above solutions 1-4 the composition is as described in table 4.2.

The amines had no significant effect of reducing the corrosion rate of aluminium in aqueous borax solution, even when included at double the original concentration.

In order to determine whether there was any inhibiting effect found at higher amine concentration levels, solutions were prepared near to saturation e.g. 1M monoethanolamine and triethanolamine. The pH of the solutions was maintained at 9.2 using boric acid powder.

Table 4.4 Corrosion rates of pure aluminium in contact with aqueous 1M amine solutions, pH 9.2, rotation speed 5Hz.

Solution	Gas	Current Density /μA cm^{-2}	Rest Potential /mV
1M triethanolamine	N_2	1.78	-748
1M triethanolamine	O_2	0.35	-685
1M monoethanolamine	N_2	0.43	-407
1M monoethanolamine	O_2	0.10	-168

In the presence of 1M amine solutions the corrosion rate of aluminium was reduced only slightly. The OCP was significantly higher than that observed when aluminium is immersed in more dilute amine solutions.

4.1.1 Discussion

The corrosion currents of the 1M solutions were lower than that of the dilute solutions. However, it was considered impractical and expensive to include the amines in the formulation at this concentration level, and given that the inhibiting effect that is observed is only slight, experiments were not pursued any further.

None of the combinations of amines in solutions 1-4 (Table 4.3) have any significant inhibiting effect on the corrosion rate of aluminium. The amines are included in the concentrate formulation as intended aluminium corrosion inhibitors. However, the exact corrosion inhibiting mechanism is not fully understood. The pH is the main factor controlling the rate of corrosion, and not in this case the concentration of the amine inhibitor. It may be possible to exclude these amines altogether and control the corrosion rate by maintaining the pH of the solution. This would have several commercial benefits.

The reasons for the eliminating the amines from the original cutting fluid formulation are as follows;

i) Cost
ii) Amines are nitrogen containing and enhance the growth rate of bacteria
iii) Mono- and diethanolamine can cause staining of aluminium aerospace alloys and are aggressive towards some additives rendering them ineffective.
iv) Microbial degradation with production of ammonia
v) They serve no purpose in the inhibition of corrosion other than maintaining the pH. It is known however, that they interact with boric acid i.e. $R\text{-}NH_3^+H_2BO_3^-$, H_3BO_3 also included in the original formulation. This enhances the overall buffering capacity of emulsion, important for inhibiting the growth of bacteria and the long term stability of the fluid [1].

Removing amines from the formulation would increase the cost effectiveness and simplicity of the working fluid, that is providing an alternative solution which is stable and maintains the pH at around 9 could be found. New oil concentrate formulations were prepared at the Production Engineering and Technology site, Castrol International (see Table 2.1). A clear concentrate could only be prepared with bicarbonate buffer as a replacement for the amine/boric acid containing water phase. No combination of decouplers was found to give a stable concentrate with the aqueous borax buffer as the water phase.

4.2 Impedance and Corrosion Rate Measurements on Aluminium in the Presence of Emulsions A and B

The corrosion rate studies that have been carried out by workers [2-5], are on aluminium in contact with oil in water emulsions, and are in conjunction with the biodegradability of the fluids. They found that degradation leads to changing pH and separation of the fluid. The pitting corrosion potential of aluminium was found to occur at more active values compared to when immersed in a sterile medium [6].

Electrochemical measurements were carried out on propriety, and experimental cutting fluid emulsions. On changing the electrolyte from a pure water phase to an oil in water emulsion, the rest potential became more negative, and the corrosion current decreased. The following results were obtained from measurements made on aluminium in contact with 5% aerated emulsions and with an electrode rotation speed of 5Hz. The results showed an approximate 10 fold decrease in the corrosion rate of aluminium, compared to those results

obtained for aluminium when immersed in an aqueous electrolyte at the same pH. On rotation for 24 hours, a further 10 fold decrease in corrosion rate was observed.

Table 4.5 Corrosion currents and impedance elements for pure aluminium in contact with an aerated oil in water emulsion pH 9, rotation speed 5Hz.

Time After Immersion	**i_c /μA cm^{-2}**	**OCP /mV**	**Capacitance /μF cm^{-2}**	**Charge Transfer Resistance /10^{4}Ω cm^2**
20 mins	0.30	-1400	10.1 ± 1.0	8.2
24 hrs	0.04	-1490	1.8 ± 0.5	9.9

Table 4.6 Corrosion currents for pure aluminium in contact with emulsion formulations A and B (Table 2.1) after 1 and 24 hrs, rotation speed 5Hz.

Emulsion	**i_c/μA cm^{-2}**		**OCP /mV**
	1hr	**24hrs**	
A	0.28	0.018	-1412
B	0.31	0.035	-1465

Within the limits of experimental error, the corrosion rates and impedance elements of aluminium in contact with emulsions A and B were found to be the same.

The graph below indicates the extent to which a pure aluminium electrode corrodes depending on the conditions to which it is exposed.

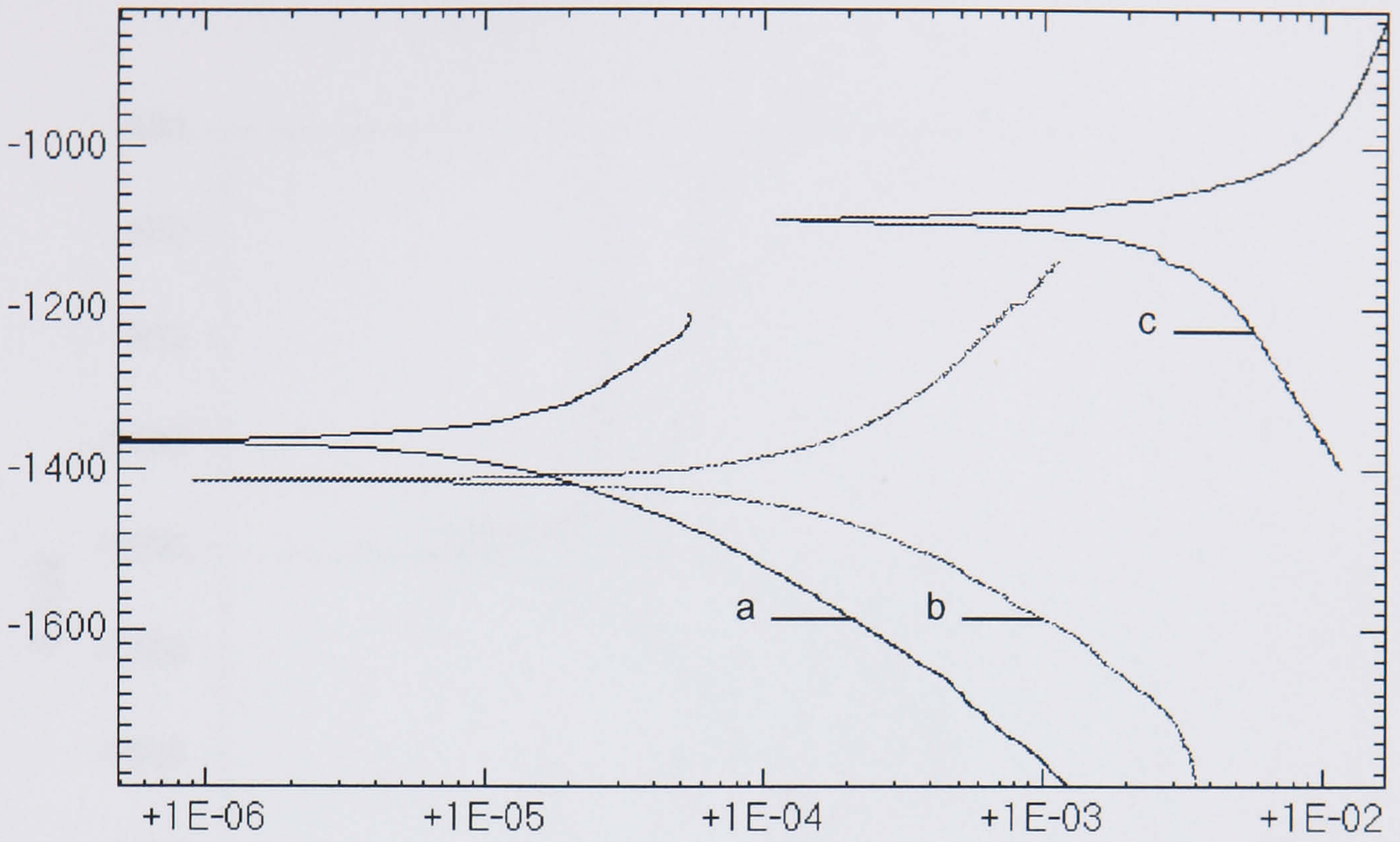

Fig. 4.1 Tafel plots indicating the extent to which a pure aluminium electrode corrodes depending on the conditions to which it is exposed, sweep rate 1mV s^{-1}; (a) 5% emulsion of concentrate B in distilled water after 24 hours (aerated), (b) 5% emulsion of concentrate B in distilled water after 1 hour (aerated), (c) 0.05 M oxygenated borax electrolyte

The behaviour of aluminium in contact with a cutting fluid emulsion is shown in Fig. 4.2 below, where it is compared to behaviour when in contact with an aqueous solution of the same pH.

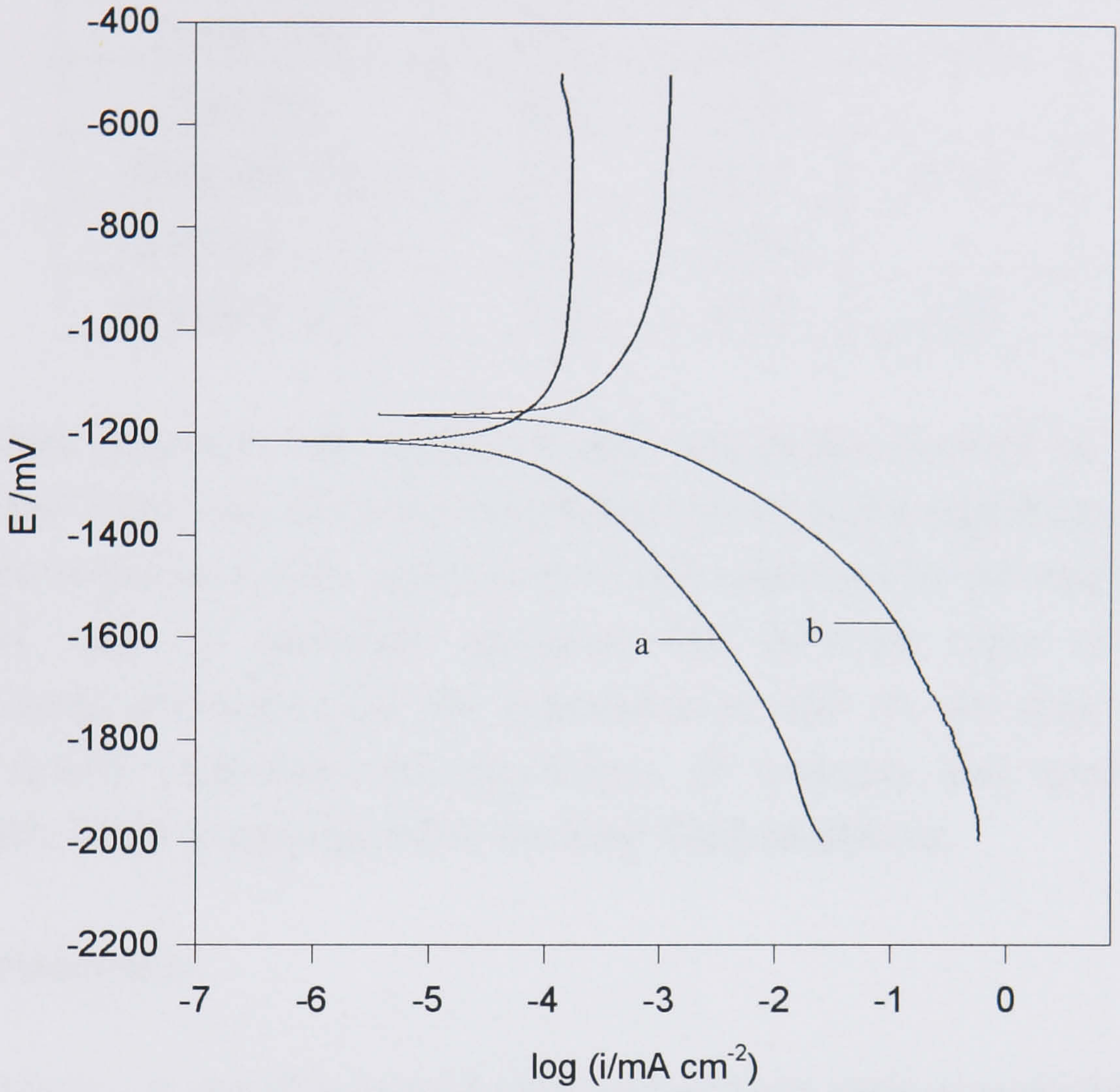

Fig. 4.2 Graph to show the anodic and cathodic corrosion currents of aluminium, sweep rate 10mV min^{-1}, in contact with (a) 5% cutting fluid emulsion (formulation A) and (b) bicarbonate buffer solution, pH 9.2.

Both the anodic and cathodic currents decrease in the presence of an emulsion.

The Effect on the Corrosion Rate of Aluminium when in Contact with Emulsions Prepared using Different Water Types.

Tafel analysis was carried out on aluminium in contact with emulsions prepared using different oil to water ratios and water types.

Table 4.7 Corrosion rates of aluminium after 1hr and 24hrs in contact with 2.5%, 5% and 10% emulsions prepared using various types of water.

Electrolyte	pH	$i_c/\mu A\ cm^{-2}$		OCP/mV
		1hr	24hrs	
Purite 5%	9.2	0.13	0.01	-1435
Tap 5%	8.8	0.23	-	-1480
Distilled 5%	9.2	0.31	0.04	-1510
Distilled 2.5%	9.2	1.60	-	-1465
Distilled 10%	9.0	0.28	0.04	-1570

Emulsions prepared with waters of different purity showed no variation in the initial and final rates of corrosion although there was a significant further 10 fold decrease in the corrosion current, when left immersed in the emulsion for 24 hrs. The pH value of emulsions prepared with different types of water differed significantly depending on the concentration and on the type of water used. These results emphasise the importance of accuracy and specification to the consumer when preparing metal working fluid emulsions.

4.2.1 Discussion

Formulations A and B prepared with and without amines respectively, were both shown to cause similar corrosion rates of aluminium when left in contact for short periods of time. It is concluded that amines do not inhibit the rate of corrosion at the concentrations at which they are included in the original formulation, in a purely aqueous phase, or as components of an emulsion.

The cutting fluid causes both the anodic and cathodic processes to be reduced in rate, so that the overall corrosion rate is reduced by a factor of approximately 10. The reduction of the rate of the cathodic process is due to the competition of the oils in the emulsion with water molecules, for contact with the metal oxide surface. The composition of the passive layer may also be modified by the presence of the hydrophobic species.

The OCP drops significantly when the emulsion is in contact with the aluminium. OCP values for aluminium are significantly more negative in the presence of an emulsion compared to when in an aqueous solution. This may be attributed to the prevention of the cathodic water reduction reaction at the oxide/solution interface, as is the case when a thick oxide layer is produced on the metal surface by anodic polarisation (see discussion 3.2). Hence, the potential on open circuit lies closer to that of the calculated equilibrium potential (-2.12V). The oil molecules form an extra protective barrier between the metal and the electrolyte solution. The composition of the passive layer may also be modified by the presence of the hydrophobic species, also resulting in a lower OCP and rate of corrosion.

On increasing the concentration from 2.5 to 10.0 %, the corrosion rate decreased. If the oil molecules were forming an additional protective layer on the oxide surface, then as the concentration increased, the corrosion current would be expected to decrease, as was observed. This is due to the decreasing rate of water reduction that occurs. This result is in agreement with results obtained by workers at Pangbourne [7]. Here PE278 fluid was tested at 3, 5, and 7 % concentrations in distilled water. The criteria used for evaluating the fluids was based on a metal thread formation test. As expected the performance decreased on dilution from 7 - 5 - 3 %, as did the corrosion rates as described above.

4.3 Scanning Electron Microscopy (SEM)

Aluminium squares 1.5cm^2 were pre-treated in 1M NaOH for 8 minutes without stirring before being immersed in various solutions (a)-(d). After exposure for 24 hrs the samples were washed with water and dried in air. Electron micrographs were obtained on an S-2400 Hitachi Scanning Electron Microscope at the University of Newcastle upon Tyne.

Figure 4.3 shows SEM micrographs of pure aluminium surfaces after exposure for 24 hours to (a) 0.05M borax pH 9.2, (b) 0.05M borax pH adjusted to 10.2, (c) 0.22M sodium carbonate + 0.82M sodium hydrogen carbonate (adjusted to pH 9.2 with sodium hydroxide solution) and (d) 5% emulsion of concentrate B in distilled water.

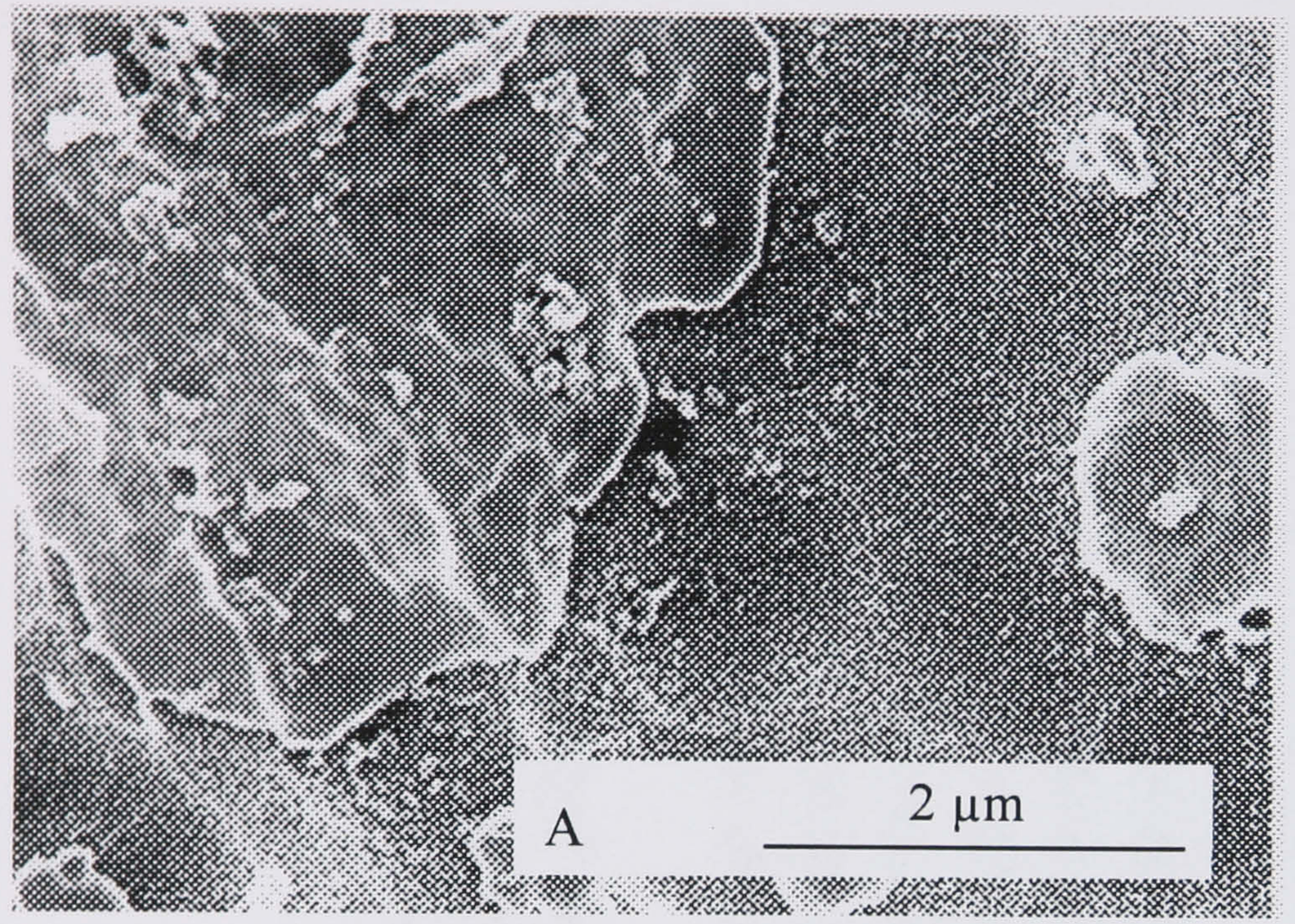

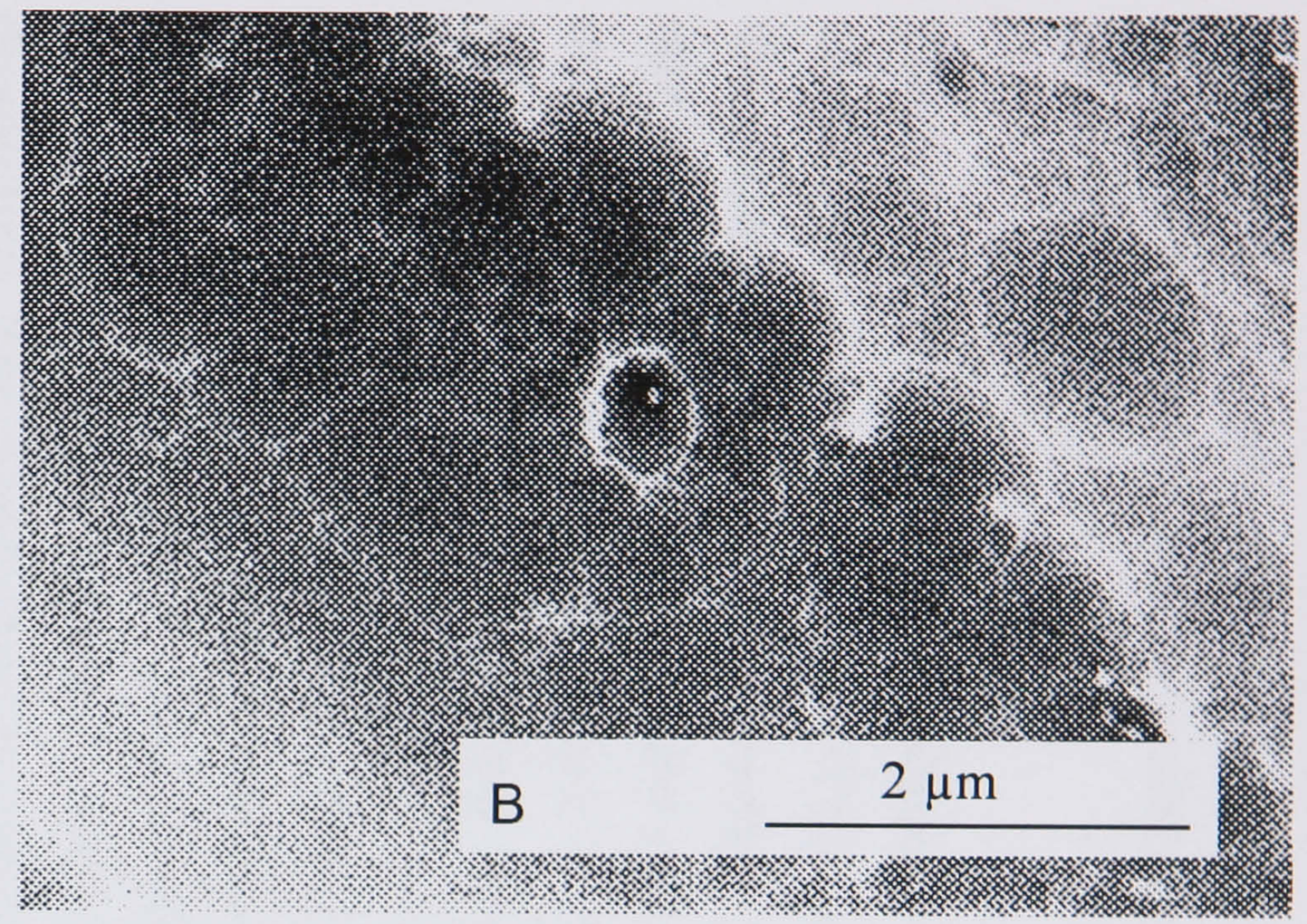

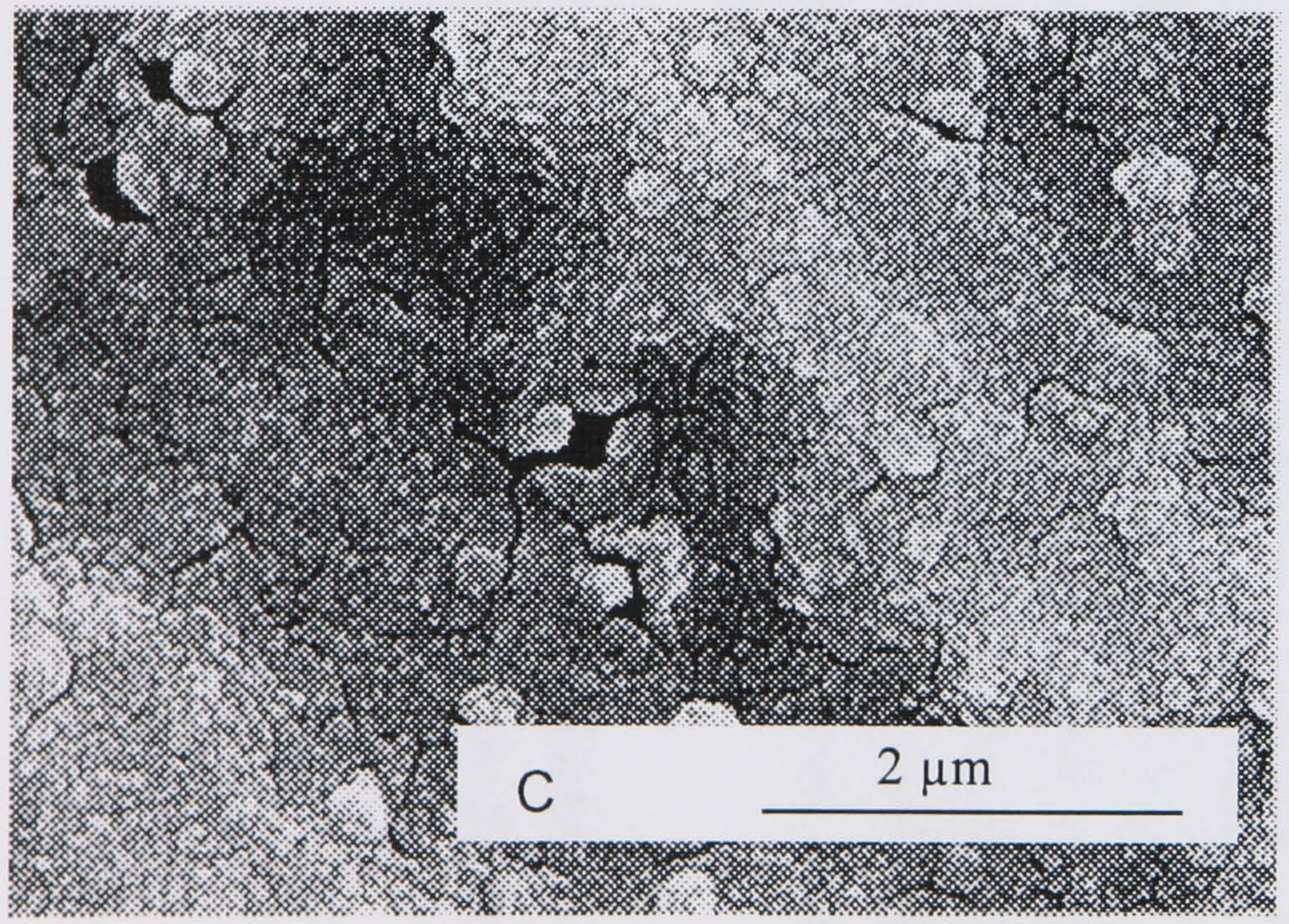

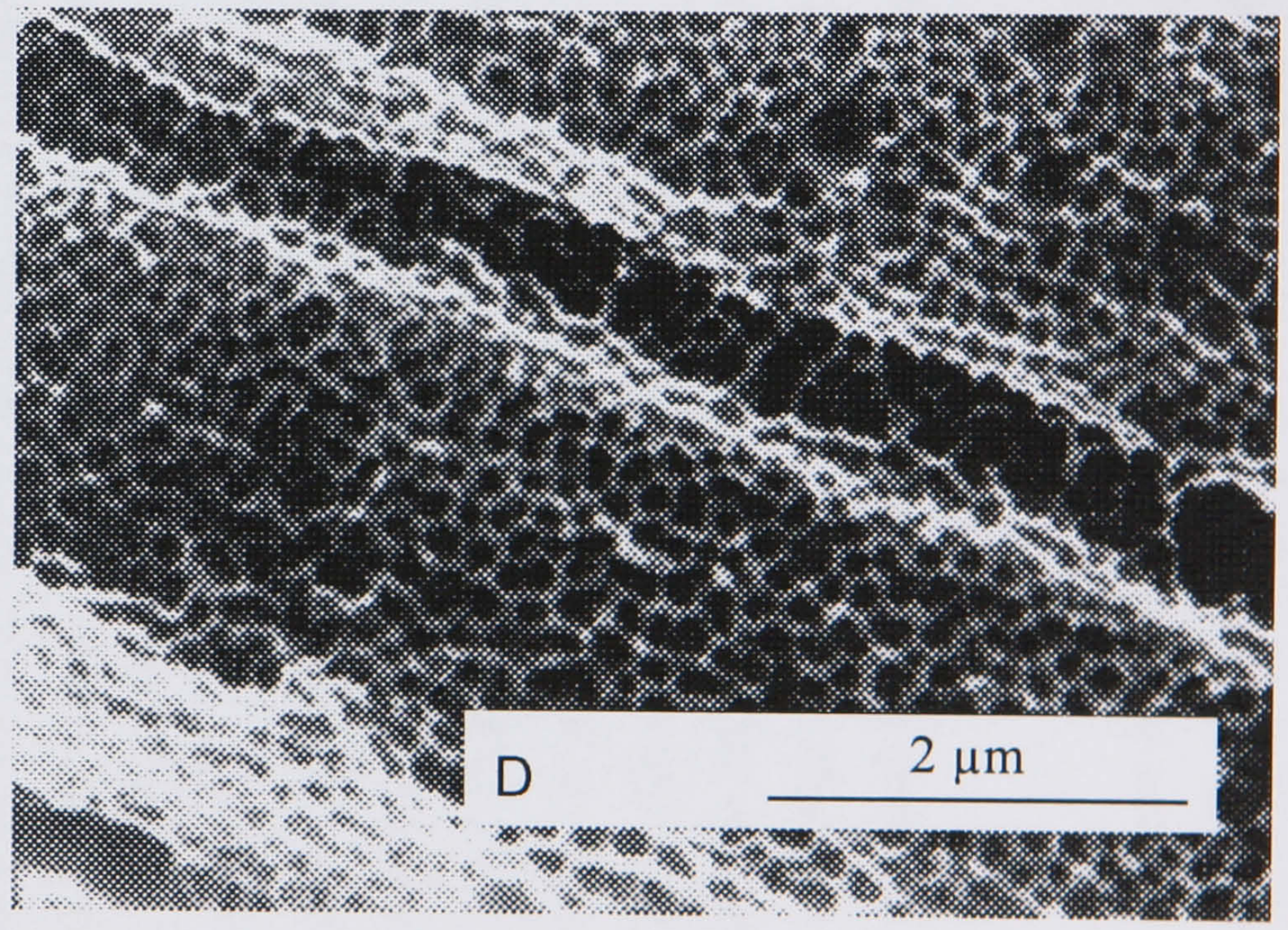

Fig. 4.3 (a)-(d) SEM Micrographs

4.3.1 Discussion

Exposure to a 5% oil in water emulsion causes a systematic 10 fold decrease in the initial corrosion rate at both pH 9 and pH 10, compared to that in an aqueous solution buffered to the same pH. This is thought to be caused by a decrease in rate of the oxygen reduction reaction at the oxide/solution interface, and the result of adsorption of a monolayer of oil onto the electrode surface acting as a physical barrier.

The nature of the surface is different depending on the type of anion present and on the pH of the electrolyte. When in contact with aqueous pH 10 solution (b), the surface appears much smoother perhaps as a result of the higher corrosion rate (being related to a greater rate of dissolution of the oxide). (a) and (c) indicate the difference in nature of the surface layer after exposure to aqueous borax and bicarbonate solutions respectively. The micrographs show that the nature of surface layer is 'pocked' and in general dependent upon the electrolyte with which it is in contact. In particular with oily emulsions, the surface appears to become regularly porous producing a 'honeycombed' effect after exposure for 24 hrs, Fig. 4.3(d). This is consistent with findings in the literature [8,9]. It is generally assumed that porous oxides are formed in electrolytes promoting oxide dissolution. The structure of porous oxides is thought to be a close packed array of columnar hexagonal cells, each containing a central pore normal to the substrate surface. From the present findings it is thought that oily molecules wet the metal oxide surface, providing an additional protective layer which is porous in nature like the oxide layer beneath it to which it adheres. This also provides evidence to substantiate the experimental findings that the corrosion rate is approximately 10 times lower in the presence of an emulsion, compared to when in contact with a purely aqueous solution.

Impedance measurements suggest that the thickness of oxide/hydroxide on the surface is initially the same as that in the water phase, but increases in thickness when left in contact with an emulsion for 24 hrs.

4.4 Challenge Tests on Amine-Free/Formulation A Variants.

Five formulations, B and A1- D1 as shown in Table 2.1, were provided for challenge testing in order to determine how these variants performed in terms of stability, compared with the original formulation A. As described in experimental section 2.10.2, 2.5% and 5.0% solutions were prepared in 100ml mineral salts in 250ml conical flasks. Solutions were challenged daily with *Cephalosporium sp.* and *Pseudomonas aeruginosa.* The initial pH of each solution was recorded and adjusted where necessary to pH 9.0, using 0.5M HCl and/or 0.1M NaOH. The pH of the solution was measured at the end of each test.

Dry weights were obtained for fungal challenge tests, using the standard method 1/PE/146 as devised and carried out by workers at Castrol International (see Appendix A).

4.4.1 Bacterial and Fungal Challenge Tests

Both 2.5% and 5% solutions of the standard formulation A remained largely sterile throughout the test period as expected.

Table 4.8 Initial and final pH of fluids after bacterial and fungal challenge tests.

Sample	Emulsion Concentration %	Initial pH (bacterial)	Final pH	Initial pH (fungal)	Final pH
A	2.5	8.61	7.93	8.61	8.12
	5.0	8.70	8.27	8.71	8.33
B	2.5	8.36	7.18	8.39	7.88
	5.0	8.51	8.07	8.51	8.09
A1	2.5	8.28	4.54	8.30	6.58
	5.0	8.49	4.52	8.47	4.90
B1	2.5	8.28	4.53	8.28	6.73
	5.0	8.44	4.55	8.44	5.31
C1	2.5	8.14	4.57	8.20	5.54
	5.0	8.38	4.70	8.34	8.03
D1	2.5	8.34	4.59	8.35	7.40
	5.0	8.53	4.55	8.51	5.27

N.B. All initial pH values were adjusted to pH 9

Bacterial Growth

Both of the 2.5 % and 5% solutions of the standard formulation A remained sterile throughout the test period. Bacterial growth was recorded at 10^5 cfu/ml on the final day of the test in the 2.5% solution.

The 2.5% solution of amine and boron free version of standard formulation A remained sterile until day 24 of the test. Contamination was recorded at 10^3 cfu/ml, which rose to $10^6/10^7$ cfu/ml over the last two days of the test. The 5% solution of this product remained sterile throughout the test period.

Both the 2.5% and 5% solutions of blends A1 and B1 were heavily contaminated throughout the test period.

The 2.5% solution of blend C1 remained sterile until day 7 of the test when contamination was recorded at 10^5 cfu/ml. This quickly rose to > 10^{10} cfu/ml, remaining at this level duration of the test. The 5% solution of blend C1 remained sterile until day 13 when contamination was recorded at 10^{10} cfu/ml. The level of contamination remained at this value for the remainder of the test.

Both 2.5% and 5% solutions of blend D1 were heavily contaminated, $10^9/10^{10}$ cfu/ml, with bacteria for the duration of the test.

Fungal Growth

Both the 2.5% and 5% solutions of amine and boron free version of formulation A were sterile throughout the test period.

Both concentrations of blend A1 gave similar results, contamination being recorded from day 1 at 10^3 cfu/ml. The level of contamination gradually increased throughout the test to a level of 10^6 cfu/ml on completion of the test.

Both concentrations of blend B1 performed similarly throughout the duration of the test. Both samples were sterile until day 7 of the test when contamination at 10^3 cfu/ml was recorded. The level of contamination increased slightly to 10^5 cfu/ml on completion of the test.

Both concentrations of blend D1 gave similar results. Both remained sterile until day 7, when contamination at 10^3 cfu/ml was recorded. The level of contamination then slowly increased to 10^6 cfu/ml over the test period.

The 2.5% solution of blend C1 remained sterile until day 14 of the test when contamination was recorded at 10^2 cfu/ml, this increased to 10^6 cfu/ml over the final two weeks of the test. The 5% solution of blend C1 also remained sterile until day 14 of the test when contamination was recorded at 10^2 cfu/ml for 4 days. The sample then became sterile but contamination at 10^2 cfu/ml was recorded on the final day of the test.

4.4.2 Biomass Accumulation

Table 4.9 Accumulation of fungal biomass during challenge testing.

Sample	Concentration %	Initial weight (g)	Final weight (g)	Biomass (mg/100ml)	Biomass Development as % of Relevant Control
A	2.5	0.3150	0.3699	54.9	0
	5.0	0.3256	0.4048	79.2	0
B	2.5	0.3408	0.4264	85.6	55.9
	5.0	0.3404	0.4259	85.5	8.0
A1	2.5	0.3470	0.5599	212.9	287.8
	5.0	0.3332	0.6239	290.7	267.0
B1	2.5	0.3358	0.5630	227.2	313.8
	5.0	0.3228	0.4693	146.5	85.0
C1	2.5	0.3245	0.6758	351.3	539.9
	5.0	0.3088	0.3911	82.3	3.9
D1	2.5	0.2979	0.4683	170.4	210.4
	5.0	0.3050	0.5523	247.3	212.2

The standard formulation A recorded an average biomass accumulation of 67mg/100ml. All of the variations of the standard formulation showed increased biomass accumulations, which corresponded with fungal growth in the challenge tests.

4.4.3 Discussion

The control standard formulation A remained free from bacterial and fungal contamination throughout the test period. This is as expected as it contains both the biocide and fungicide components.

The amine/boron free version performed as well as the control in the fungal challenge test. Again this was as expected since the formulation contains both the biocide and fungicide. The 2.5% solution of this product did become contaminated towards the end of the test period. The 5% solution remained free from bacterial contamination throughout the test.

Blend A1 became heavily contaminated with both fungi and bacteria as expected as the formulation contains no biocide or fungicide. Blend D1 containing both the biocide and fungicide showed unexpectedly high levels of growth for both concentrations throughout the test. The fungal results are similar to those for blend B1.

In summary, all of the variations performed worse than the standard formulation A, in terms of microbial growth. It can not therefore solely be the action of the biocides and fungicides that inhibits the growth of bacteria in the emulsion. The buffering action of the boric acid and amines, together with the anti-bacterial properties of the boric acid included in the water phase of the concentrate, provide added protection against microbial growth, which is essential as far as the long term stability of the fluids is concerned. In order to pursue the bicarbonate/carbonate formulation further in terms of large scale production, more work is necessary. An amine free concentrate with boric acid included would be one possibility taking the present results into account.

4.5 Buffering capacity

Acid-base titrations were carried out in order to determine the relative buffering capacities of the standard emulsion and the new concentrate formulation B, as described in experimental section 2.3.5.

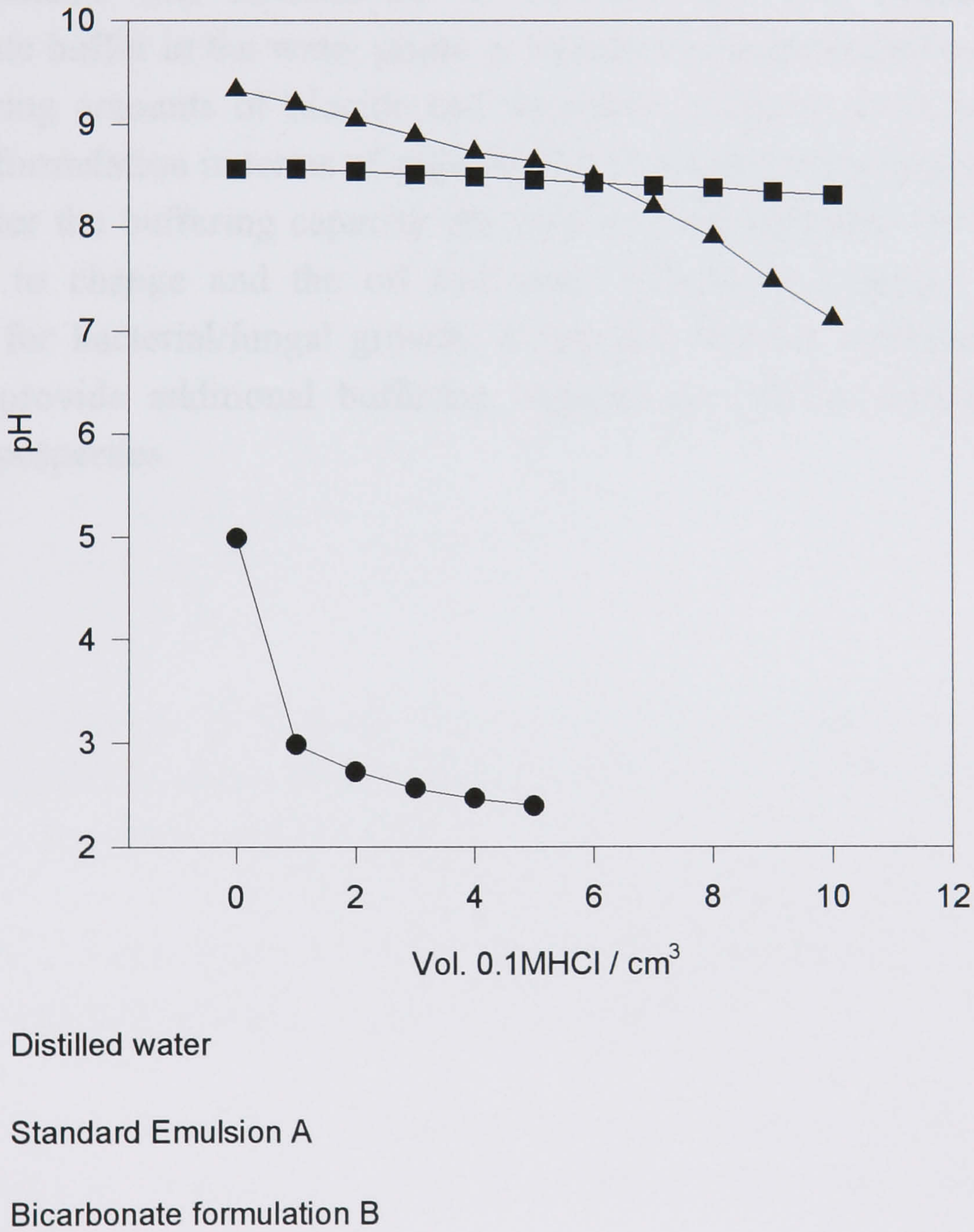

Fig. 4.4 Buffering capacity curves obtained for distilled water and emulsions A and B vs. 0.1M HCl.

The results can be expressed as the volume of acid required to create a change of 0.1 pH units. Distilled water has no buffering capacity and requires less than

0.1cm^3 of 0.1M HCl to make a 0.1 unit change in pH. Conversely, the standard emulsion needed approximately 5.0cm^3 of acid to create the same change in pH, whilst the experimental emulsion B, required about 1.0 cm^3.

4.5.1 Discussion

These results show that the buffering capacity of the original standard emulsion is greater than that of the new formulate. Because the difference is almost negligible we could conclude that this has no significance in practical terms to the make up of the concentrate. It is only until after a period of time has elapsed that the effects become noticeable. Results from the challenge tests (section 4.4.1), indicate that formulation A variations (A1-D1) prepared with the bicarbonate buffer in the water phase in replace of the boron/amine complex and with varying amounts of biocide and fungicide, perform much worse than the standard formulation in terms of stability. This becomes more apparent with time. The weaker the buffering capacity the greater is the tendency for the pH of the emulsion to change and the oil and water phases to separate, providing an interface for bacterial/fungal growth. It appears that the boron/amine complex together provide additional buffering capacity as well as having some anti-bacterial properties.

References

[1] G. C. J. Morris, 'Preparation and Assessment of Hydrolytic Stability of Boric Acid/Alkanolamine Condensates and Boric Acid/Alkanolamine/Fatty Acid Condensates for Use in Methal Cutting Fluids', Wolverhampton Polytechnic, (1992) pp. 12-14.

[2] J. F. D. Stott, 'What progress in the understanding of microbially induced corrosion has been made in the last 25 yrs? A personal viewpoint', *Corr. Sci.*, **35**, (1993) pp. 667-673.

[3] H. W. Rossmore, 'Biostatic fluids, friendly bacteria, and other myths in metal working microbiology', *Lub. Eng.*, **49** (1993) pp. 253 - 260.

[4] B. M. Rosales, E. S. Ayllon, and M. C. Leiro, 'Accelerated test for determining microbiological-influenced corrosion resistance of aluminium alloys', *New methods for corrosion testing of aluminium alloys*, ASTM STP 1134, (1992) pp.50 -59.

[5] S. C. Dexter, D. J. Duquette, O. W. Siebert, and H. A Videla, 'Use and limitations of electrochemical techniques for investigating microbiological corrosion', *Corrosion*, NACE, **47** (1991) pp. 307-317.

[6] R. C. Salvarezza, M. F. L. de Mele and H. A. Videla, 'Redox potential and the microbiological corrosion of aluminium and it's alloys in fuel/water systems', *Br. Corros. J.*, **16** (1981) pp.162-168.

[7] K. Airey, 'Industrial and Marine Group Laboratory Report', TI 5924, (1992-1993) Castrol International, Pangbourne, Reading.

[8] A. Despic and V. P. Parkhutik, *Modern Aspects of Electrochemistry*, Electrochemistry of aluminium, Vol.20, (1959) pp. 401 - 501, edited by J. O'M. Bockris, Plenum.

[9] S. Ono and N. Masuko, 'The duplex structure of cell walls of porous anodic films formed on aluminium', *Corr. Sci.*, **33** pp. 503-507 (1992).

CHAPTER 5

GENERATION OF FRESH METAL SURFACES AND ELECTROCHEMICAL MEASUREMENTS *IN SITU*

5.0 Generation of Fresh Metal Surfaces and Electrochemical Measurements *in Situ*.

An experiment was devised whereby a rotating disc of aluminium was lowered onto a stationary glass frit, situated beneath it. In this way, electrochemical measurements could be made, *in situ* whilst the aluminium was being cut away.

Results for an abraded electrode and a stationary electrode, in aqueous and emulsion electrolytes are reported. Potential transients were also obtained from which information about the rate of oxide recovery could be deduced.

5.1 Corrosion Rates With and Without Abrasion of the Electrode Surface.

Fig. 5.1 shows the logi-E relationship for an electrode, with and without continuous abrasion, in situ with an aqueous bicarbonate buffer solution, (pH 9.2).

Cathodic currents increased by a factor of approximately 3 on abrasion. The jagged profile in Fig. 5.1(b) is attributed to the irregular nature of the abrasion process. This was reduced when the electrode was abraded in the presence of an emulsion, due to the lubricating action of the cutting fluid.

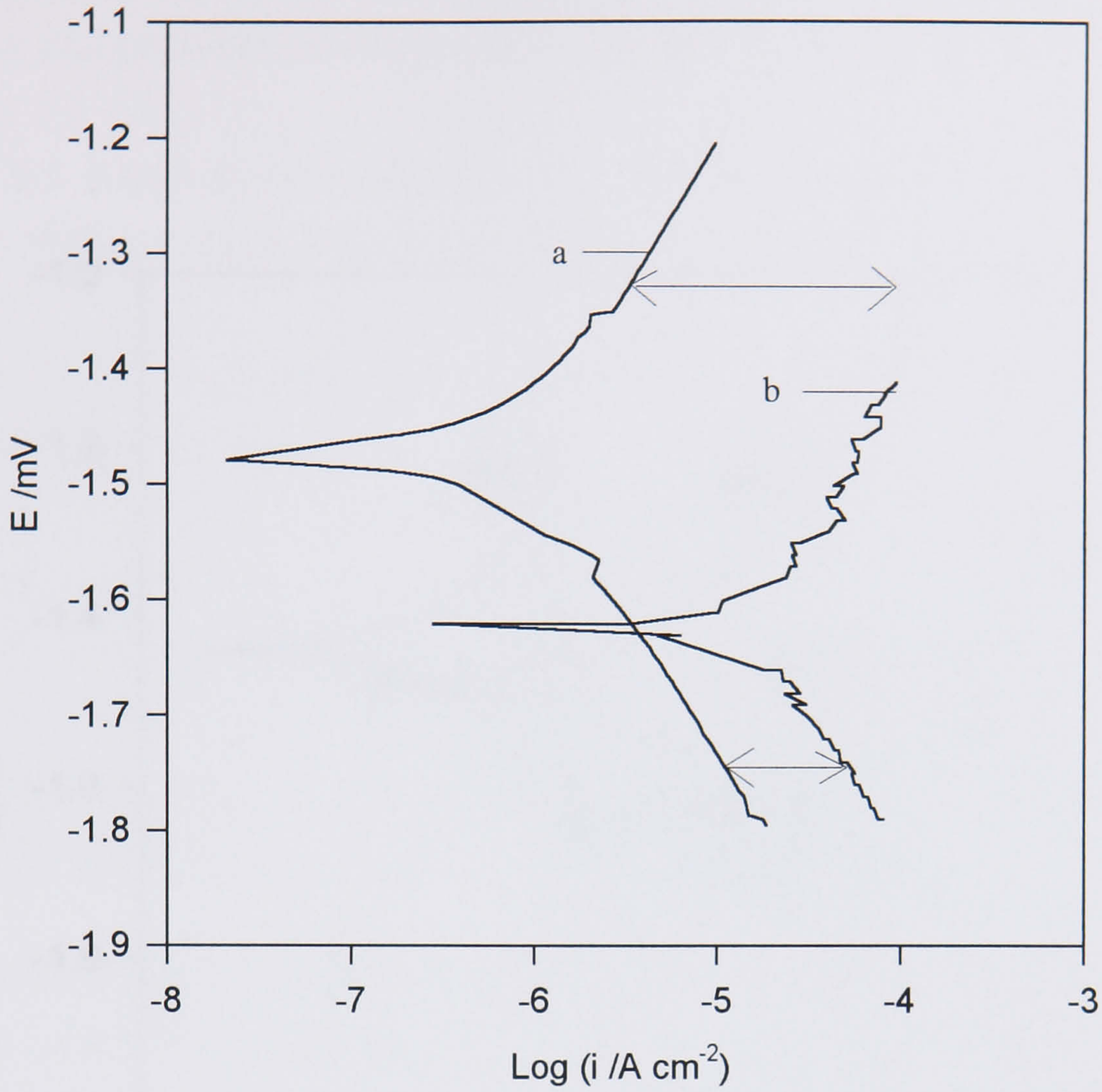

Fig. 5.1 Logi-E relationship obtained with (a), and without (b), continuous abrasion of a pure aluminium surface in contact with an aerated bicarbonate buffer solution pH9.2, rotation speed 5Hz, 5mV s^{-1}.

Both the anodic and cathodic Tafel lines shifted by a considerable factor with abrasion of the surface (Fig. 5.2).

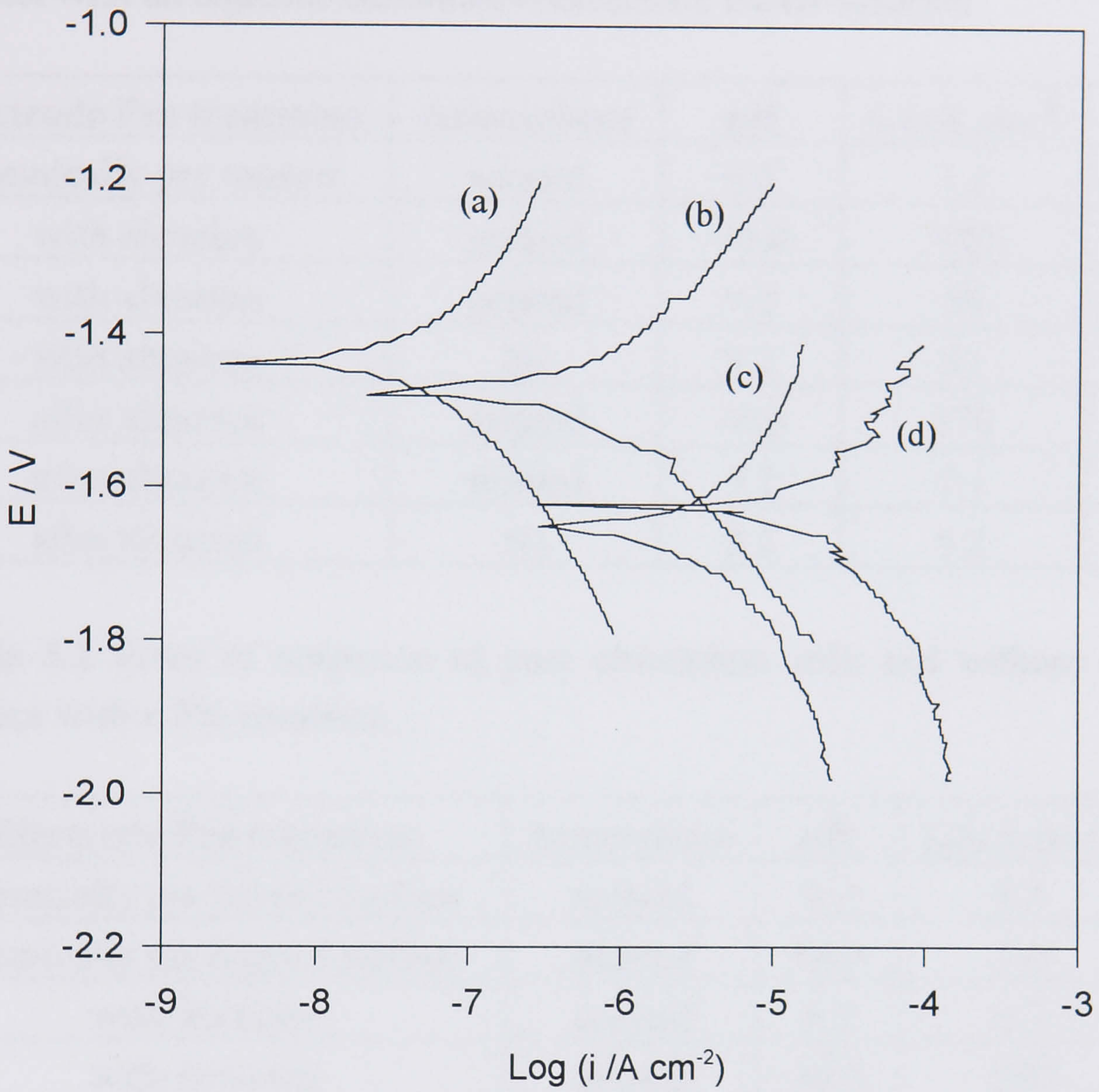

Fig. 5.2 Logi-E relationships for an aluminium surface in contact with various aerated electrolytes pH 9.2, rotation speed 5mV s^{-1}, (a) 5% emulsion after abrasion, (b) bicarbonate solution after abrasion, (c) 5% emulsion during continuous abrasion, (d) bicarbonate buffer solution during continuous abrasion,.

Results obtained on abrasion of the electrode in the absence of oxygen (nitrogen saturated), showed a decrease in the corrosion rate compared to results obtained in oxygenated solutions. This is comparable to the corrosion rate observed in the absence and presence of oxygen for a chemically pre treated surface.

Table 5.1 Rates of corrosion of pure aluminium with and without abrasion in contact with an aqueous carbonate/bicarbonate buffer solution.

Electrode Pre treatment	Atmosphere	pH	$i_c/\mu A\ cm^{-2}$	OCP /mV
chemically pre treated	aerated	9.2	1.3	-1000
with abrasion	aerated	10.0	950	-1700
with abrasion	aerated	9.2	58	-1650
with abrasion	N_2	9.2	51	-1630
after abrasion	aerated	10.0	170	-1580
after abrasion	aerated	9.2	7.1	-1480
after abrasion	N_2	9.2	5.2	-1480

Table 5.2 Rates of corrosion of pure aluminium with and without abrasion in contact with a 5% emulsion.

Electrode Pre treatment	Atmosphere	pH	$i_c/\mu A\ cm^{-2}$	OCP /mV
chemically pre treated surface	aerated	9.2	0.3	-1400
chemically pre treated surface	aerated	10.0	7.0	-1500
with abrasion	aerated	9.2	6.7	-1650
with abrasion	aerated	10.0	220	-1600
with abrasion	N_2	9.2	25	-1510
after abrasion	aerated	9.2	0.8	-1480
after abrasion	aerated	10.0	63	-1600
after abrasion	N_2	9.2	4.3	-1480

Corrosion rates were estimated from the logi-E plots. Typical values are shown in Table 5.1 for aqueous solutions. The corrosion rate of a mechanically pre treated aluminium surface is a factor of approximately 5 times higher than a chemically pre treated electrode under identical conditions, for both aqueous solution and an emulsion.

The increase in corrosion rate that is observed when the solution pH is increased form pH9.2 to 10.0 is greater when the metal surface is being abraded compared to after it has been abraded.

5.1.1 Discussion

On abrasion of the aluminium electrode;

1. The OCP becomes more negative

2. The corrosion current increases

To explain these observations, the anodic and cathodic currents must have increased by different amounts. If the cathodic slope and the anodic slope had shifted to higher current values by the same amount on abrasion of the surface, then the OCP would have remained the same. The diagram below shows 2 possibilities that would lead to a decrease in the OCP. Figure (5.3) shows the consequence of an increasing anodic dissolution rate. The OCP value drops and the corrosion current increases, as is observed experimentally on abrasion of the electrode.

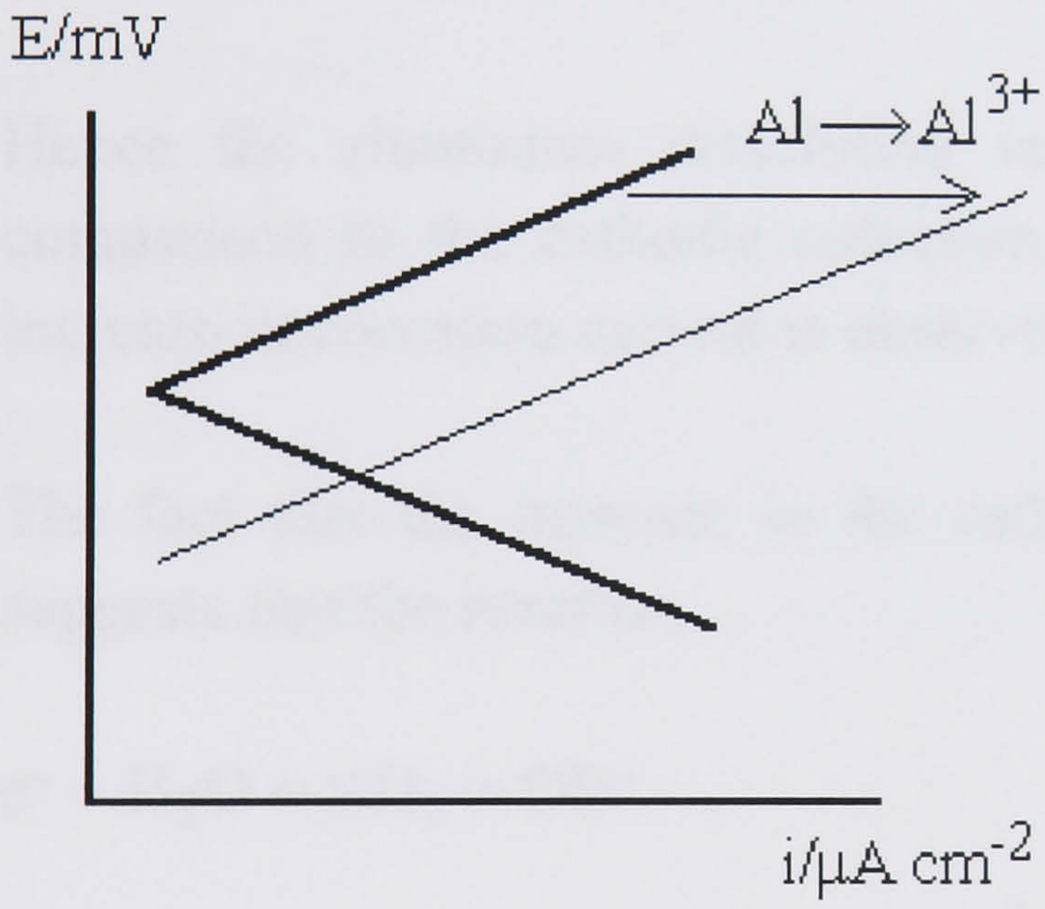

Figs. 5.3 Schematic to illustrate how, on abrasion of the electrode, the corrosion rate increases and the rest potential decreases as a result of an increase in rate of the metal dissolution reaction.

This is consistent with the fact that the aluminium oxidation/dissolution rate has exceeded the cathodic hydrogen evolution reaction by a factor of approximately 20, as indicated by the arrows in Fig. 5.1.

There are two reasons why this should be the case;

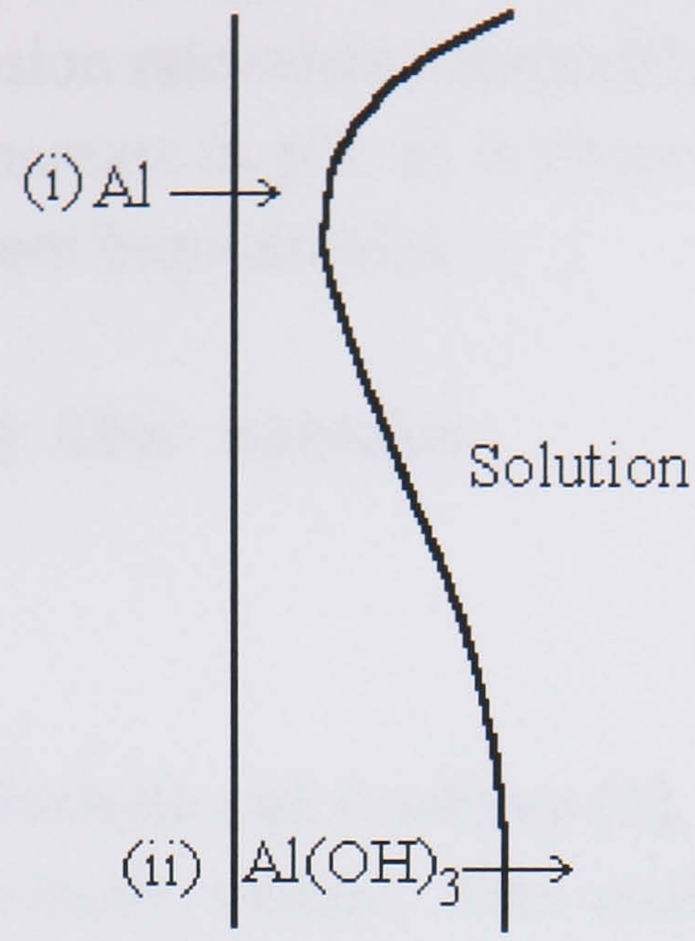

i) Repair of $Al(OH)_3$

ii) Normal Al loss as $Al(OH)_4^-$

Hence the aluminium dissolution reaction increases to a greater extent in comparison to the cathodic reduction, and a decrease in OCP and an overall increase in corrosion current is observed.

The fact that the increase in the cathodic current is as low as a factor of 3 suggests that the reaction,

$$e^- + H_2O = \tfrac{1}{2}H_2 + OH^-$$

on bare aluminium, is similar to that on film covered aluminium.

Since the abrasion experiments (where some of the cathodic current must come from direct reaction at the bare metal) cause the cathodic currents to increase by a factor of only 3, it be can postulated that the water content of the passive film must be very high. This is in agreement with previous results (Chapter 3), which suggest that the mechanism of cathodic reduction involves the reduction of water incorporated into the passive layer.

The relatively low increase in corrosion current observed on abrasion, with unit increase in pH, can be explained by considering the direct reaction of the bare metal surface with the solution. New oxide is formed, which is subsequently removed by the abrasive action of the electrode in contact with the frit, and so on.

The rate of corrosion is not as a direct result of, or dependent upon, the rate of chemical removal of the oxide by dissolution as aluminate. This, as previously discussed, is dependent upon the pH of the solution (refer to section 3.2). A significant rise in the corrosion rate when continually abrading the surface is not seen, therefore, with unit increase in pH, as is observed with unit increase in pH for an electrode which has not been abraded.

5.2 Open Circuit Recovery After Abrasion

5.2.1 Introduction

A technique described by Burstein and Cinderey [1], allows a travelling chisel to guillotine the working electrode surface. This enabled the OCP of a freshly generated electrode surface and its subsequent evolution with time to be measured. The work described here differs from the guillotine method, in that it does not provide a means of measuring kinetic data in the first milliseconds of oxide recovery. A similar technique of continuous surface renewal has been described by Tomashov [2], who studied the kinetics of some electrode processes of other metals.

The potential rise was observed to be linear in log(t/s) between 100 and 1000 seconds, after the start of the potential recording. However, no information regarding the initial stages of recovery are reported. Repassivation of the surface oxide in the first milliseconds was not explored in any detail as carried out by Burstein, due to the relative inaccuracy of the cutting procedure.

5.2.2 Recovery Transients

The transients shown in Figs. 5.4, 5.5, 5.6, and 5.7, show how the corrosion potential varied with log(t/s) after and during continuous abrasion. Before abrasion of the electrode, the OCP value was equal to that of the passivated rotating disc in solution. The graphs are shown in terms of log(t/s) to allow the full range of recorded time of approximately 1500 seconds, to be analysed. The potential range covered in this time is $-1.69V < E < -1.28V$ (vs Hg/HgO) for an aqueous bicarbonate buffer solution of pH 9.2. For 1M NaOH solution the OCP drops to -1.78V on abrasion, and recovers to a potential of only -1.58V over the same period of time. The sudden drop in potential is due to the release of the rotating electrode onto the glass frit, Fig. 5.5(b). Most of the oxide layer is removed at this stage and the OCP drops significantly to approximately -1.69V.

On release of the rotating electrode from the glass frit, there is a sudden increase in potential (Figs. 5.5 and 5.6). This is an indication of the rapid initial rate of 'recovery' of the repassivating surface. Recovery then continues at a slower rate until the potential on open circuit is re-established.

Extrapolation of the linear section of the repassivation transient in Fig. 5.5(d), indicates a time resolution of milli seconds, at the equilibrium potential, (-2.12V vs Hg/HgO).

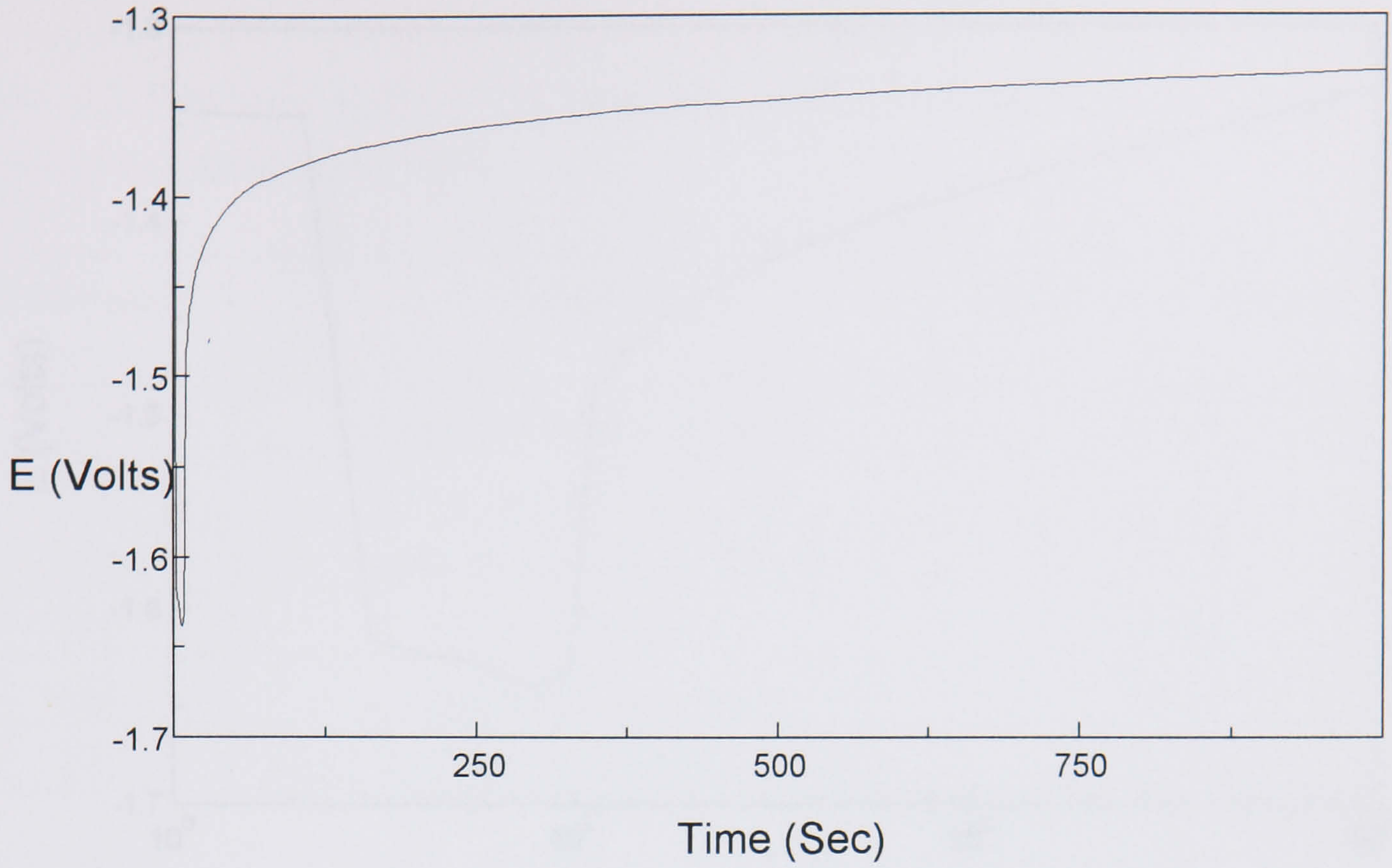

Fig. 5.4 Open circuit recovery profile for Al in contact with an aqueous buffer solution during and after abrasion. Results are recorded on a linear time scale.

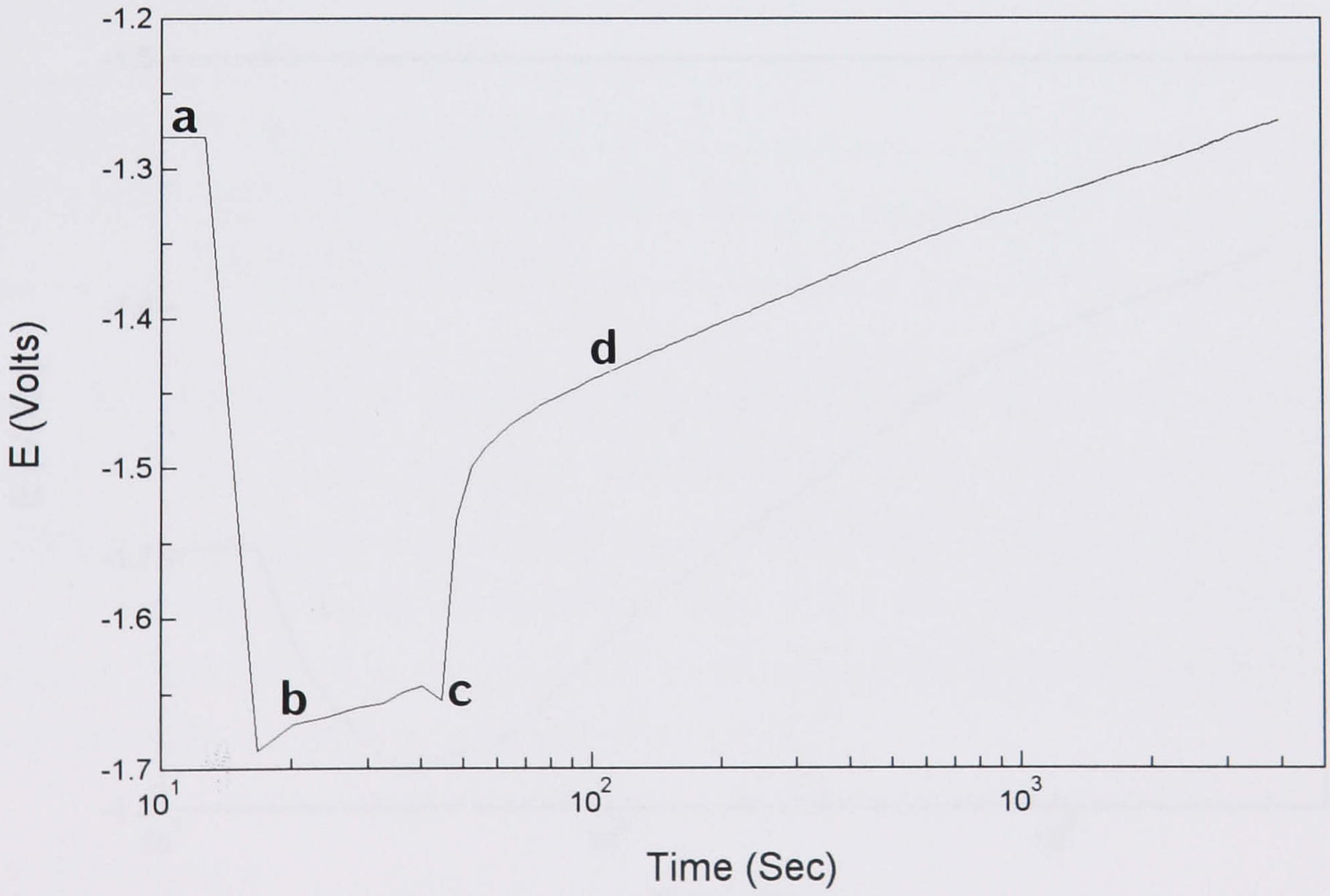

Fig. 5.5 Open circuit potential transient for pure Al in contact with a 0.05M aqueous borax solution, pH 9.2, rotation speed 5Hz (a) passivated rotating disc in solution (b) aluminium in contact with glass frit (c) release of pressure, abraded metal surface in contact with electrolyte (d) repassivating metal surface.

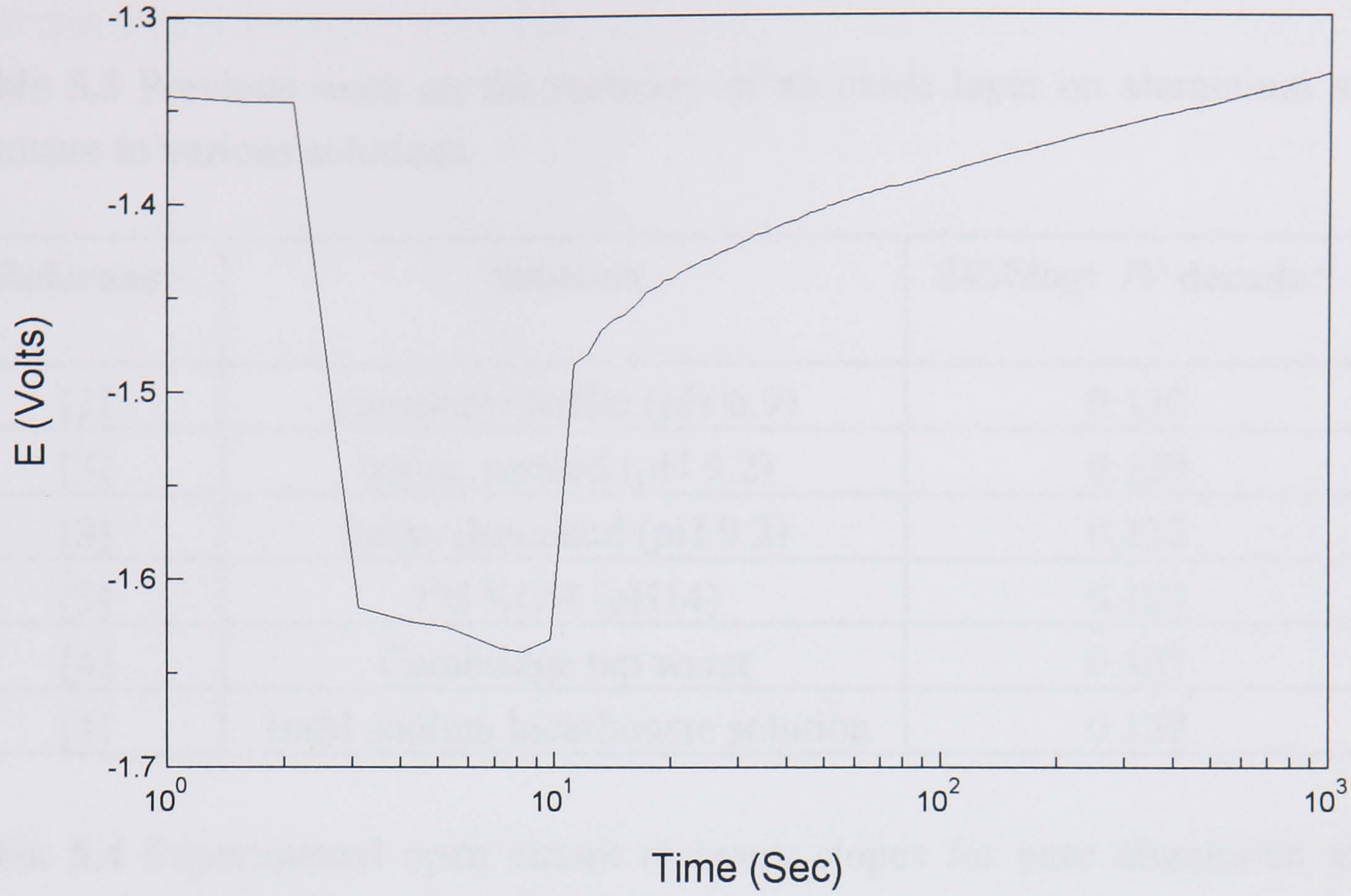

Fig. 5.6 Recovery transient for aluminium in contact with a 5% cutting fluid emulsion (formulation A).

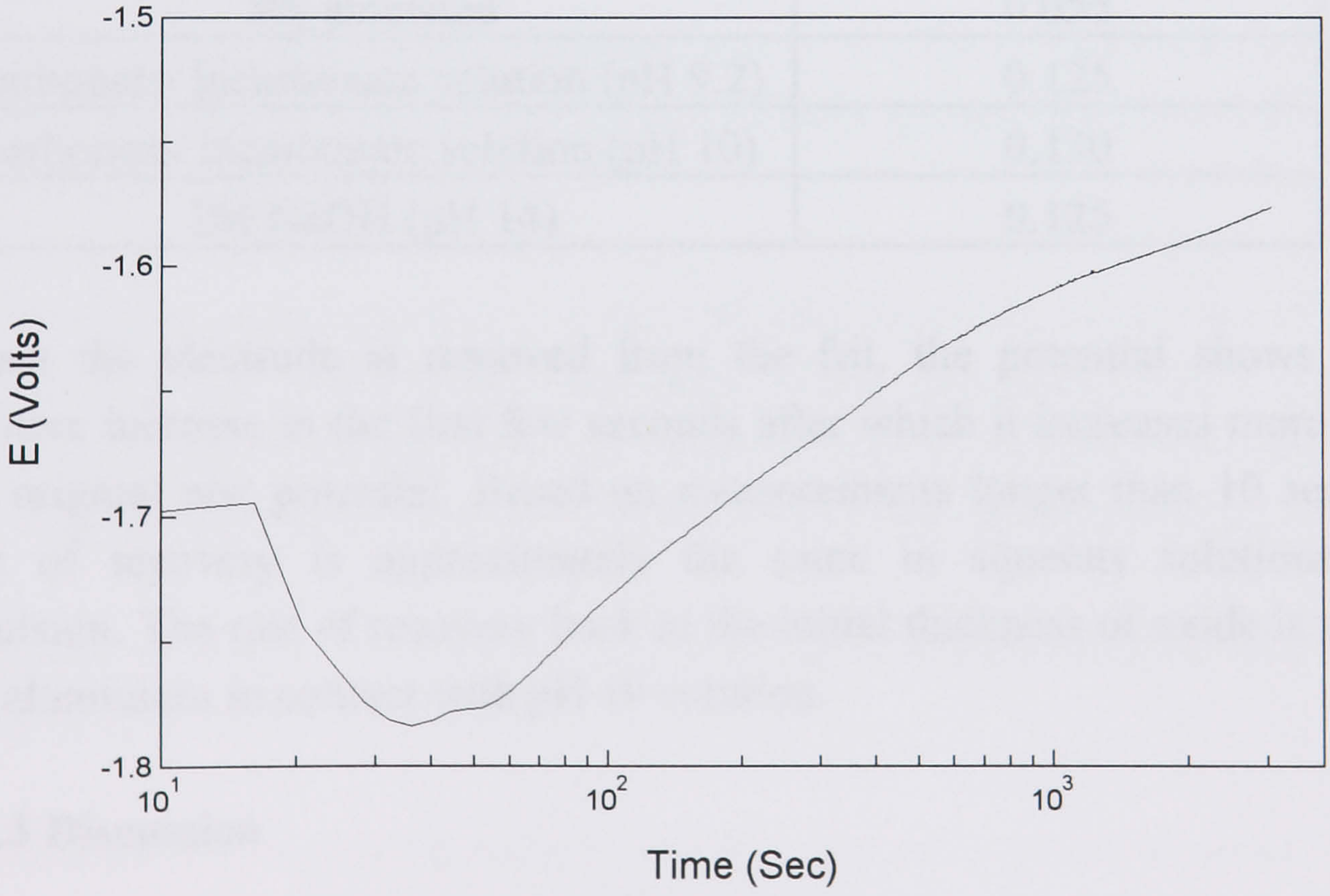

Fig. 5.7 Recovery transient for a fresh aluminium surface in contact with a 1M NaOH solution, pH 14.

Some results have been analysed from previous work found in the literature, and are summarised in Table 5.3 below.

Table 5.3 Previous work on the recovery of an oxide layer on aluminium after exposure to various solutions.

Reference	Solution	$\delta E/\delta \log t$ /V decade^{-1}
[1]	phosphate buffer (pH 6.9)	0.130
[3]	borax, aerated (pH 9.2)	0.129
[3]	borax deaerated (pH 9.2)	0.132
[3]	1M KOH (pH14)	0.125
[4]	Cambridge tap water	0.107
[4]	1mM sodium bicarbonate solution	0.129

Table 5.4 Experimental open circuit recovery slopes for pure aluminium after exposure to various electrolyte solutions.

Solution	$\delta E/\delta \log t$ /V decade^{-1}
0.05M borax, aerated (pH 9.2)	0.350
5% emulsion	0.055
carbonate/ bicarbonate solution (pH 9.2)	0.125
carbonate/ bicarbonate solution (pH 10)	0.130
1M NaOH (pH 14)	0.125

When the electrode is removed from the frit, the potential shows a sudden positive increase in the first few seconds after which it increases more slowly to the original rest potential. Based on measurements longer than 10 seconds, the rate of recovery is approximately the same in aqueous solutions and the emulsion. The rate of recovery back to the initial thickness of oxide is most rapid for aluminium in contact with pH 10 solution.

5.2.3 Discussion

On abrasion of the electrode, the OCP drops to approximately -1.69V. This value is positive by approximately +0.43V to the calculated equilibrium potential (see section 1.4.1) for the reaction $Al = Al^{3+} + 3e^-$, at pH 9. The latter however, is unlikely to be achieved by an experimental technique of this nature, due to the need for extremely high time resolution. Extrapolation of the linear section of the

repassivation transient in Fig. 5.5(d) indicates a time resolution of milli seconds for a potential of -2.12V (vs Hg/HgO). However, this value is unreliable. The inaccuracy may be attributed to the relatively simplistic nature of the equipment used here, and shows the difficulty encountered when trying to measure kinetic characteristics of such a system at the equilibrium potential. Burstein and Cinderey used a cutting speed of 1m s^{-1} so that a 1mm diameter wire was cut through in 1ms. They found in a similar experiment that the time resolution required to reach such low electrode potentials on extrapolation gave t = 0.4 μs [1].

The quantity of bare aluminium at the electrode surface, on abrasion, is small and dependent upon the force with which the rotating disc is applied to the glass frit. The OCP falls to more negative values the greater the force that is applied, as a result of more bare aluminium being exposed to the solution.

These measurements are made under electrolyte immersion hence the recorded potentials cannot have been due to air coming into contact with the electrode surface prior to any electrochemical measurement, as is the case with chemical pre treatment. The oxide film that develops is formed by a reaction with the solution. There are several other factors to take into account when comparing the corrosion currents of chemically and mechanically pre treated metal surfaces;

i) Surface area. The glass frit used to abrade the metal will creates a roughened surface on the metal so that the area is actually greater than that calculated from the diameter of the disc.

ii) According to the equation $v = \omega r$, the velocity at the outer edge of the disc is greater than that at the centre, and there is non uniformity across the electrode surface. However, the pressure and length of time of abrasion was made identical for each measurement to ensure that the results were as reproducible as possible.

iii) Glass particles becoming embedded in the soft aluminium surface may affect the potential on open circuit.

iv) Mechanical action should be fast to minimise surface heating. The pH is temperature dependent as is the relationship between current and potential.

5.3 Effect of pH

The graph in Fig. 5.8 below, shows recovery slopes measured *in situ* for an abraded aluminium disc, in contact with an emulsion and an aqueous solution, in the presence and absence of oxygen, at pH values 9, and 10.

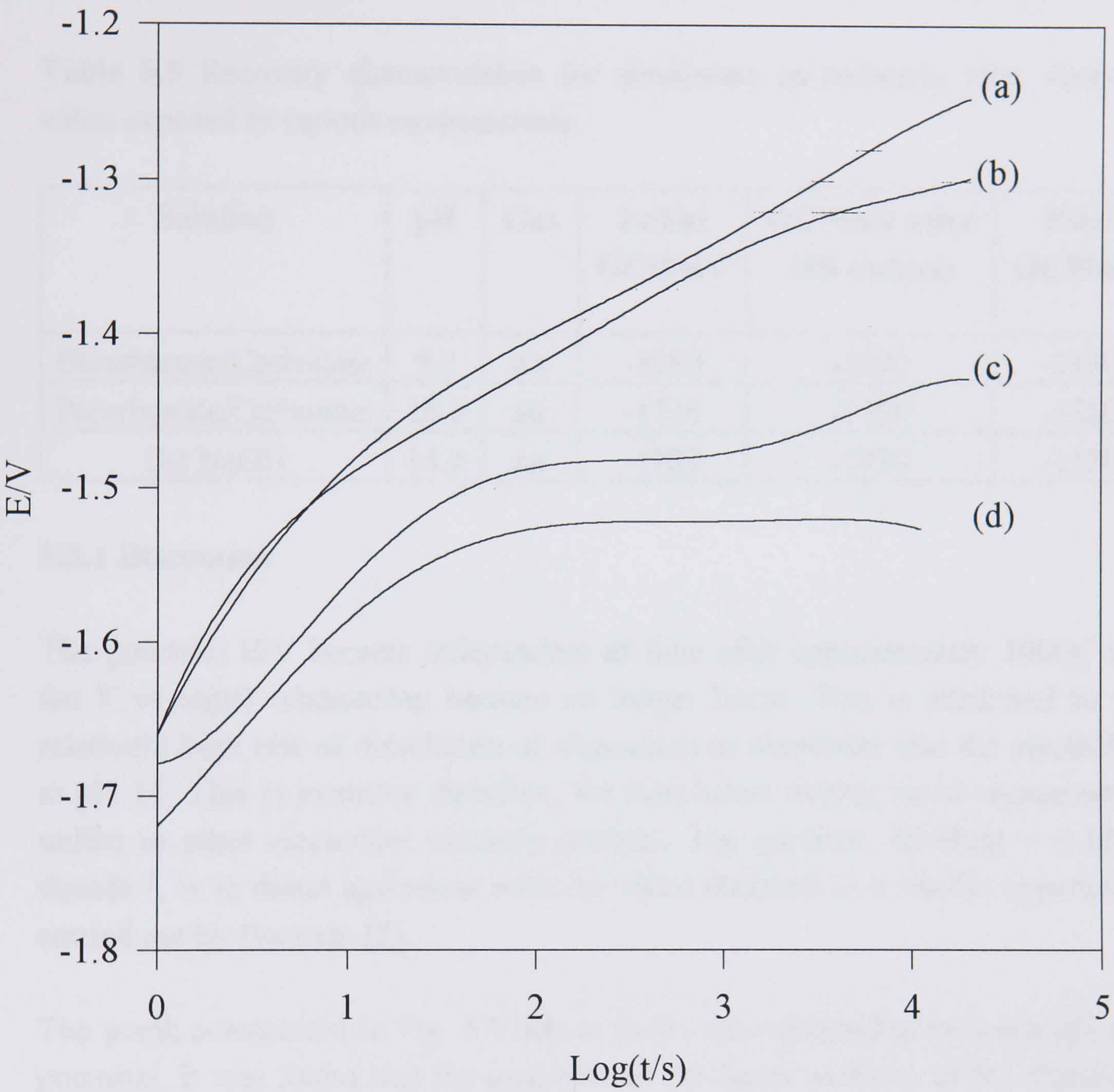

Fig. 5.8 Recovery slopes measured *in situ* for an abraded aluminium disc in contact with various electrolytes, rotation speed 5Hz; (a) oxygenated 5% emulsion, (b) 5% emulsion in the absence of oxygen, (c) aqueous bicarbonate/carbonate solution pH 9.2, (d) aqueous bicarbonate/carbonate solution pH 10.

With increasing pH it was observed that lower potentials arose during the abrasion period, and although the initial rise in potential was less rapid the final

steady state potential was achieved relatively quickly, Fig. 5.8(d). For aluminium in contact with 1M NaOH solution, the rate of dissolution of the oxide was very high and film recovery was slow. The initial sharp rise in potential that was observed at pH 9.2 is not apparent at pH 14. This is illustrated by the relatively shallow slope shown in Fig. 5.7. The potential E/V becomes independent of t after approximately 1000s, and the E vs logt relationship is no longer linear.

Table 5.5 Recovery characteristics for aluminium immediately after abrasion when exposed to various environments.

Solution	pH	Gas	Initial OCP/mV	OCP/mV after 100 seconds	Final OCP/mV
Bicarbonate/Carbonate	9.2	air	-1680	-1490	-1430
Bicarbonate/Carbonate	10.0	air	-1720	-1530	-1520
1M NaOH	14.0	air	-1780	-1730	-1570

5.3.1 Discussion

The potential E/V became independent of time after approximately 1000s, and the E vs log(t) relationship became no longer linear. This is attributed to the relatively high rate of dissolution of aluminium as aluminate into the electrolyte at pH 14. This is evidence therefore, for dissolution *during* metal repassivation unlike in other electrolyte recovery profiles. The gradient, $\delta E/\delta \log t = 0.125V$ $decade^{-1}$, is in direct agreement with the value obtained in a similar experiment carried out by Burstein [5].

The graph constructed in Fig. 5.9 below shows the relationship between pH and potential. It was found that the gradients of the linear sections of the transients are equivalent for pH values 9.2, 10.0 and 14.0, within the limits of experimental error i.e. $\delta E/\delta \log t$ is independent of pH.

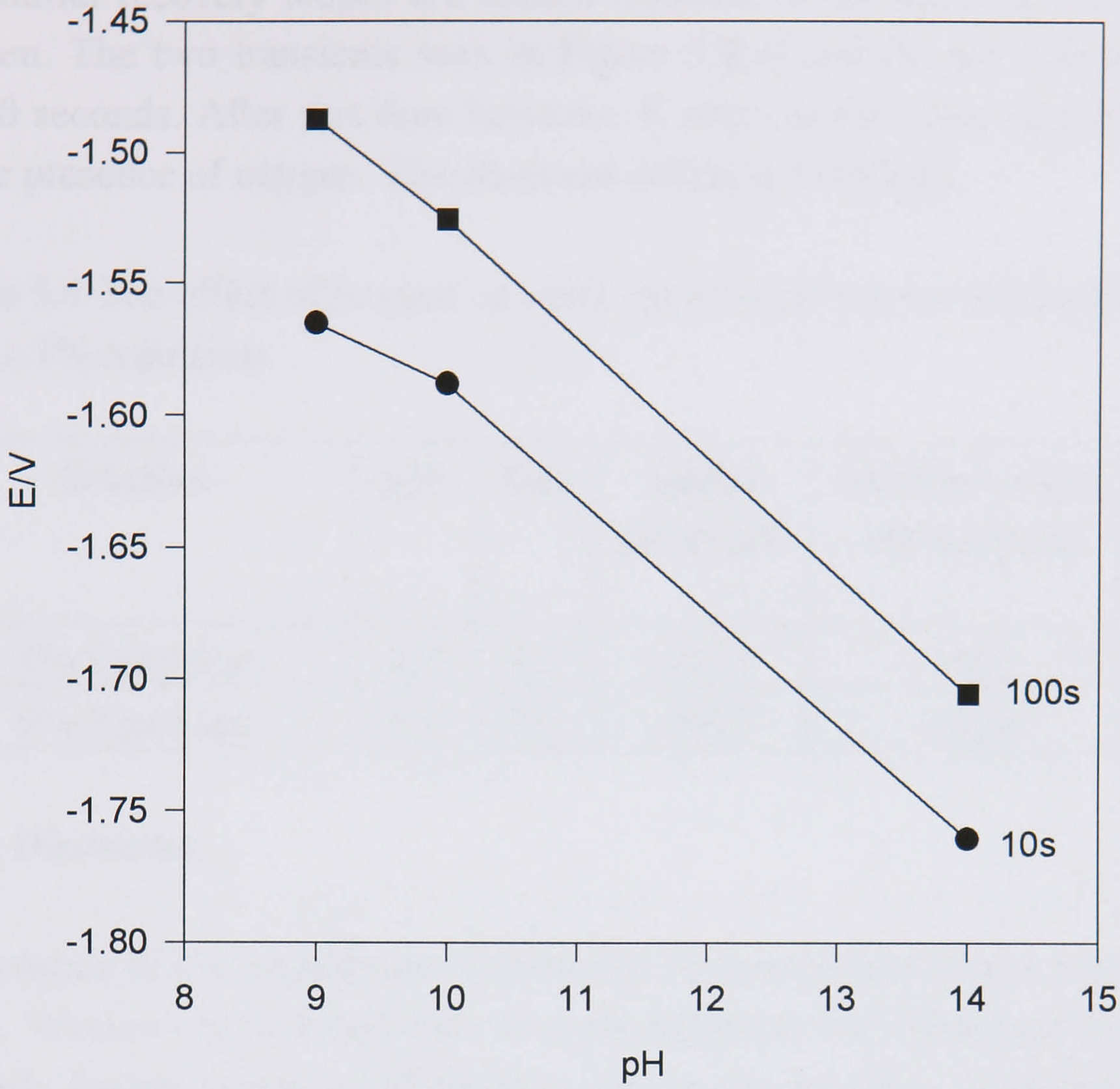

Fig 5.9 Graph to show the relationship between pH and open circuit potential for aluminium in contact with aqueous solutions, 10s and 100s after abrasion.

Decade time intervals were selected from the point at which the electrode was removed from the frit. The average gradient value is equal to -0.04V decade^{-1}. This is more positive than the Nernstian slope of -0.0562V decade^{-1} as predicted by Burstein and Cinderey [5] where,

$$\delta E/ \delta pH = -2.303RT/F.$$

This may be attributed to the difference in the nature of the two experiments. The validity of this equation is uncertain however. It is derived from complex mathematics and assumes that E_{oc} and E_{oa} are the only parameters to vary with pH, and that $E_{oc} - E_{oa}$ is independant of pH.

5.4 Effect of Oxygen

The initial recovery slopes are almost identical in the absence and presence of oxygen. The two transients seen in Figure 5.8(a) and (b) are coincident for the first 8 seconds. After this time however, E starts to rise more rapidly with log(t) in the presence of oxygen. The observed difference is slight.

Table 5.6 The effect of oxygen on open circuit recovery for aluminium in contact with a 5% emulsion.

Solution	pH	Gas	Initial OCP/mV	OCP/mV after 100 seconds	Final OCP/mV
5% Emulsion	9.2	O_2	-1655	-1400	-1250
5% Emulsion	9.2	N_2	-1655	-1420	-1300

5.4.1 Discussion

The origins of the logarithmic relationship between E and t have been dealt with, [3-6]. Workers have found that in some solutions the deviations from linearity towards higher values of $\delta E/\delta \log t$ is due to the presence of dissolved oxygen. This effect can be seen most clearly for transients (a) and (b) in Fig. 5.8. It has been reported that as the potential rises with time, the cathodic overpotential for hydrogen evolution decreases and the rate of reaction is reduced, so that the transient reaches a regime in which the growth of oxide is limited by the rate of mass transport of oxygen to the metal surface. From the findings presented in recent experiments, it would seem more reasonable to suggest that the growth of the oxide becomes limited by the formation of aluminate ions at the metal/solution interface as discussed in section 3.2. Earlier rotation speed experiments suggest only a slight dependence on the mass transport of oxygen to the surface.

5.5 Computer Simulation

5.5.1 Introduction

A computer transform programme was written in order to simulate a theoretical oxide film growth model (see Appendix B). This is a programme for calculating the way in which the OCP varies after abrasion of the electrode surface has stopped. Once the abrasion stops, any current which flows causes the oxide layer

to thicken. The resultant profiles were compared to the original potential transients using the parameter $\delta E / \delta \log t$ /V dec^{-1}.

Each of the 5 Figures 5.10-5.14, represent a computer simulated oxide recovery transient. In each case, one of the parameters has been changed in order to establish the repassivation profile that one would expect to observe when each of the variables are systematically altered. The parameter that has been changed is indicated in the title of the graph. The values that were varied have been listed in the corresponding line in the programme, and highlighted in bold type.

It is assumed that the growth of the oxide film occurs with 100% current efficiency, and with no alternative oxidative processes, such as metal dissolution and the formation of other forms of barrier oxide layers. Hydrogen evolution is considered as the only cathodic reduction process that takes place. It is also assumed that the kinetics of the hydrogen evolution reaction are controlled directly by the Tafel equation (1.6).

A more accurate transient results for larger values of n typically 20000, where n is the number of computer iterations.

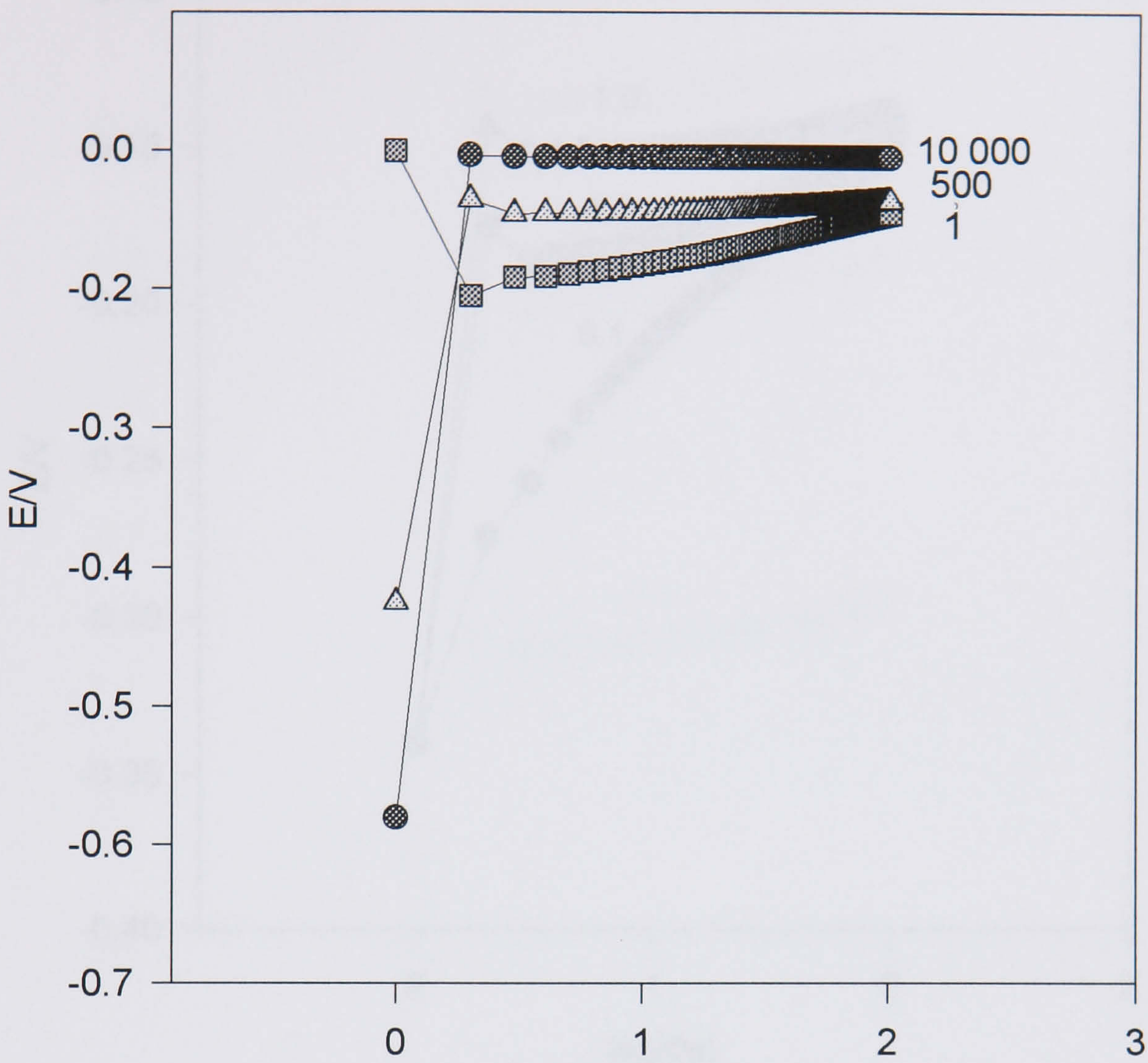

Fig. 5.10 Computed simulated transients showing the effect of the magnitude of the initial current on the oxide recovery.

```
1     cell(1,1)=1, 500, 10 000
2     cell(1,3)=0.5
3     cell(1,5) = 0.1 + 0.12*log(cell(1,1))

4     for n =1 to 100 step 1 do
5     cell(1,2) =  cell(1,3) + cell(1,1)/500
6     cell(1,3) = cell(1,2)
7     h =0.1 + 0.12*log(cell(1,1))
8     cell(4,n) = cell(1,1)
9     cell(2,n) = - h
10    cell(3,n) = n
11    cell(1,1) = exp((1+cell(1,5) - h)/cell(1,2))
12    cell(5,n) =cell(1,3)
13    cell(6,n) = log(n)
```

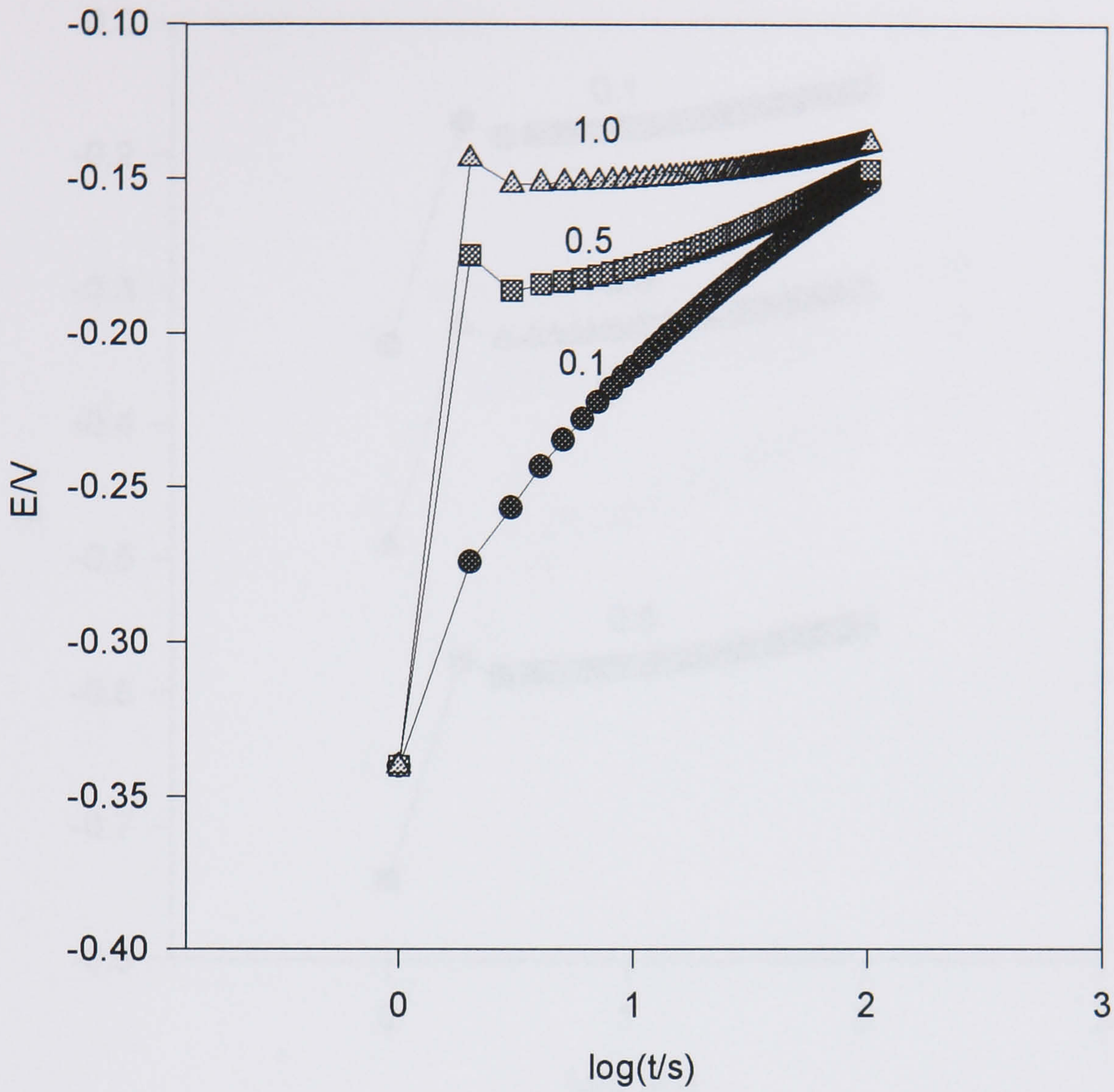

Fig. 5.11 Computer simulatd transients showing the effect of initial oxide thickness on the recovery profile.

```
1     cell(1,1)=100
2     cell(1,3)=0.1, 0.5, 1.0
3     cell(1,5) = 0.1 + 0.12*log(cell(1,1))

4     for n =1 to 100 step 1 do
5     cell(1,2) =  cell(1,3) + cell(1,1)/500
6     cell(1,3) = cell(1,2)
7     h =0.1 + 0.12* log(cell(1,1))
8     cell(4,n) = cell(1,1)
9     cell(2,n) = - h
10    cell(3,n) = n
11    cell(1,1) = exp((1+cell(1,5) - h)/cell(1,2))
12    cell(5,n) = cell(1,3)
13    cell(6,n) = log(n)
```

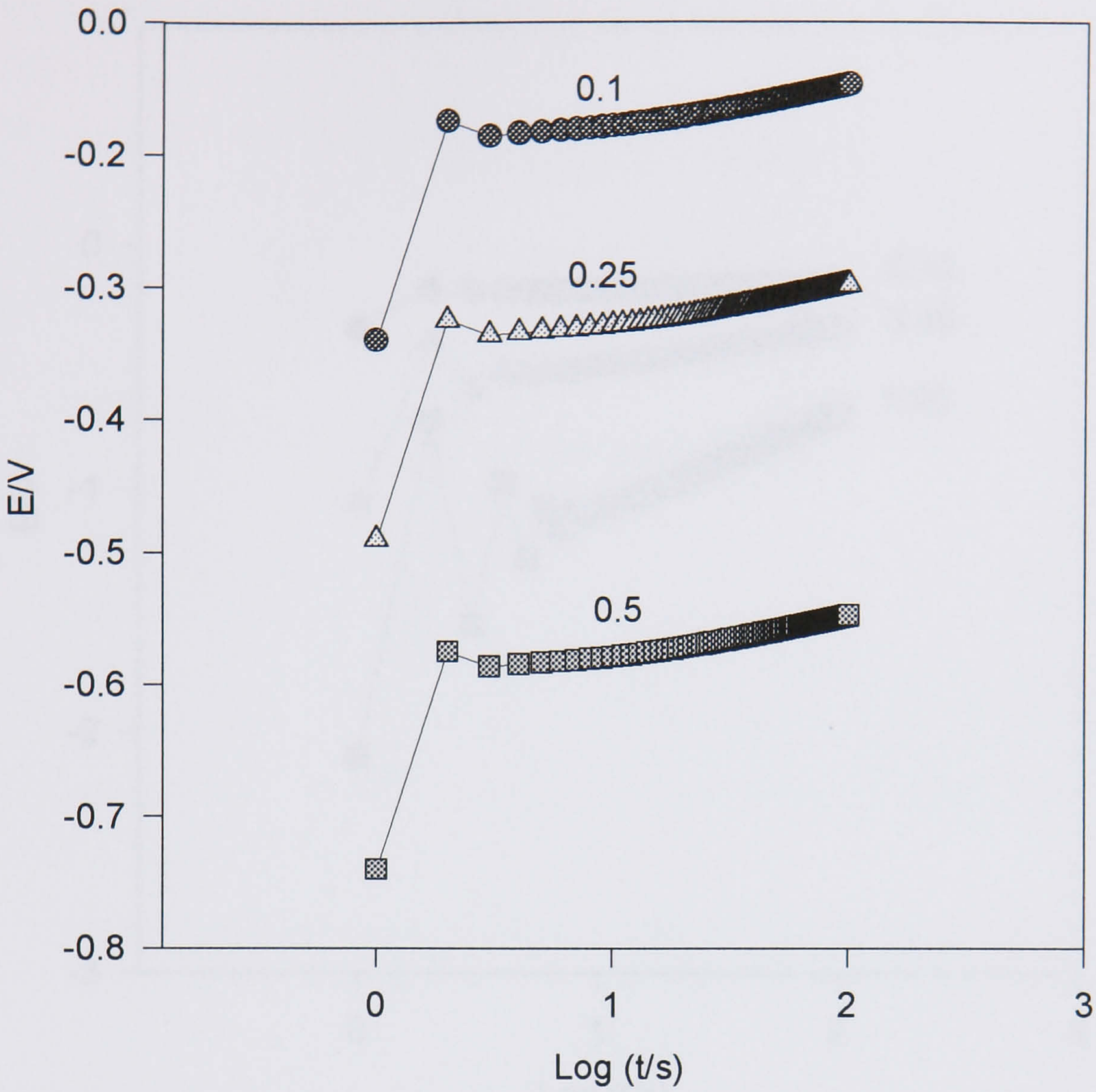

Fig. 5.12 Computer simulated oxide recovery transients with Tafel parameter 'a' as the variable.

```
1     cell(1,1)=100
2     cell(1,3)=0.5
3     cell(1,5) = 0.1, 0.25, 0.5 + 0.12*log(cell(1,1))

4     for n =1 to 100 step 1 do
5     cell(1,2) =  cell(1,3) + cell(1,1)/500
6     cell(1,3) = cell(1,2)
7     h =0.1,0.25,0.5 + 0.12*log(cell(1,1))
8     cell(4,n) = cell(1,1)
9     cell(2,n) = - h
10    cell(3,n) = n
11    cell(1,1) = exp((1+cell(1,5) - h)/cell(1,2))
12    cell(5,n) = cell(1,3)
13    cell(6,n) = log(n)
```

Line 3. Tafel Parameter b

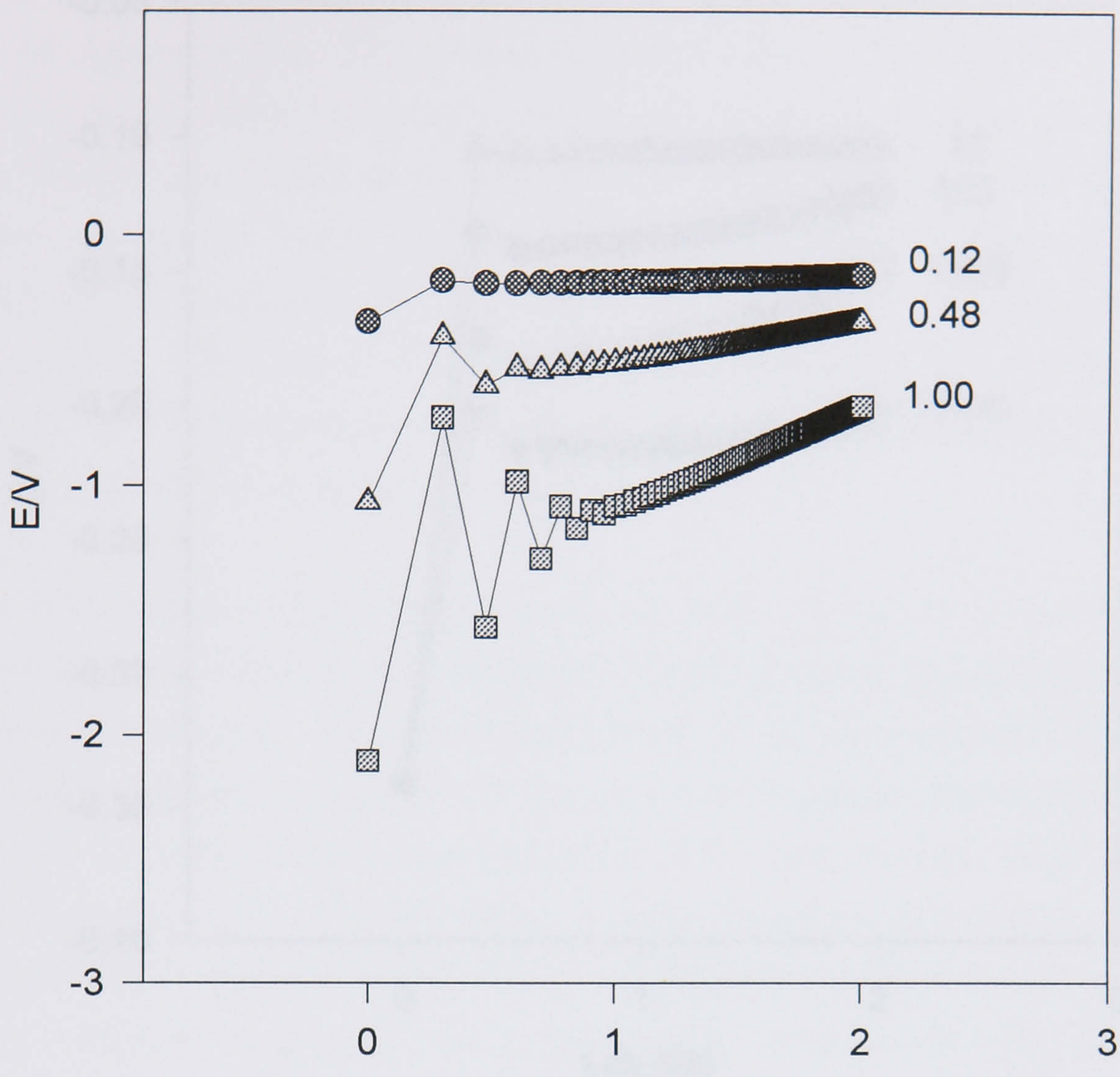

Fig. 5.13 Computer simulated transients of oxide recovery with the Tafel parameter 'b' as the variable.

```
1     cell(1,1)=100
2     cell(1,3)=0.5
3     cell(1,5) = 0.1 + 0.12, 0.48, 1.0*log(cell(1,1))

4     for n =1 to 100 step 1 do
5     cell(1,2) = cell(1,3) + cell(1,1)/500
6     cell(1,3) = cell(1,2)
7     h = 0.1 +0.12, 0.48, 1.0*log(cell(1,1))
8     cell(4,n) = cell(1,1)
9     cell(2,n) = - h
10    cell(3,n) = n
11    cell(1,1) = exp((1+cell(1,5) - h)/cell(1,2))
12    cell(5,n) = cell(1,3)
13    cell(6,n) = log(n)
```

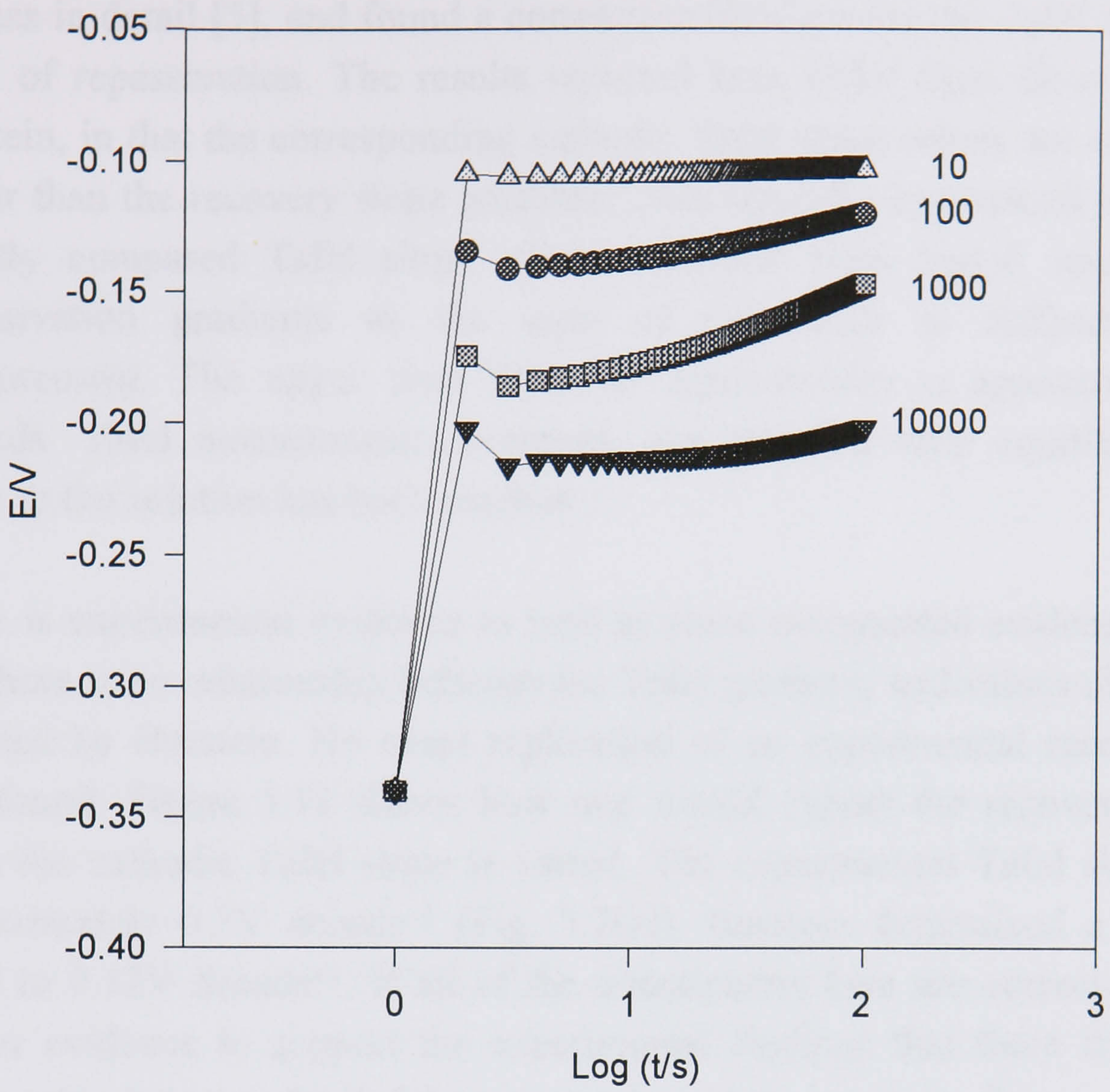

Fig 5.14 Computer simulated transients for oxide recovery with oxide thickness as the variable.

```
1     cell(1,1) =100
2     cell(1,3) =0.5
3     cell(1,5) = 0.1 + 0.12*log(cell(1,1))

4     for n =1 to 100 step 1 do
5     cell(1,2) = cell(1,3) + cell(1,1)/10, 100, 1000, 10000
6     cell(1,3) = cell(1,2)
7     h =0.1 + 0.12*log(cell(1,1))
8     cell(4,n) = cell(1,1)
9     cell(2,n) = - h
10    cell(3,n) = n
11    cell(1,1) = exp((1+cell(1,5) - h)/cell(1,2))
12    cell(5,n) = cell(1,3)
13    cell(6,n) = log(n)
```

5.5.2 Discussion

Burstein and Cinderey studied the kinetics of the cathodic hydrogen evolution process in detail [5], and found a correlation between the the Tafel slope and the slope of repassivation. The results reported here differ from those reported by Burstein, in that the corresponding cathodic Tafel slope values are systematically higher than the recovery slope gradients. It is not fully understood why Burstein directly compared Tafel slope values obtained from logi-E relationships to repassivation gradients as the state of the oxide is different for each measurement. The upper time limit for repassivation is approximately 1500 seconds. Tafel measurements however, are obtained after equilibrium of the oxide in the solution has been reached.

There is experimental evidence as well as some computated evidence to suggest that there is no relationship between the Tafel gradient, and values of $\delta E/\delta \log t$ as reported by Burstein. No exact replication of an experimental recovery profile was found. Figure 5.13 shows how one would expect the recovery to change when the cathodic Tafel slope is varied. The experimental Tafel slope value is approximately 0.3V decade^{-1} (Fig. 5.2(a)). Burstein determined a Tafel slope equal to 0.12V decade^{-1}. If all of the assumptions here are correct, then this is further evidence to support the experimental findings that there is no obvious relationship between the Tafel parameter b, and the recovery slope.

References

[1] G. T. Burstein and R. J. Cinderey, ' The potential of freshly generated metal surfaces determined from the guillotined electrode - A new technique', *Corros. Sci.*, **32** (1991) p.1195.

[2] N. D. Tomashov and L. P. Vershinina, 'Kinetics of some electrode processes on a continuously renewed surface of solid metal'. *Electrochim. Acta*, **15** (1970) pp.501-517.

[3] G. T. Burstein and C. Liu, 'Time resolved electrochemical impedance of the guillotined aluminium electrode', *Electrochim. Acta*, **39** (1994) p.873.

[4] R. J. Cinderey and G. T. Burstein, 'The repassivation potential of aluminium in water', Short Communication, *Corros. Sci.*, **33** (1992) pp.499-502.

[5] G. T. Burstein and R. J. Cinderey, 'Evolution of the corrosion potential of repassivating aluminium surfaces', *Corros. Sci.*, **33** (1992) p.475.

[6] G. T. Burstein and C. Liu, 'The cathodic reaction during repassivation of aluminium in open circuit', *Corros. Sci.*, **37** (1995) pp.1151-1162

The graph below in fig. 6.2 indicates the effect of pH on the corrosion rate of a zinc rich aluminium alloy.

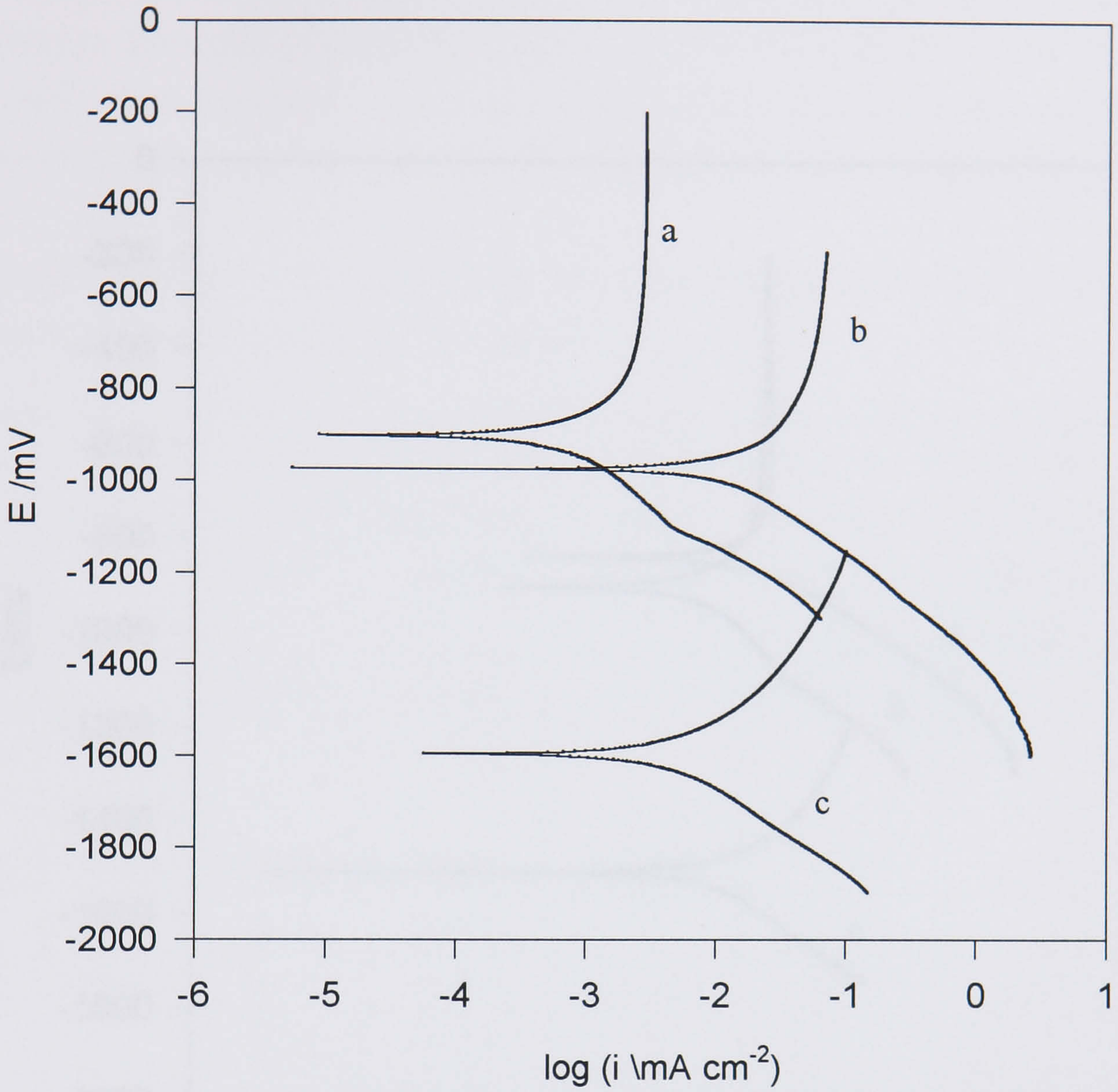

Fig. 6.2 Logi-E relationships for aluminium alloy 7075 in contact with a deaerated bicarbonate buffer solution, rotation speed 5Hz, sweep speed 1mV s^{-1} a) pH 9.2, b) pH 10 and c) pH 10, (pure aluminium).

The observed trend is similar to that found for pure aluminium in aqueous solutions (**Fig** 3.3), with a systematic increase in the anodic current for unit increase in pH. The cathodic currents of the alloys are again similar to one another within the limits of reproducibility. The cathodic currents of the alloys at pH 9 and 10, are both significantly greater than that of pure aluminium. The anodic dissolution rate of 7075 at pH 10, is comparable to that of pure aluminium at the same pH.

Finally, Tafel plots were obtained for the alloys when immersed in a 5% emulsion, pH 9.2. Again, the results were compared to those obtained for pure aluminium.

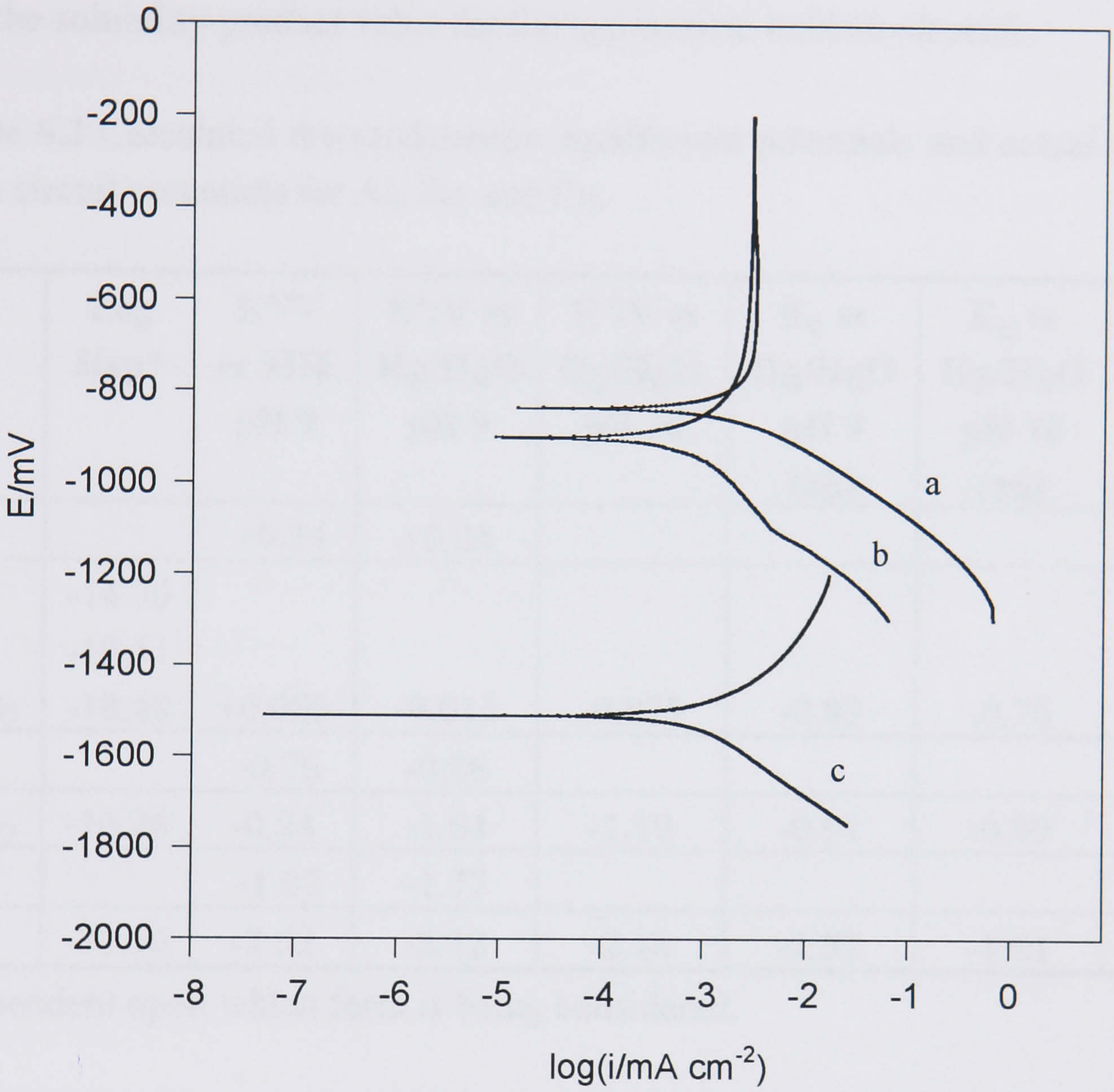

Fig. **6.3** Logi-E relationships for aluminium and aluminium alloys in contact with a 5% emulsion, pH 9.2, rotation speed 5Hz, sweep speed 1mV s^{-1}, a) alloy 2024, b) alloy 7075 and c) pure aluminium.

The OCP values for both alloys are systematically higher than that for pure aluminium. Corrosion rates for the alloys are lower in the emulsion at pH 9.2 compared to when in an aqueous solution at the same pH. These results correspond to those obtained for pure aluminium (Fig 4.1). The anodic dissolution current for both the copper and zinc alloys are similar within the limits of experimental error.

6.2.2 Discussion

Thermodynamic Considerations

The figures tabulated below in Table 6.2 show the differences between the equilibrium potential (E°), and the experimental OCP (E_c) values, at pH 9 and 10. Equilibrium potential values were calculated using the Nernst equation (1.1), and the solubility product value for the appropriate oxide/hydroxide.

Table 6.2 Calculated thermodynamic equilibrium potentials and actual observed open circuit potentials for Al, Zn, and Cu.

	Log Ksp*	**E°/V *vs* SHE pH 9**	**E°/V *vs* Hg/HgO pH 9**	**E°/V *vs* Hg/HgO pH 10**	**E_c *vs* Hg/HgO pH 9 (aq)**	**E_c *vs* Hg/HgO pH 10 (aq)**	**E_c *vs* Hg/HgO pH 9 emulsion**
Cu/Cu^{2+}		+0.34	+0.24				
Cu/Cu_2O	-14.70						
Cu/CuO	-19.51						
$Cu/Cu(OH)_2$	-18.48	+0.085	-0.015	-0.075	-0.83	-0.76	-0.83
Zn/Zn^{2+}		-0.76	-0.86				
$Zn/Zn(OH)_2$	-16.26	-0.94	-1.04	-1.10	-0.91	-0.99	-0.85
Al/Al^{3+}		-1.67	-1.77				
Al/Al_2O_3	-33.50	-2.02	-2.12	-2.18	-1.52	-1.61	-1.25

* dependent upon which form is being considered.

The actual OCP for pure aluminium measured *vs* the mercury/mercuric oxide reference electrode, is positive to the calculated equilibrium potential for Al/Al_2O_3. This explains in terms of thermodynamics, why there is always a protective layer of oxide on the metal surface. The same is true of the $Zn/Zn(OH)_2$ equilibrium. The corrosion potential vs Hg/HgO at pH 9 for $Zn/Zn(OH)_2$ is approximately equal to -0.91V, which is 0.13V positive to that of the calculated equilibrium potential. Thermodynamically therefore we would expect to find zinc oxide/hydroxide formed at pH 9 and pH 10 as is observed for aluminium. For copper however, the experimental corrosion potential measured is approximately 0.82V negative to the calculated equilibrium potential for $Cu/Cu(OH)_2$. Hence from thermodynamics the copper metal species is expected to exist at pH values 9 and 10, as opposed to the copper oxide/hydroxide species. If the copper metal exists incorporated into the aluminium oxide layer or at the metal oxide interface, then it will take up the potential applied in linear sweep

measurements. If, however, copper is loosely bound at the electrode surface, then it may form the oxide/hydroxide.

Pourbaix diagrams for copper and zinc are shown in Figs 6.5 and 6.6 [2]. The origin and limitations of these diagrams have been discussed in section 1.3.4. The analysis of these diagrams provides further confirmation that at pH values 9 and 10, copper is thermodynamically more stable when present as copper metal on open circuit, as opposed to copper oxide. Zinc hydroxide is expected to exist on open circuit when in contact with water at 25°C, as opposed to zinc metal. Fig. 6.7, shows the influence of pH on the corrosion rate of zinc. It shows that the corrosion rate is minimal in the pH region 9-11, and increases rapidly to approximately 700g/dm^2.day, at low and high pH values.

Corrosion Rates

It is known that copper reduces the corrosion resistance of aluminium more than any other alloying element. This is mainly due to the fact that copper is almost always present in 'micro-constituents' [1]. These are usually the source of most problems with electrochemical corrosion, since they lead to non uniform attack at specific areas of the alloy surface.

The alloying metals create localised redox couples at the grain boundaries so that the potential on open circuit is altered by an amount dependent upon the individual electrode potential of the alloying element present. The copper electrode potential is approximately 2V positive to that of aluminium, and hence the rest potential of alloy 2024 appears more positive than that for pure aluminium under the same conditions. The effect is less significant for 7075, the zinc containing alloy, since the standard electrode potential for zinc is about 1V positive to that for pure aluminium.

i) pH 9, aqueous solution

The corrosion rates of both alloys are significantly higher than that of pure aluminium under similar conditions. The cathodic current which arises due to the reduction of species at the oxide/solution interface (essentially hydrogen evolution) has been enhanced by some effect created by the incorporation of copper/zinc atoms into the oxide layer. This may alter the structure of the oxide/hydroxide in some way. A more porous oxide layer would allow electrons to tunnel through the layer more easily or alternatively, allow the penetration of reductants into the layer. Another possible explanation would be that the energy barrier for electron tunnelling has been lowered due to foreign metal atoms

accumulating either at the metal/oxide interface, or at the oxide/solution interface.

In addition, the anodic dissolution current is significantly higher compared to that of pure aluminium. This is an indication that the presence of Cu, or $Zn(OH)_2$ incorporated into the aluminium oxide film, enhances the loss of aluminate into the electrolyte solution.

There are various ideas as to where copper is thought to accumulate on the surface of an aluminium copper alloy on polarisation of the metal. Various workers have carried out research into the incorporation of copper species at the alloy/film interface. Paez *et al* [3] made electrochemical measurements on an Al-3.5 wt% Cu alloy. They reported that the incorporation of copper species is related to the clustering processes at the alloy/film interface, which leads to significant enrichment of copper in the form of relatively short lived copper oxide fingers.

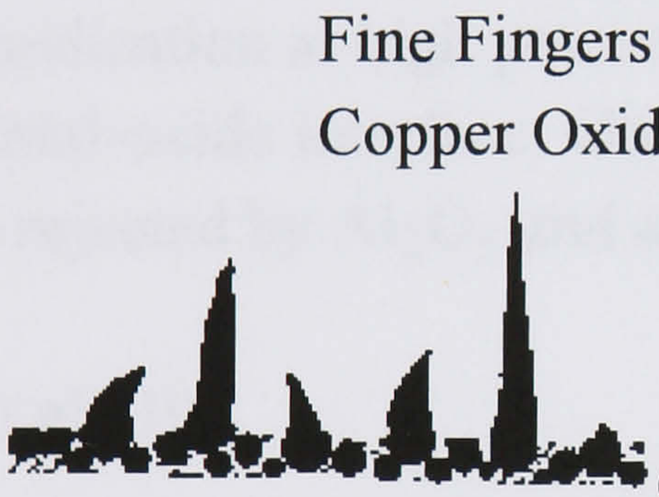

Fig. 6.4 Incorporation of copper species from the copper enriched layer developed at the alloy/film interface for an aluminium - copper alloy

They concluded that isolated copper atoms in the alloy may enter the alumina film at the alloy/film interface. The majority of copper atoms are considered to form clusters with vacancies, the development of which is responsible for interfacial enrichment of copper, which eventually leads to a steady-state copper concentration, at the alloy/film interface.

Mackintosh *et al* [4] studied the rate of motion of metallic foreign atoms introduced into the surface layers of aluminium specimens, relative to aluminium ion movement. Species with lower oxidation potentials than aluminium were oxidised and incorporated into the Al_2O_3. Species with higher oxidation potentials than aluminium were not oxidized and remained incorporated within the metal. A sample of copper implanted beneath the surface of the metal was found to be 100% present at the oxide/metal interface after anodic oxidation.

Strehblow et al [5] investigated the incorporation of copper in the anodic oxide of a copper rich aluminium alloy at high potentials. They concluded that copper is not incorporated into the oxide phase unless the potential drop at the metal/oxide interface is increased by an additional over voltage. This is due to the significant difference of the standard electrode potentials for the formation of the corresponding oxides and hydroxides. This of course is dependent upon the pH of the electrolyte.

It was found that in a 0.1M borax solution which is known to have a low solubility for copper oxide and hydroxide, copper accumulates at the surface of the specimen during potentiodynamic sweeps [6]. Films were shown to have similar corrosion properties to those of pure copper and at pH 9.2, the polarisation curves obtained were closely related to those of pure copper. Anions with complexing properties for copper ions resulted in an increased solubility for copper oxide/hydroxide helping to form a copper free surface.

It has been shown by Strehblow, Melliar-Smith, and Augustyniak [7], that the oxide film does not contain any copper and its failure during gavanostatic anodization at high potentials is closely related to an enrichment of copper at the metal-oxide interface. Observations by Chiu and Chang [8], indicate that copper is rejected by Al_2O_3 and accumulates at the Al_2O_3/Al interface.

ii) pH 10

Unit increase in pH causes an approximate 10 fold increase in corrosion rate for both alloys. This is a similar effect to that observed on pure aluminium. An explanation for this in terms of hydroxide solubility, is found in section 3.2. Anodic dissolution currents at pH 10 are comparable for 7075 and pure aluminium, something which is not observed at pH 9. At higher pH values, the dissolution of aluminate from the surface must be the more dominant factor controlling the corrosion rate of the metal. Contributions towards the corrosion current from mixed potentials and changes in the structure of the protective oxide/hydroxide with incorporation of foreign metal complexes, appear less significant.

iii) Emulsions

For pure aluminium in contact with a cutting fluid emulsion, the corrosion rate is reduced by a factor of approximately 10, compared to that when in contact with an aqueous solution of the same pH (section 4.1) It has also been shown that the absence of oxygen significantly reduces the rate of corrosion of aluminium

(section 3.1.1). It should be noted that the results presented here are for aluminium in contact with aerated emulsion and with aqueous solutions which are deaerated. It is therefore difficult to make any clear statements regarding the effect the emulsion has on the alloys compared to pure aluminium, although it is expected that the corrosion rate varies in a similar manner.

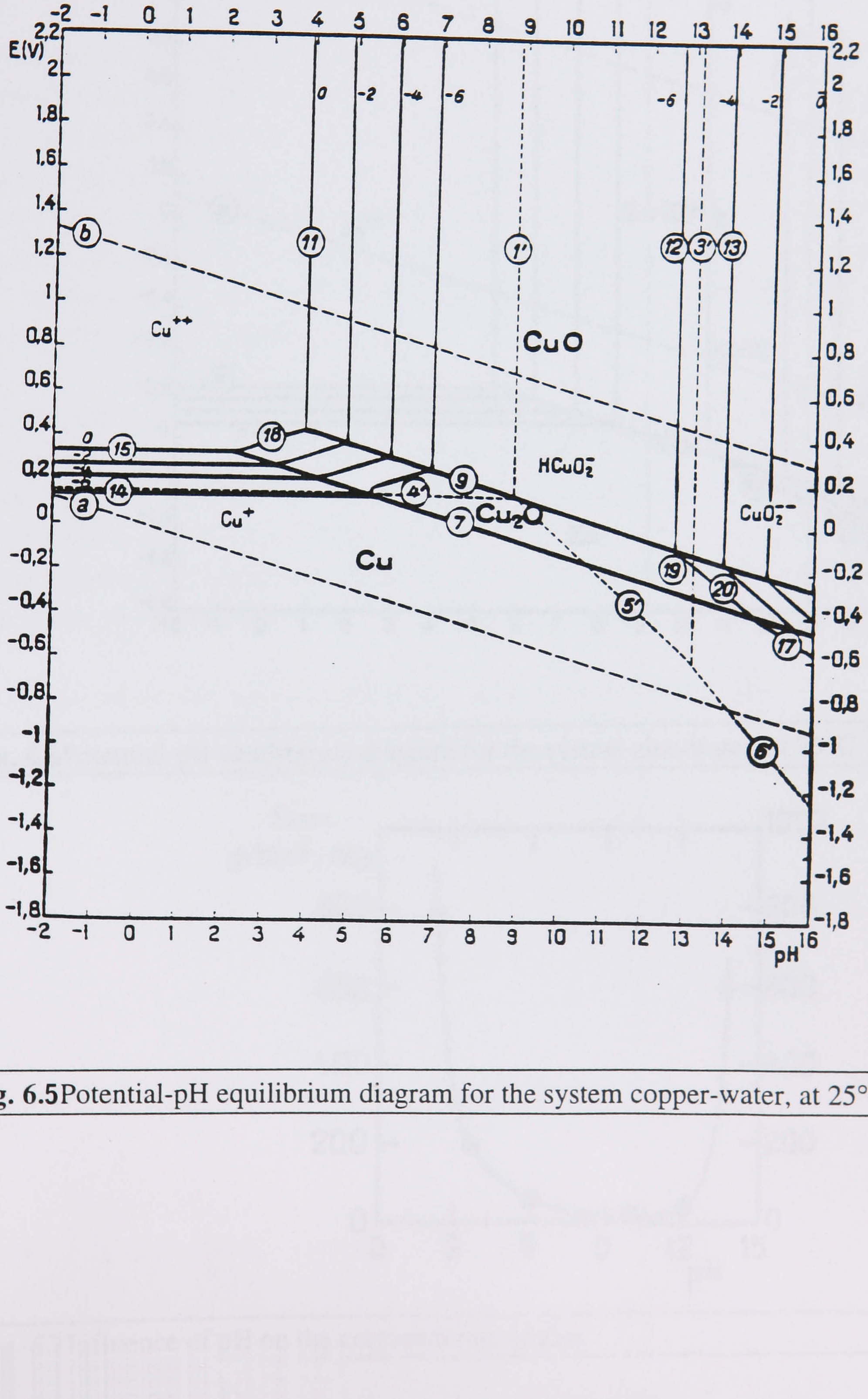

Fig. 6.5 Potential-pH equilibrium diagram for the system copper-water, at 25°C.

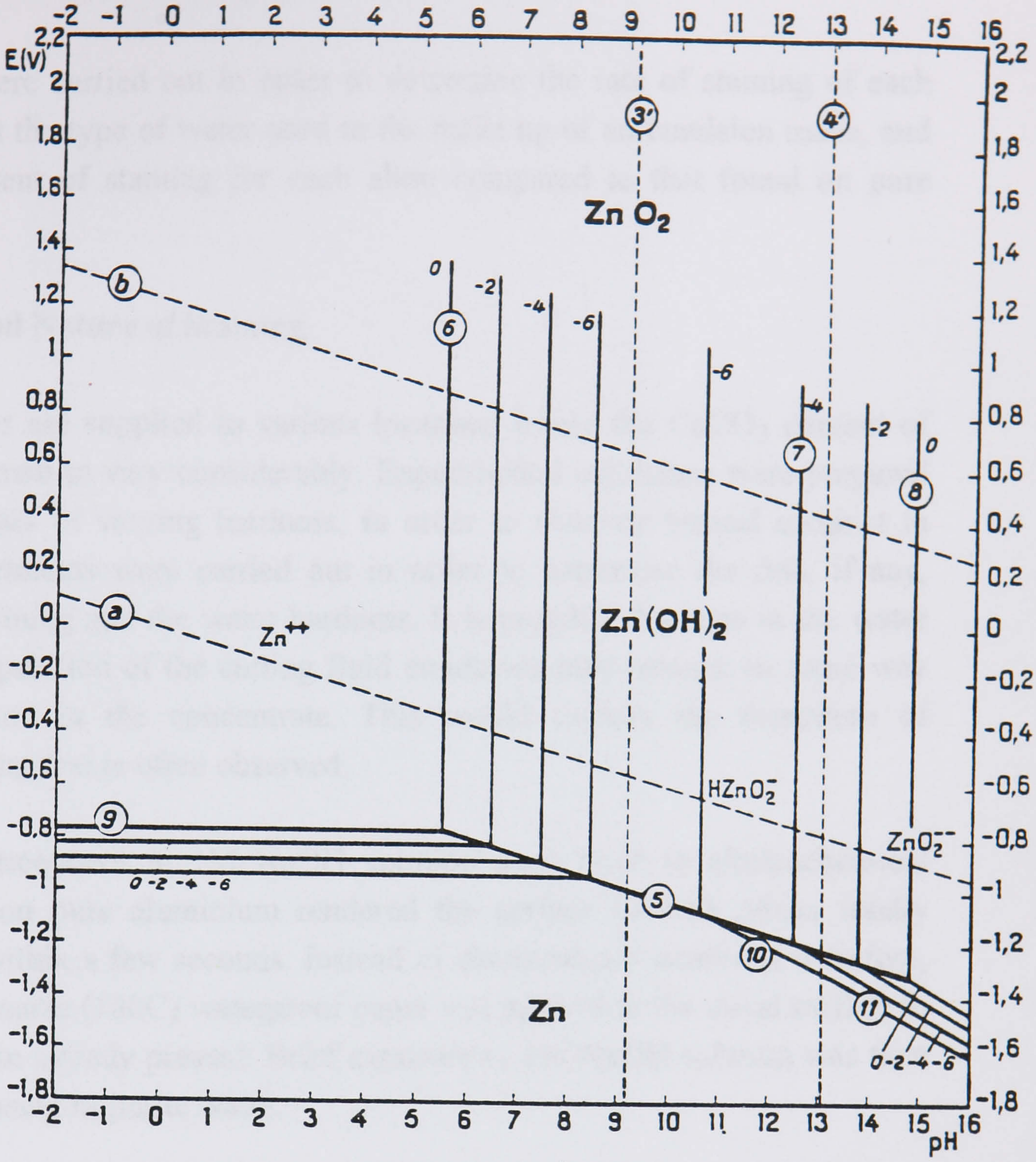

Fig. 6.6 Potential-pH equilibrium diagram for the system zinc-water, at 25°C

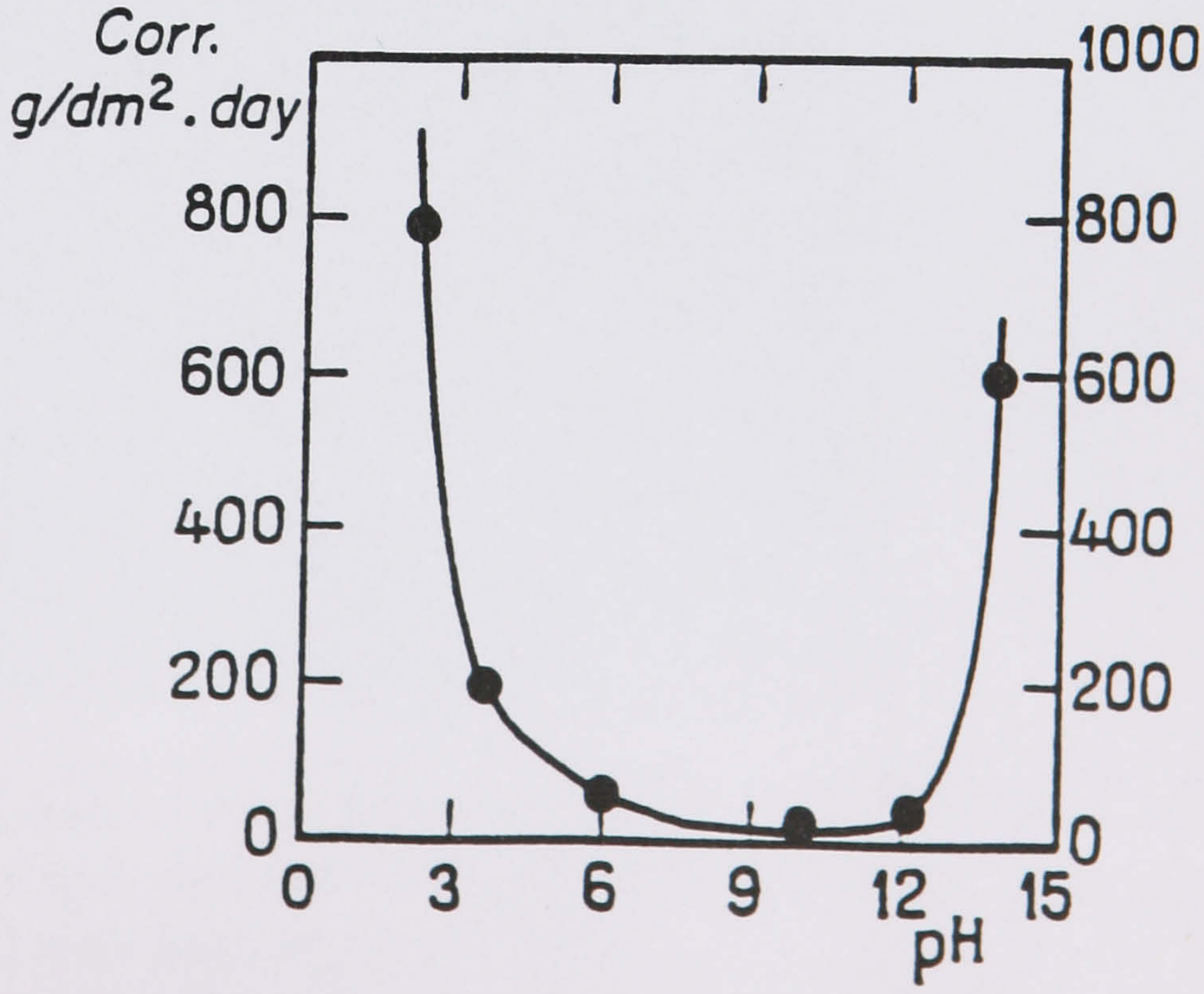

Fig. 6.7 Influence of pH on the corrosion rate of zinc

6.3 Staining of Aluminium Alloys

Experiments were carried out in order to determine the rate of staining of each alloy, the effect the type of water used in the make up of an emulsion made, and the general extent of staining for each alloy compared to that found on pure aluminium.

6.3.1 Extent and Nature of Staining

Oil concentrates are supplied to various locations where the $CaCO_3$ content of the water is known to vary considerably. Experimental emulsions were prepared using water types of varying hardness, in order to simulate typical conduct in industry. Experiments were carried out in order to determine the link, if any, between the staining and the water hardness. It is possible that ions in the water used in the preparation of the cutting fluid emulsions may interact in some way with components in the concentrate. This would explain the formation of unsightly staining that is often observed.

Chemical pre treatment in 1M NaOH solution used prior to electrochemical measurements on pure aluminium rendered the surface of both alloys totally stained black within a few seconds. Instead of chemical pre treatment therefore, abrasion with coarse (180C) waterproof paper was applied to the metal surface to remove any stain already present. Brief exposure to 1M NaOH solution was then made before rinsing in purite water.

Photographs of stained aluminium alloy surfaces are shown in Fig. 6.8.

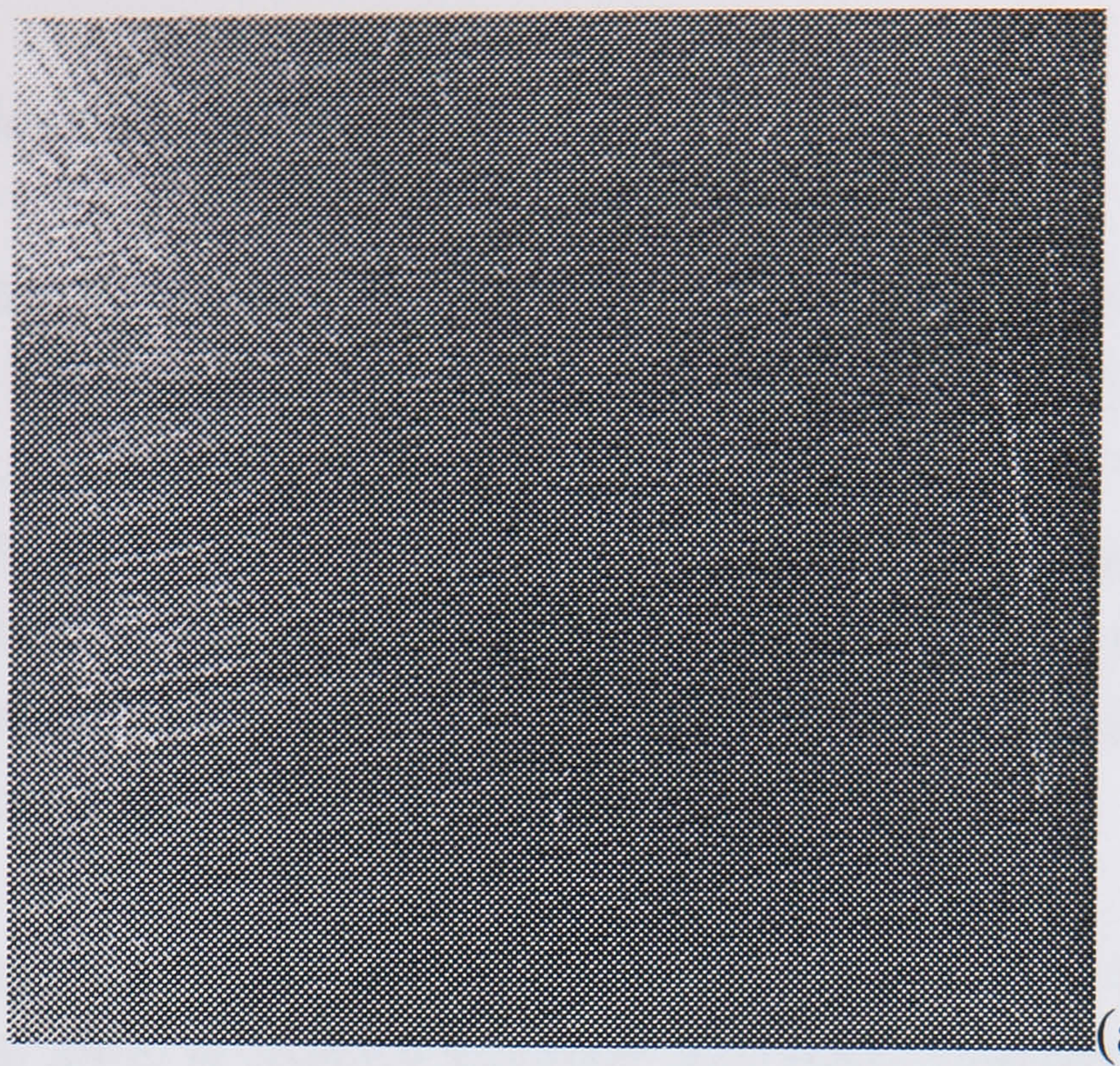

(a)

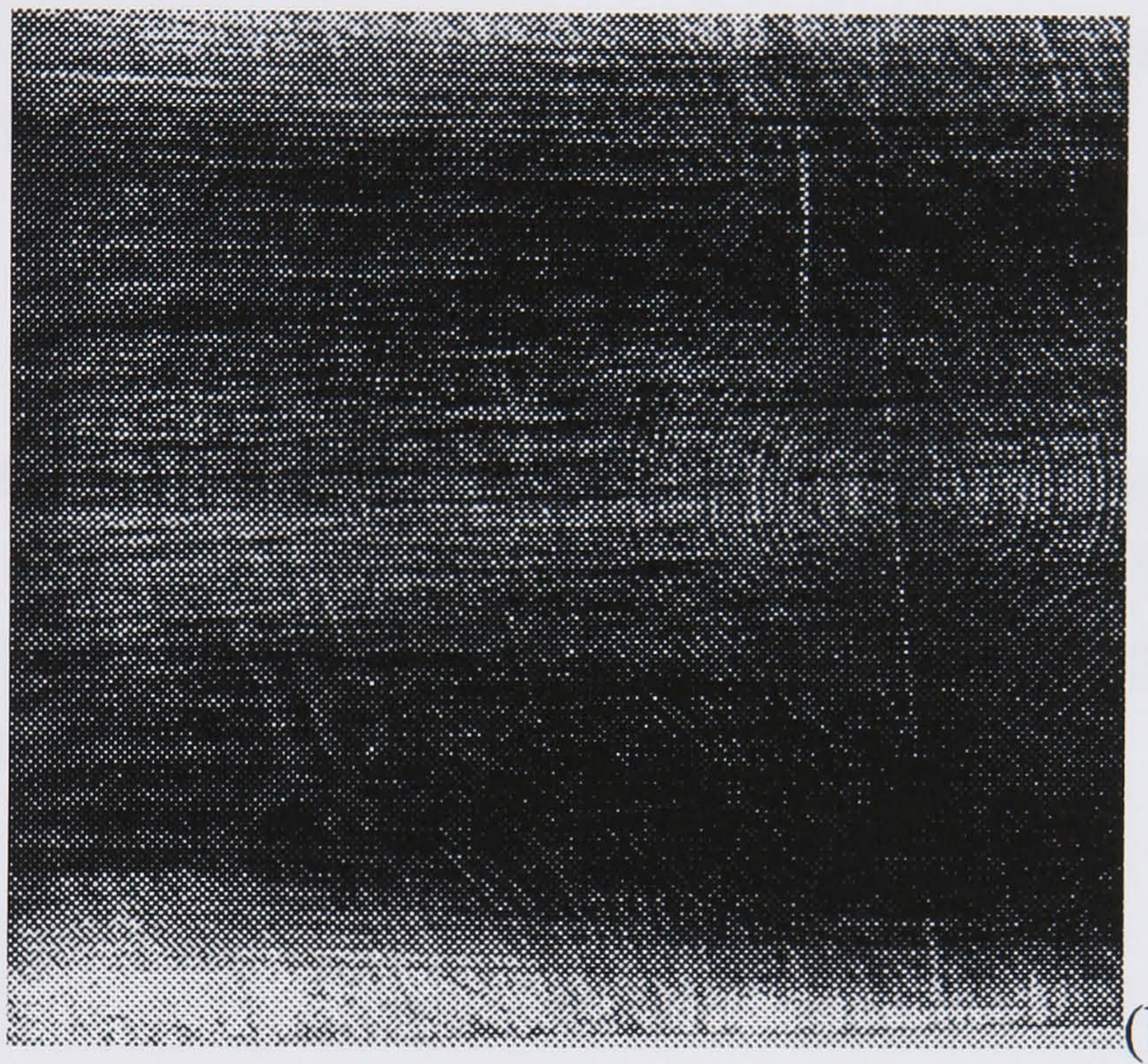

(b)

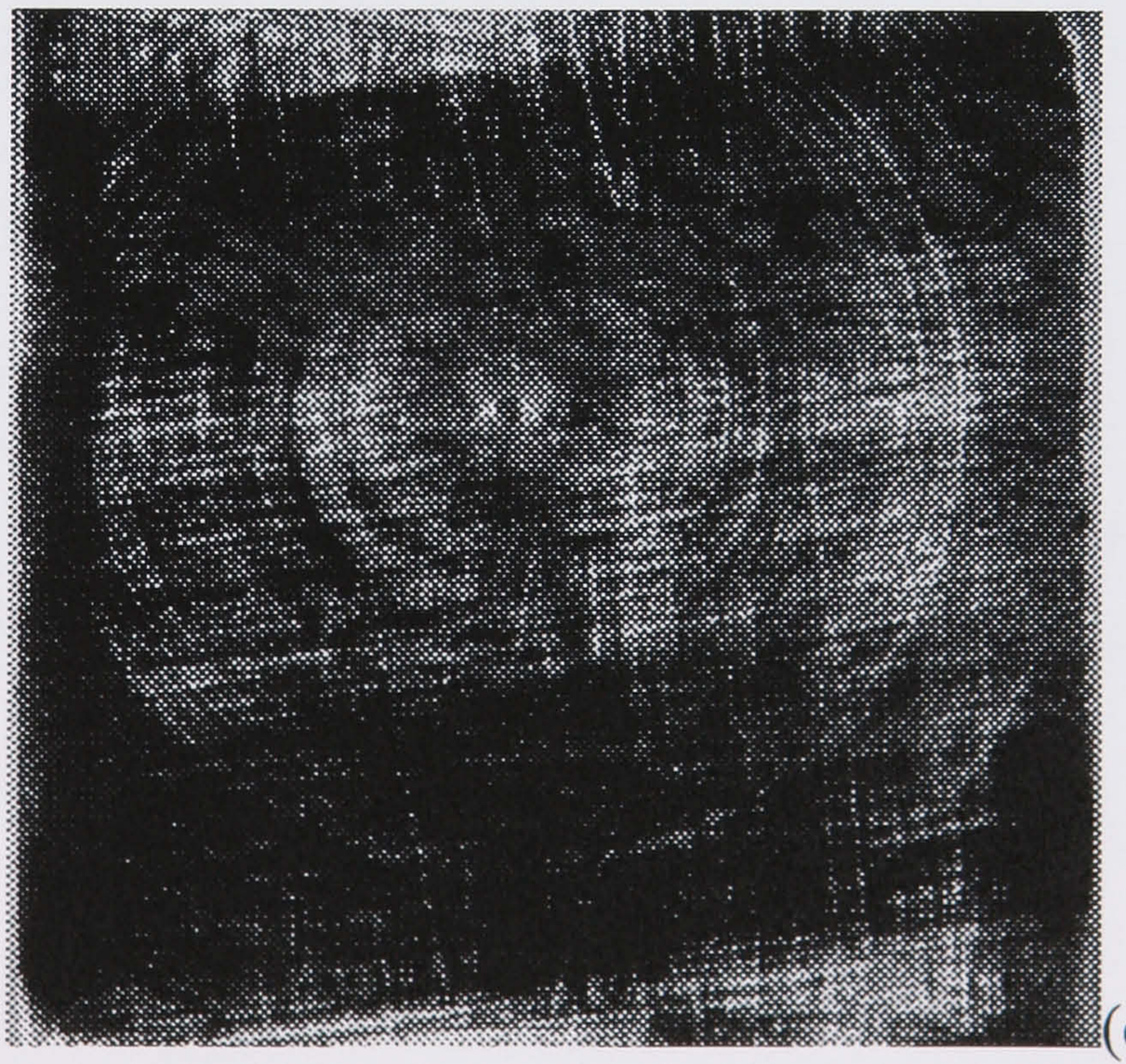

(c)

Fig. 6.8 Photographed stained alloy surfaces; (a) 2024, after 24hrs exposure to 10% emulsion prepared with distilled water, (b) 7075, after 24 hrs exposure to a 10% emulsion prepared with hard water (400ppm $CaCO_3$), (c) 2024, after 24 hrs exposure to a 10% emulsion prepared with hard water (400ppm $CaCO_3$).

Visual Observations

Sample (a) became rather dull in appearance after exposure to the emulsion, and after 2 to 3 days became almost fully stained. This was true for both metal alloys in contact with a 10% emulsion prepared with distilled water. Samples (b) and (c) show the extent of staining of both alloys, after 24hrs in contact with an emulsion prepared from hard water containing 400 ppm $CaCO_3$. It is clear from these results that the presence of $CaCO_3$ in the water is a contributory factor towards the nature and extent of the staining.

Although it is not clear from the photographs produced here, the staining present on the copper rich alloy is slightly 'mottled', and more 'copper' in colour. It is also apparent that the zinc alloy forms a darker stain compared to that observed on the copper rich alloy.

EDAX

In order to determine the nature of the stain material on the surface of each alloy, metal samples were prepared for examination by EDAX as described in experimental section 2.3.11. Samples 1 and 2 were mechanically pre treated and the remaining samples were chemically pre treated.

Table 6.3 EDAX - Elemental distribution of metallic species on the surface of pure aluminium 99.999% and aluminium alloys 2024 and 7075 after immersion in various electrolytes for 100 hrs.

Sample No.	Alloy	Solution	CuK	ZnK	AlK	Ca K	Total (elemental weight %)
1	2024	400ppm $CaCO_3$, 10% emulsion	2.10	0.35	97.50	0.05	90.46
2	7075	"	0.80	3.65	95.45	0.05	89.93
3	2024	Purite	5.30	0.05	94.65	0.10	56.90
4	7075	"	1.70	8.55	89.85	0.20	59.64
5	2024	400ppm $CaCO_3$, 10% emulsion	2.60	0.20	96.9	0.45	63.41
6	7075	"	1.10	4.25	94.55	0.05	69.86
7	Pure Al	"	0.05	0.05	100.00	0.00	92.46
8	2024	purite, 10 % emulsion	3.75	0.35	96.3	0.00	74.89
9	7075	"	0.80	3.60	95.6	0.05	77.17
10	pure	"	0.00	0.05	99.90	0.05	90.81

Analysis

i) Mechanical vs chemical pre treatment (sample 1 *vs* 5, and sample 6 *vs* 2)

There is no significant elemental difference between mechanically and chemically pre treated samples. The % total elemental weight however indicates that a thicker surface layer is present on the mechanically pretreated samples.

7075 - 0.5% more Zn found in the surface of the chemically pretreated sample.
2024 - 0.5% more Cu, and 0.15% less Zn, in the chemically pretreated sample.

ii) $CaCO_3$ vs Purite (samples 5 *vs* 8, 6 *vs* 9, and 7 *vs* 10)

0.45% more calcium is detected on the surface of sample 5 left in an emulsion made up in hard water containing 400ppm $CaCO_3$. There are no other significant differences in the metallic surface compositions.

7075 - 0.3% more Cu, 0.75% more Zn 0.05% more Ca, found in the 400ppm $CaCO_3$ emulsion immersed sample.

2024 - 1.15% less Cu, 0.15% less Zn, 0.45% more Ca, in 400ppm $CaCO_3$ emulsion immersed sample.

No significant elemental differences were found for pure aluminium.

iii) Purite water vs emulsion (samples 3 and 4, vs samples 5 and 6)

A significant amount of the metal alloying element was found on samples immersed in purite. The same samples left in an emulsion showed smaller traces of the alloying metal at the surface.

7075 - 0.9% more Cu, 4.95% more Zn in the purite immersed sample.
2024 - 1.55% more Cu, 0.3% less Zn in the purite immersed sample.

6.3.2 Rate of Stain Formation

An experiment was designed in order to determine the time taken for the surface of the alloy to change colour when in contact with aqueous solutions of increasing pH. Samples of both aluminium alloys were polished using coarse (180C) waterproof paper, and immersed in aqueous solutions of varying pH. The time was noted before the alloy was completely covered in stain material.

At pH 10, the alloy was polarised both anodically and cathodically, and the colour of the electrode was analysed after each sweep. Potential sweeps of approximately 500mV were made. They were initiated 100mV in a positive and negative direction from the OCP, at a rate of 1mV/s.

Table 6.4 Time taken for complete surface staining of pure aluminium samples immersed in aqueous bicarbonate buffer solutions of varying pH.

pH	Time for Taken to form Stain 2024	Time for Taken to form Stain 7075
9.0	days	days
10.0	with anodic polarisation only	no discolouration observed on polarisation
11.0	80 mins	45 mins
13.5	3 mins	2 mins

Staining occurs rapidly within minutes on both alloys when in contact with a strongly alkaline solution. The rate of staining decreases for both alloys, with decreasing strength of alkalinity of solution. The copper rich alloy generally stains at a faster rate than the zinc rich alloy.

6.3.3 Discussion

Table 6.5, 'The hydrolysis of metal complexes of Al, Cu, and Zn, at 25°C', constructed from Figs 3.6, 6.9, and 6.10 [9], helps to explains why the extent of staining increases with increasing pH, and also provides evidence to explain the origin of the 'copper' coloured surface, which develops on alloy 2024.

Table 6.5 The hydrolysis of metal complexes of Al, Cu, and Zn, at 25°C.

Equilibrium	pH	Log Conc^n
$Al(OH)_3 \equiv [Al(OH)_4]^-$	9	-5.0
$Al(OH)_3 \equiv [Al(OH)_4]^-$	10	-4.0
$Al(OH)_3 \equiv [Al(OH)_4]^-$	11	-3.0
$Cu(OH)_2 \equiv [Cu(OH)]^+$	9	-9.5
$Cu(OH)_2 \equiv [Cu(OH)_3]^-$	10	-10.0
$Cu(OH)_2 \equiv [Cu(OH)_3]^-$	11	-9.0
$Zn(OH)_2$ (s) $\equiv Zn(OH)_2$ (aq)	9	-5.8
$Zn(OH)_2$ (s) $\equiv [Zn(OH)_3]^-$	10	-6.5
$Zn(OH)_2$ (s) $\equiv [Zn(OH)_3]^-$	11	-5.8

The oxide/hydroxides of the alloying elements Cu and Zn are much less soluble than the corresponding aluminium oxide/hydroxide. This relationship becomes more apparent with increasing pH. Thus, in aqueous solution, the aluminium species preferentially dissolves leaving an excess of Cu/Zn species at the surface, depending on which alloy is being considered. From thermodynamic considerations we would expect copper metal to be present at the interface as opposed to copper oxide/hydroxide species. As the aluminium hydroxide dissolves in solution a copper metal rich layer in time will be exposed giving rise to a copper coloured stain on the surface. In the case of the zinc alloy the thermodynamics tends towards the more favourable zinc oxide/hydroxide species at pH 9 and 10, which depending on the stoichiometry, is black. Again, as the aluminium dissolves in the solution, a zinc oxide rich surface results.

Previous work by Bombara and Bernabai [10], showed that at pH values intermediate between the passivity range and the alkaline corrosion range,

aluminium develops a film, sometimes so dark that is referred to as 'black oxide'. These films were found to be far from being protective, undergoing micro-cracking with time, with penetrating pits forming at the intersection of cracks. The darkness is thought to be due to the incorporation of metal particles from the reaction;

$$3Al^{+} = Al^{3+} + 2Al$$

subvalent Al^{+} ions giving metallic Al, and normal trivalent ions. This is a possible explanation or contributary factor towards the alloy staining that is observed in the present work.

It is surprising to discover that the stain formed on the surface of a zinc rich alloy is dark in colour, when zinc oxide in its powdered form is normally white. Copper oxide is dark in colour due to the non stoichiometric nature of the copper which may exist as Cu^{I} and Cu^{II}. Electrons are free to move around to a certain extent throughout the structure, the oxide behaving like a semi-conductor. It is these electronic transitions which give rise to light absorption, and the oxide appears dark in colour. The same is true for zinc oxide but to a lesser extent. Zinc is less stoichiometric than copper, Zn^{I} not being as stable as Zn^{II}.

The effect of the staining is exaggerated at higher values of pH owing to the 10 fold increase in solubility of aluminium oxide/hydroxide with unit increase in pH.

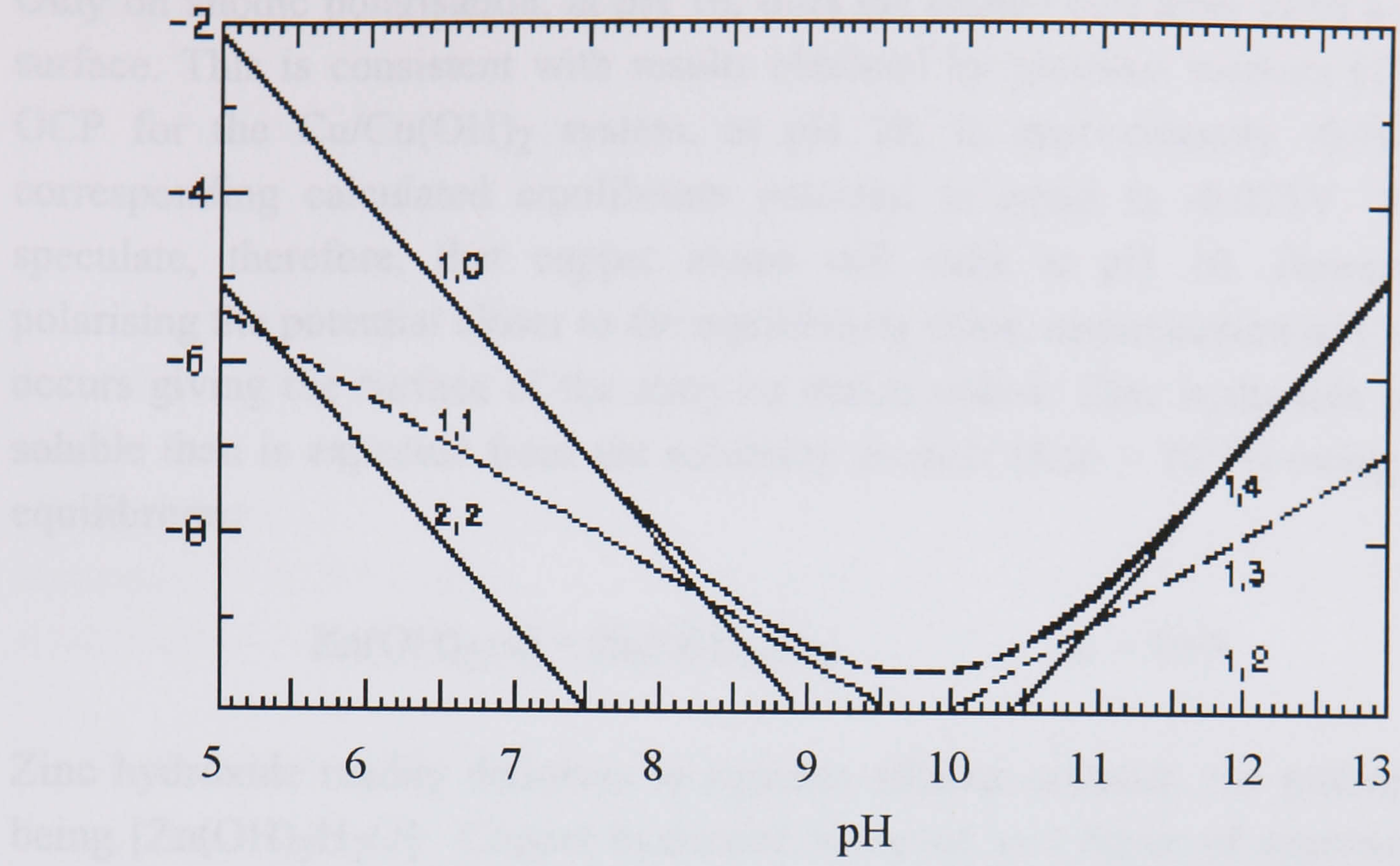

Fig. 6.9 Distribution of hydrolysis products (x,y) at 25°C in solutions saturated with CuO. The minimum is dashed because of the uncertainty with which the $Cu(OH)_2$ and $Cu(OH)_3^-$ species are known.

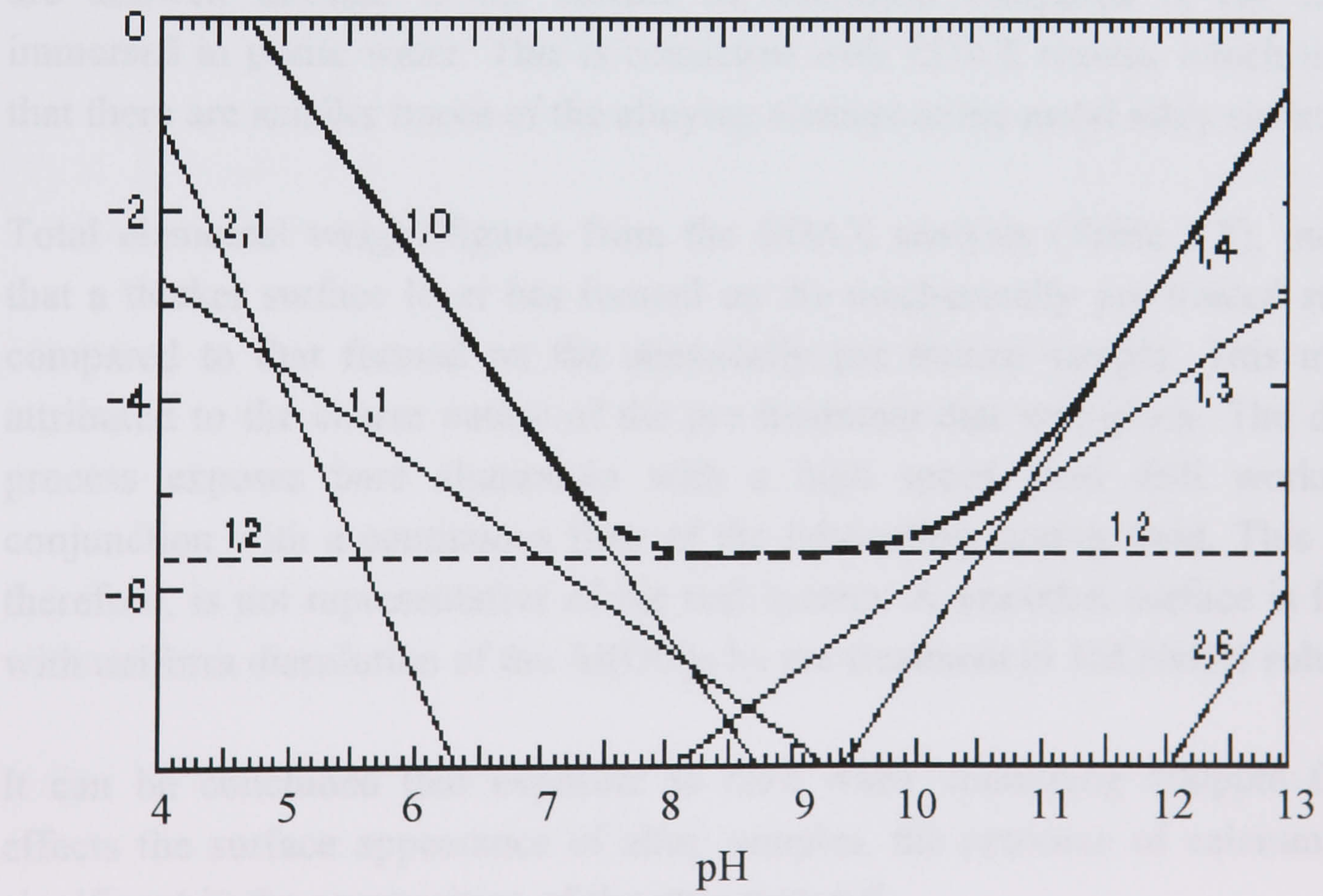

Fig. 6.10 Distribution of hydrolysis products (x,y) at 25°C in solutions saturated with ZnO. The minimun is dashed because of the uncertainty with which the $Zn(OH)_2$ species is known.

Only on anodic polarisation, at pH 10, does the copper rich alloy form a stained surface. This is consistent with results obtained by previous workers [11]. The OCP for the $Cu/Cu(OH)_2$ system, at pH 10, is approximately -0.76V, the corresponding calculated equilibrium potential is equal to -0.075V. We can speculate, therefore, that copper atoms will exist at pH 10. However, on polarising the potential closer to the equilibrium value, accumulation of $Cu(OH)_2$ occurs giving the surface of the alloy its darker colour. Zinc hydroxide is more soluble than is expected from the solubility product ($Ksp = 10^{-11}$) owing to the equilibrium;

$$Zn(OH)_2\ (s) = Zn(OH)_2\ (aq) \qquad K = 10^{-6}$$

Zinc hydroxide readily dissolves in aqueous alkaline solution, the principle ion being $[Zn(OH)_3H_2O]^-$. Copper hydroxide however, is a factor of approximately 10^3 times less soluble than zinc hydroxide, at the same pH (refer to Figs 6.5 and 6.6).

From earlier work on aluminium immersed in an emulsion, it was shown that an additional protective layer forms on the metal surface. If the same is true of the aluminium alloy samples it is possible that less of the various alloying elements are allowed through to the surface on corrosion compared to the samples immersed in purite water. This is consistent with EDAX results, which indicate that there are smaller traces of the alloying element at the metal alloy surface.

Total elemental weight figures from the EDAX analysis (Table 6.3), indicates that a thicker surface layer has formed on the mechanically pre treated surface, compared to that formed on the chemically pre treated sample. This may be attributed to the coarse nature of the pre treatment that was given. The drilling process exposes bare aluminium with a high speed steel drill working in conjunction with a continuous flow of the lubricating cutting fluid. This result, therefore, is not representative of the real system. A smoother surface is formed with uniform dissolution of the $Al(OH)_3$ by pre treatment in 1M NaOH solution.

It can be concluded that exposure to hard water containing 400ppm $CaCO_3$ effects the surface appearance of alloy samples, the presence of calcium being significant in the composition of the stain material.

References

[1] I. J. Polmear, *Light Alloys*, *Metallurgy of the Light Metals*, E. Arnold, New York (1989).

[2] Marcel Pourbaix, 'Atlas of electrochemical equilibria in aqueous solutions', 2nd Edition, NACE, Cebelcor, Houston, Texas p.388, p.409.

[3] M. A. Paez, T. M. Foong, C. T. Ni, G. E. Thompson, K. Shimizu, H. Habazaki, P. Skeldon and G. C. Wood, 'Barrier type anodic film formation on an Al-3.5 wt% Cu alloy', *Corr. Sci.*, **38** (1996) pp. 59-72.

[4] W. D. Mackintosh, F. Brown and H. H. Plattner, 'Mobility of foreign atoms during the anodic oxidation of aluminium', *J. Electrochem. Soc.*, **121** (1974) pp.1281- 1286.

[5] H. H. Strehblow and C. J. Doherty, 'Examination of Al-Cu films during anodic oxidation', *J. Electrochem. Soc.*, **125** (1978) pp.30-33.

[6] H. H. Strehblow, C. J. Melliar-Smith, and V. M. Augustyniak, 'Examination of Al-Cu films during the galvanostatic formation of anodic oxide', *J.Electrochem. Soc.*, **125** (1978) pp. 915-919.

[7] H. H. Strehblow, C. J. Melliar-Smith, and V. M. Augustyniak, submission to *J. Electrochem Soc.*, (1978).

[8] Re-Long Chiu, Peng-Heng Chang and Chih-Hang Tung, 'Al_2O_3 films formed by anodic oxidation of Al-1% Si-0.5% Cu films', *J. Electrochem Soc.*, **142** (1995) pp. 525-531.

[9] C. F. Baes, Jr. and R. E. Mesmer, '*The Hydrolysis of Cations*' Wiley, New York (1976).

[10] G. Bombara and U. Bernabai, 'Corrosion of aluminium in multimetal water systems', *Br. Corros. J.*, **11** (1976) pp.25-30.

[11] G. Meyer-Rodenbeck, T. Hurd and A. Ball, 'On the abrasive-corrosive wear of aluminium alloys', *Wear*, **154** (1992) pp. 305-317.

CHAPTER 7

CONCLUSIONS

7.0 Main Conclusions and Suggestions for Future Work

7.1 Introduction

In this thesis, corrosion in relation to the drilling of aluminium and aluminium alloys in the presence of cutting fluid emulsions has been studied. The main objective of this work was to determine the corrosion rate of aluminium and aluminium alloys when in contact with various weakly alkaline solutions. An investigation into some of the mechanistic aspects of aluminium corrosion in an environment similar to that experienced by aluminium metal during the drilling procedure, was also carried out. Another aspect of the work involved the formulation of new cutting fluid emulsions which avoided the use of amines. Factors such as cost and availability of the replacement constituents were taken into account, as well as environmental constraints, product stability, and aesthetics.

Chemical pre-treatment of the electrode surface, though used extensively in the work reported here, was not considered to be representative of the actual drilling process that occurs, where a fresh aluminium surface is generated mechanically. A cell was therefore designed which enabled a rotating disc of aluminium to be lowered onto a stationary glass frit situated beneath it. A bare metal surface was exposed to the electrolyte solution contained within the cell, and the electrochemical measurements were made *in situ*. An investigation into the nature of oxide recovery was also carried out using this technique. The results were compared to those obtained by Burstein and Cinderey in a similar experiment.

Techniques used have included, linear sweep potentiometry, Tafel analysis, impedance analysis, SEM, and EDAX.

7.2 Main Conclusions

1. For aluminium in contact with aqueous solutions, in the pH range 7-10, the corrosion rates varied between 10^{-7} and 10^{-5}A cm^{-2}. This is comparable to the results found in the literature. Corrosion rates were higher (about a factor of 10 times) in the presence of oxygen, compared to those in a de-oxygenated solution. In the absence of oxygen, the open circuit potential was 200-300 mV more negative compared to that found in an oxygenated solution at the same pH.

2. Each unit increase in pH between 8.2 and 11 was found to give an approximate 10 fold increase in the corrosion current of aluminium in aqueous solution. This is as expected and is consistent with the degree of solubility of the oxide layer.

3. Mechanistic studies show that the rate of the cathodic reaction which occurs when aluminium corrodes in weakly alkaline solution i.e.

$$e^- + H_2O = \tfrac{1}{2}H_2 + OH^-$$

is a function of the electrode potential, and not of the solution pH. Since the thickness of the anodic film on aluminium varies with pH, the reaction rate is concluded to be independent of film thickness. These observations are consistent with a mechanism which can be described by the reduction of water molecules which are incorporated into the anodic film. The slow step in the anodic reaction i.e.

$$Al + 4OH\text{-} = Al(OH)_4^- + 3e^-$$

is the formation of aluminate from the anodic film on the electrode surface.

4. Impedance measurements showed that the electrode/solution interface behaves as a resistance in parallel with a capacitance. The capacitance values indicate a very thin surface film of oxide/hydroxide on the aluminium in most cases.

5. The aluminium corrosion rate is approximately 10 times lower when the metal is in contact with a typical metal working fluid compared to when in contact with an aqueous borax buffer of the same pH. The cutting fluid causes both the rate of the anodic and cathodic processes on aluminium to be reduced (in comparison to when in contact with an aqueous solution), so that the overall corrosion rate is reduced by a factor of approximately 10. The reduction of the rate of the cathodic process is due to the competition of the oils in the emulsion with water molecules for contact with the metal surface. There is some evidence to suggest that the composition of the passive layer is also modified by the presence of the hydrophobic species from the oil.

6. The corrosion rate of aluminium in contact with a cutting fluid emulsion is independent of the presence of amines.

7. The corrosion rate of a mechanically pre-treated metal surface can successfully be estimated *in situ*, by a method of continuous surface renewal as described. The corrosion rate of a mechanically pre-treated aluminium surface is a factor of 7 times higher than for a chemically pre-treated electrode under identical conditions. Abrasion of the surface causes the aluminium oxidation/dissolution rate to increase to a greater extent (by a factor of nearly 20) relative to the

cathodic reaction. This is attributed to, i) the repair of $Al(OH)_3$ and ii) the normal loss of aluminium as $Al(OH)_4^-$.

8. Both aluminium alloys 2024 and 7075, corrode at a greater rate compared to that of pure aluminium when under similar conditions. The cathodic current increases due to an effect brought about by the incorporation of copper/zinc atoms in to the aluminium oxide layer thus altering its structure. A unit increase in pH causes an approximate 10 fold increase in the corrosion rate for both alloys. This is a similar effect that is observed on pure aluminium.

9. Staining occurs rapidly on both of the alloys when in contact with strongly alkaline solutions. In general, the copper rich alloy stains at a faster rate compared to the zinc rich alloy. The effect of the staining is exaggerated at higher values of pH, again owing to the 10 fold increase in solubility of aluminium oxide/hydroxide with unit increase in pH.

10. Exposure to hard water containing 400ppm $CaCO_3$ effects the surface appearance of alloy samples. The presence of calcium in the water used to dilute the oil concentrate, is a contributory factor in the composition of the stain material found on the metal surface.

7.3 Suggestions for Future Work

Following the discussion in section 4.3.1 regarding the nature of the aluminium metal surface after exposure to a 5% cutting fluid emulsion, it was concluded that the surface is regularly porous producing a 'honeycomb' effect after exposure for 24 hours (Fig. 4.3(d)). It would be of interest to determine whether this effect is caused by the chemical reaction between the aluminium oxide/hydroxide and ester groups from the cutting fluid, the ester groups subsequently forming an additional protective barrier against corrosion. This information would provide an insight into the mechanism of corrosion of aluminium in contact with cutting fluids. FTIR would also be a useful technique for determining the presence of carbonyl groups on the surface. Ellipsometry is another useful technique for this application.

None of the work carried out so far has allowed us to obtain details of the composition of the stain material found on the surface of both aluminium alloys. Careful analysis of the aluminium alloy surface following immersion in solutions of high pH, and in calcium carbonate containing solutions using the same techniques as above would be advantageous. Once the nature of the stain material

is known, then steps can be taken in order to reduce the extent of staining of the alloy when in contact with the various staining solutions.

Often the cutting fluid is recycled throughout the drilling procedure which means that the fluid may be in use over long periods of time. During this time swarf particles accumulate saturating the fluid with aluminate ions. It is also known that the emulsion becomes less stable with time, the oil and water phases separating as a result. Particle size analysis carried out on the emulsion after various lengths of time after use, would provide useful information about the relationship between the short term aluminium corrosion rate and the particle size of oil droplets in the fluid with time.

It is important to remember that although it is the aluminium that is being drilled, the corrosion of which has been considered in this work, the drilling tools are usually made of stainless steel. Corrosion of the machine tools would lead to increased power consumption, poor finish on the metal subject and the introduction of foreign ions into the emulsion - a possible cause of emulsion instability. Would it be beneficial to include a stainless steel corrosion inhibitor within the fluid? There is scope here therefore for some corrosion rate measurements on stainless steel in contact with cutting fluid emulsions.

At present the fluid is designed for use in contact with selected aluminium alloys. It would be of interest to explore the effectiveness of the cutting fluid in contact with some other alloys and indeed ultimately design a fluid which would be universally acceptable for use in contact with most aluminium alloys.

Finally, it is known that during drilling, temperatures up to 1000°C are reached at the tip of the drill. All of the work carried out in this thesis has been at room temperature. Corrosion rate measurements made at elevated temperatures would present a more accurate analysis of the corrosion process that occurs during the drilling procedure.

APPENDIX A

Measurement of Microbial Survival 1/PE/146

Castrol International Marketing and Technology Division

Metalworking Technology Department Procedure

Contents:

1. Flowchart for Measuring Microbial Survival

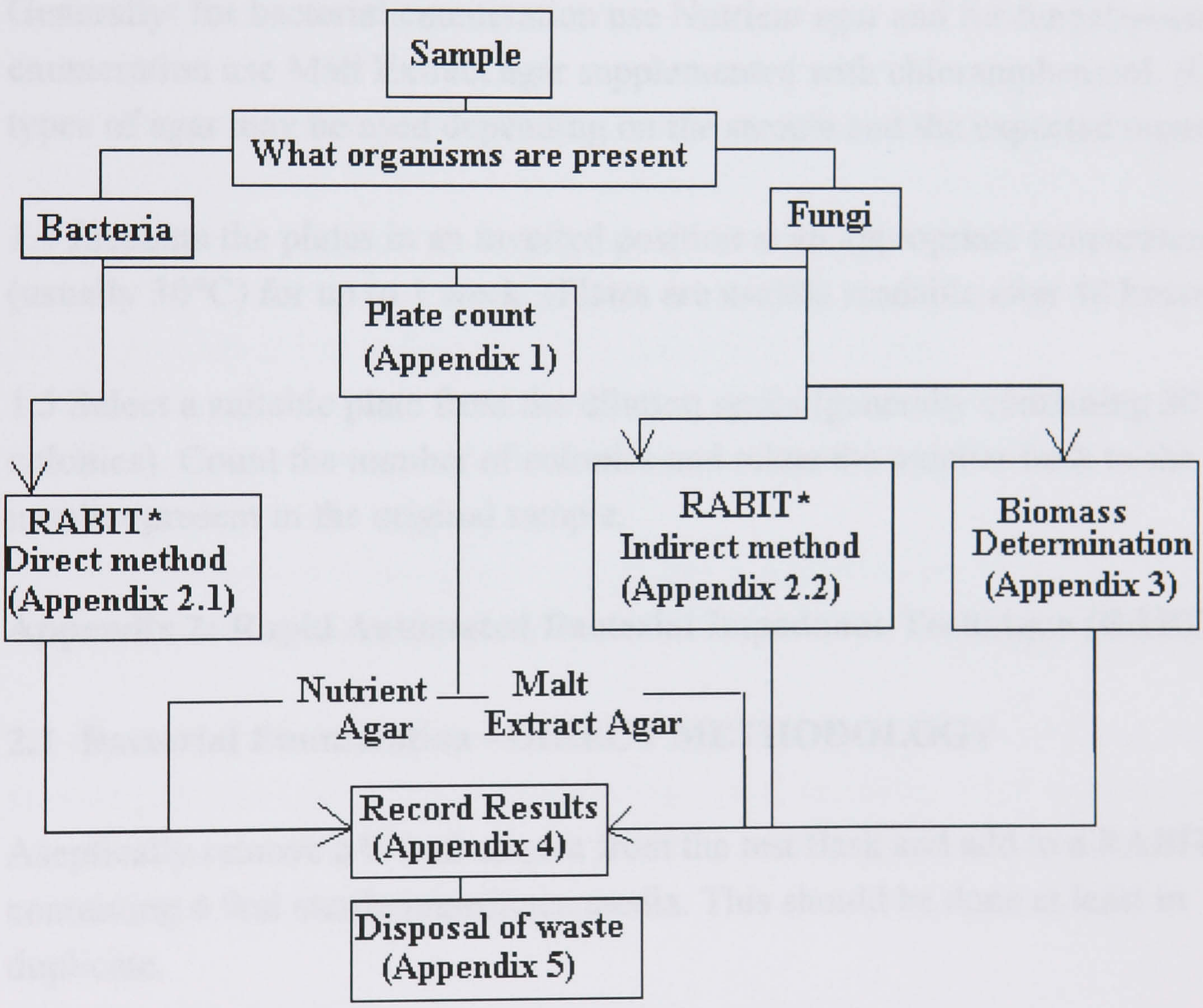

* The two RABIT methods (direct for bacteria and indirect for fungi) are only suitable for standard test organisms. Any samples in which the microbial population is varied, or unknown should be plate counted.

Appendix 1: Conventional Plate Counts

1.1 Aseptically remove a 1 ml aliquot from the sample. Add this to a test tube containing 9ml sterile deionised water. Mix tube contents thoroughly using a 'whirly-mixer'.

1.2 Remove 1 ml from this tube and transfer to another clean tube containing 9ml sterile water. This process is repeated until a decimal dilution series has been prepared to a suitable level (at the informed discretion of the operator).

1.3 Place 0.1 ml of the neat and dilution tube samples on separate labelled plates and spread over agar surface using sterile spreader.

Generally: for bacterial enumeration use Nutrient agar and for fungal/yeast enumeration use Malt Extract agar supplemented with chloramphenicol. (Other types of agar may be used depending on the sample and the expected organisms).

1.4 Incubate the plates in an inverted position at an appropriate temperature (usually 30°C) for up to 1 week. (Plates are usually readable after 48 hours).

1.5 Select a suitable plate from the dilution series (generally containing 20 to 200 colonies). Count the number of colonies and relate the number back to the number present in the original sample.

Appendix 2: Rapid Automated Bacterial Impedance Technique (RABIT)

2.1 Bacterial Enumeration - DIRECT METHODOLOGY

Aseptically remove a 0.1 ml aliquot from the test flask and add to a RABIT tube containing 4.9ml sterile impedance media. This should be done at least in duplicate.

The numbers of bacteria are determined using the RABIT as described in the suppliers operation instructions.

2.2 Fungal Enumeration - INDIRECT METHODOLOGY

Aseptically remove a 0.1 ml aliquot from the test flask and inoculate a Tryptone Soya agar slope. Place inoculated slope into 'aged' indirect RABIT tube and replace bung securely.

The numbers of fungi are determined using the RABIT as described in the suppliers operation instructions. (NOTE the detection criterion is negative, as downward curves are seen).

Appendix 3: Fungal Biomass Determination - DRY WEIGHTS

Can be used at the end of a routine challenge test or as an experimental procedure in its own right (for fungistasis testing).

3.1 Select and number individually appropriately sized Whatman 541 fast, ashless filter papers. Dry each filter paper and weigh on a balance to 4 decimal places.

3.2 Place filter paper in buchner funnel and apply vacuum.

3.3 .Pour contents of experimental flask (or equivalent) into funnel.

3.4 When filtration is complete, rinse residual material out of flask into filter paper with a minimum of 100ml deionised water.

3.5 Place a minimum of 20ml Petroleum Ether (80-100°) into test flask, rinse around flask then pour onto fungal residue on filter paper. (NOTE: if at any stage a residue remains in flask, or an oily residue remains on the filter paper, washings can continue until it is removed).

Observe all safety precautions for handling solvents.

3.6 Remove filter paper from buchner apparatus and place in a tin-foil envelope in an oven at 70°C for at least 48 hours.

3.7 Remove filter papers from oven and place undisturbed in desicator cabinet to cool.

3.8 Weigh filter papers and biomass on a balance to four decimal places.

3.9 Calculate dry weight of fungal material in mg/ml test fluid.

3.10 Ensure all original experimental flasks, any contaminated equipment and all non solvent washings are autoclaved before washing. Where applicable, soaking in a 1% Virkon solution may be a suitable alternative.

3.11 Before disposing of solvent washings, add a suitable amount of Virkon powder to disinfect any water present. Leave for at least 1/2 hour before disposing of solvent in approved manner. Residual Virkon may be flushed to drain with plenty of water.

Appendix 4: Recording of Results

All results should be recorded on appropriate forms and stored under the correct Tl number in the Microbiology Filing System.

Appendix 5: Waste Disposal

All contaminated plates, Rabit tubes, water tubes, filter papers etc must be autoclaved prior to disposal (see l/PE/011 waste disposal).

Appendix 6: References

6.1. Solvents on Site - A Summary Castrol Publication, April 1981

6.2. Solvents and You - HSE Leaflet Ind (G) 93 (L) dated 9/90

APPENDIX B

COMPUTER SIMULATION FOR THEORETICAL OXIDE FILM GROWTH

A computer transform programme was written in order to simulate a theoretical oxide film growth model. This is a programme for calculating how the open circuit potential varies after abrasion of the electrode surface has stopped. Once abrasion has stopped any current which flows will cause the oxide layer to thicken. The resultant profiles were compared to the original potential transients using the parameter $\delta E / \delta \log t$ /V dec^{-1}.

Line 1 gives the initial current value. This decays with time as the oxide film thickens. Thickness after a given time t is represented by line 2. Line 3 is a form of the Tafel Equation where the parameters a and b can be altered in order to fit the experimental data, depending on the hydrogen evolution rate (η=a +blogi, hydrogen overpotential /V). The unit of time is given by n, shown in line 4. A more accurate potential transient is given for larger values of n typically 20000. Line 5 evaluates the thickness of the oxide layer which is increased by the flow of current. Line 11 gives the current flow through the oxide and proportional to the thickness of the repassivating layer.

Programme 1 Example of a maths transform performed in sigma plot.

```
Line
1        cell(1,1)=10
2        cell(1,3)=0.5
3        cell(1,5) = 0.1 + 0.2*log(cell(1,1))

4        for n =1 to 20 step 1 do
5        cell(1,2) =  cell(1,3) + cell(1,1)/1000
6        cell(1,3) = cell(1,2)
7        h =0.1 + 0.2* log(cell(1,1))
8        cell(4,n) = cell(1,1)
9        cell(2,n) = - h
10       cell(3,n) = n
11       cell(1,1) = exp((1+cell(1,5) - h)/cell(1,2))
12       cell(5,n) =cell(1,3)
13       cell(6,n) = log(n)
```

This a typical set of data points given on execution of the programme (many more rows are usually present. 20 are shown here as stipulated in line 4 of the programme). Column 3 shows the time increments starting at 1.0000 in cell(1,1). Cell (1,4) gives the initial current value of 10.0000 and can be seen to subsequently decay to 7.3525. Column 5 represents the potential in volts plotted on the y-axis of the graph, and column 6 log (col.3) or (t) plotted on the x-axis.

Table 1 Data worksheet for simulated oxide recovery as determined computationally by programme 1 above.

	1	2	3	4	5	6
1	7.3346	-0.3000	1.0000	10.0000	0.5010	0.0000
2	0.5153	-0.2734	2.0000	7.3596	0.5017	0.3010
3	0.5153	-0.2777	3.0000	7.7381	0.5025	0.4771
4		-0.2767	4.0000	7.6472	0.5033	0.6021
5	0.3000	-0.2766	5.0000	7.6391	0.5041	0.6990
6		-0.2764	6.0000	7.6170	0.5048	0.7782
7		-0.2761	7.0000	7.5975	0.5056	0.8451
8		-0.2759	8.0000	7.5777	0.5063	0.9031
9		-0.2757	9.0000	7.5582	0.5071	0.9542
10		-0.2755	10.0000	7.5387	0.5078	1.0000
11		-0.2752	11.0000	7.5195	0.5086	1.0414
12		-0.2750	12.0000	7.5004	0.5093	1.0792
13		-0.2748	13.0000	7.4814	0.5101	1.1139
14		-0.2746	14.0000	7.4626	0.5108	1.1461
15		-0.2744	15.0000	7.4439	0.5116	1.1761
16		-0.2741	16.0000	7.4253	0.5123	1.2041
17		-0.2739	17.0000	7.4069	0.5131	1.2304
18		-0.2737	18.0000	7.3886	0.5138	1.2553
19		-0.2735	19.0000	7.3705	0.5145	1.2788
20		-0.2733	20.0000	7.3525	0.5153	1.3010

The curve below shows the form of the open circuit recovery where

1. The H evolution is given by $\eta = 0.2 + 0.1\log i$
2. The oxide growth is given by exp(driving potential/thickness)

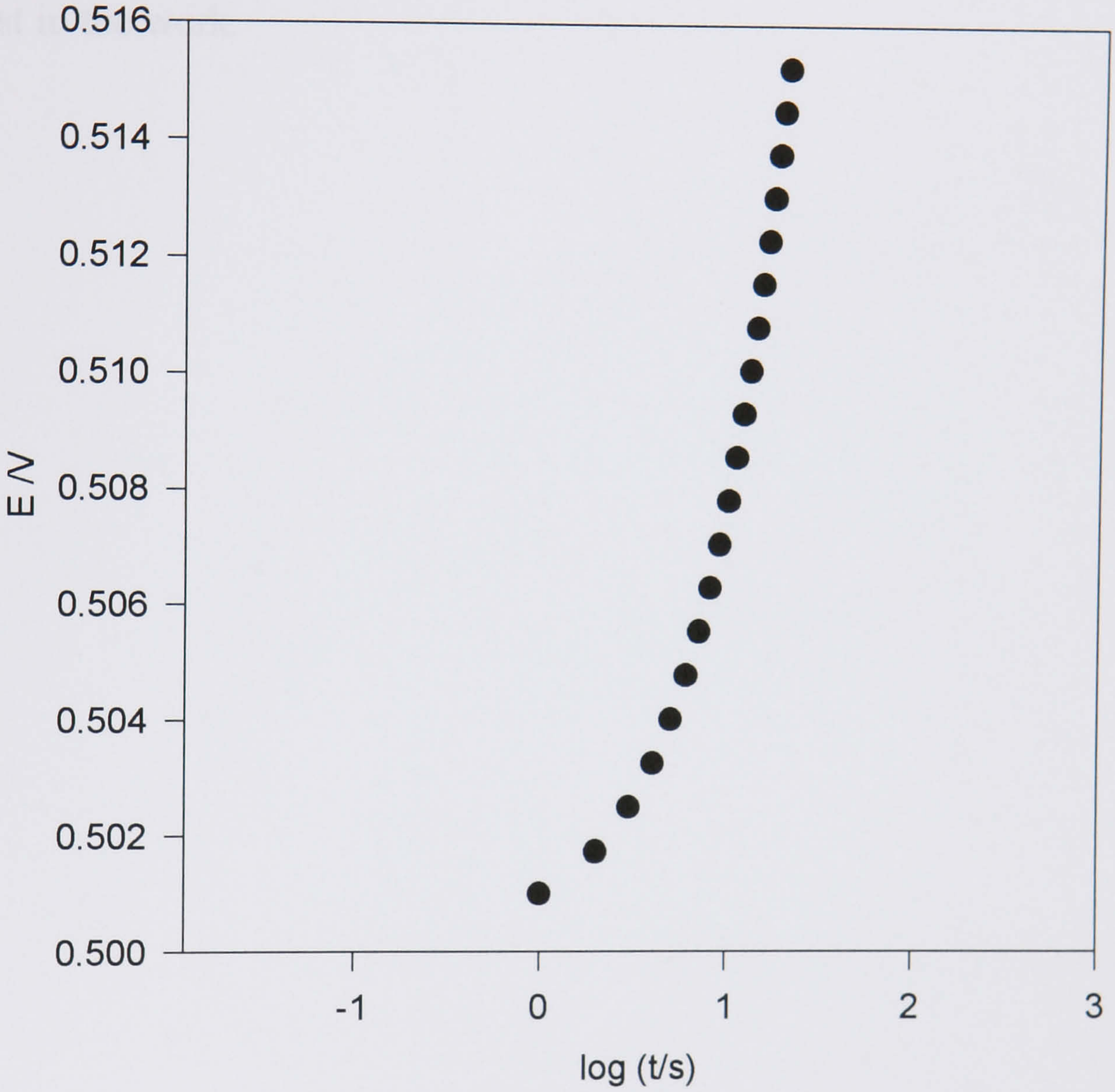

Fig. 1.0 Theoretical oxide recovery transient

Acknowledgments

Thankyou to my academic supervisor, Professor Ron Armstrong for all his help and advice during my six years as a student at Newcastle University. Also thankyou to Dr. Ken Airey and Dr Brian Walsh my industrial supervisors at Castrol International, for their help in organising this project and continued interest in the work.